Multi-responsive hydrogel structures from patterned droplet networks

Florence Downs

Brasenose College

University of Oxford

A thesis submitted for the degree of

Doctor of Philosophy

Michaelmas 2018

Acknowledgements

I would like to gratefully thank everyone who contributed to this thesis.

Firstly, my supervisors, whose meticulous approach to science, creative input and encouragement throughout have greatly advanced my scientific development. Professor Hagan Bayley, for the opportunity I have had to undertake my DPhil in his group, and for all the advice and training I have received from him in doing so. Dr Michael Booth, whose continual and patient mentorship throughout my DPhil, I cannot express enough gratitude for.

My special thanks go to the wonderful Dr David Lunn, who initiated the use of responsive hydrogels with droplet networks, and whose experimental input and intellectual guidance ensured rapid progress was made at all stages of the project.

Dr Linna Zhou, Dr Ravinash Krishna Kumar, Alessandro Alcinesio, Dr Michael Booth and Dr Stuart Box, for unlocking the secrets to droplet printing and sharing them with me. Dr David Lunn and George Klemperer for their optimisation work with the gold nanoparticles. Josh Roundtable, for illuminating experiments during his rotation. Dr Michael Booth and Dr David Lunn, for proofreading this thesis.

The entire Bayley group, for insightful discussions and being a joy to work with over the last three years. Special mention to the absolute rays of sunshine that are Vanessa Restrepo Schild and Dr Michael Booth: thank you for always staying hydrated with me. Also, Dr Ravinash Krishna Kumar and Alessandro Alcinesio, for making LG6 such an excellently soundtracked lab (despite libellous claims from elsewhere) and for always having time for discussions with me, scientific or otherwise.

The Synthetic Biology Centre for Doctoral Training, funded by the EPSRC and BBSRC, for the studentship that enabled this work. Brasenose College, for providing additional support and excellent people.

Finally, I would like to thank my family and friends, and Jake, who I probably definitely couldn't have done it without.

Abstract

Responsive hydrogels that undergo controlled shape changes in response to a range of stimuli are of widespread interest for use in microscale soft robotics and biomedical devices. However, existing fabrication methods cannot easily produce patterned multi-material structures. This thesis describes a novel approach for producing 2D- and 3D-patterned, multi-material, multi-responsive hydrogels, on a µm to mm scale, templated by droplet networks. Droplet networks are assemblies of aqueous droplets formed in a lipid-containing oil, and connected by droplet interface bilayers (DIBs). Within the compartmentalised structure of a droplet network, 3D patterning of multiple types of aqueous droplet is possible. Initially, nanolitre *N*-isopropylacrylamide (NIPAm) pre-gel droplets were assembled into networks in a range of 2D and 3D geometries. Polymerization across the lipid bilayers then resulted in continuous poly(*N*-isopropylacrylamide) (PNIPAm) hydrogel structures that reversibly contracted when heated and cooled. Exploiting the ability to modulate the temperature response of PNIPAm, and form multi-material structures using droplet networks, enabled the fabrication of structures capable of non-uniform shape changes, such as curling. Subsequently, additives were incorporated into the hydrogel structures that imparted additional functionality, including light-controlled shape change and magnetically controlled locomotion. By utilising a mechanism for dual temperature control, this would allow the fabrication of a magnetically controlled gripper-like device. Finally, the adaptation of a 3D droplet printer to automate the fabrication of PNIPAm hydrogel structures is described. With the droplet printer, networks composed of picolitre droplets were produced, which will allow higher resolution patterning. Furthermore, automated droplet generation enables the precise placement of hundreds to thousands of droplets. Successful implementation of this technology will allow the formation of multi-material responsive hydrogels from networks composed of thousands of droplets, patterned to a resolution of tens of microns.

Contents

List of Abbreviations

AAc . . . . . acrylic acid

AAm . . . . . acrylamide

3-APTMS . . (3-aminopropyl)trimethylsiloxane

α-KGA . . . . α-ketoglutaric acid

AuNPs . . . . gold nanoparticles

BMA . . . . . butyl methacrylate

DIB . . . . . droplet interface bilayer

DMSO . . . . . dimethyl sulfoxide

DPhPC 1,2-diphytanoyl-*sn*-glycero-3-phosphocholine

EBBA . . . . . ethidium bromide bis(acrylamide)

GOx . . . . . glucose oxidase

LCST . . . . . lower critical solution temperature

MBA . . . . . methylene bis(acrylamide)

NIPAm . . . . *N*-isopropylacrylamide

PAAc . . . . . poly(acrylic acid)

PAAm . . . . . polyacrylamide

PBS . . . . . phosphate-buffered saline

PEGDAAm . poly(ethylene glycol) diacrylamide

PEGDA . . . . poly(ethylene glycol) diacrylate

PEG_{800}-SH . . poly(ethylene glycol) methyl ether thiol, $M_w = 800$

POPC 1-palmitoyl-2-oleoyl-*sn*-glycero-3-phosphocholine

PMMA . . . . poly(methyl methacrylate)

PNIPAm . . . poly(*N*-isopropylacrylamide)

SPR . . . . . surface plasmon resonance

UCST . . . . . upper critical solution temperature

TR-DHPE . . Texas Red®-1,2-dihexadecanoyl-sn-glycero-3-phosphoethanolamine

1 Introduction

1.1 Responsive hydrogels

Hydrogels are water-swollen, crosslinked networks of hydrophilic polymer chains[1] with wide-ranging and tunable properties[2]. Due to their high water content and physicochemical similarity to biological extracellular matrices, hydrogels are ideal for a variety of biomedical applications[3]. In particular, their utility has been widely demonstrated in drug delivery[4] and tissue engineering[5]. Design strategies to enhance their performance have been aided by advances in the chemical and engineering sciences[2,3]. The integration of chemically and biologically active moieties has elevated the hydrogel matrix beyond a structural role, whilst innovative assembly techniques have enabled the creation of structures with complex, defined architectures[2].

Responsive hydrogels are a hydrogel subset that are able to undergo structural changes in response to external stimuli[6]. Additional functionalities resulting from their capacity to be externally controlled have advanced and broadened their possible applications beyond those of non-responsive hydrogels. Outside of biomedical applications, the versatility of these materials extends their use to diverse fields such as sensors[7], actuators[8], soft robotics[9], optics[10,11] and wearable materials[12,13]. However, a major limitation of current methods used to fabricate

responsive hydrogels is that they cannot readily be adapted to form 3D patterned, multi-material structures. There is therefore a need for a simple method with which 2D and 3D patterning of multi-material structures is possible.

1.1.1 Physical properties

Physically, gels have properties that render them both liquid-like and solid-like[14]. Despite being structurally disordered and primarily composed of a liquid solvent[15], solid-like properties result from the crosslinked polymeric network, such as the capacity to be deformed with a characteristic shear modulus[14]. The polymeric network is a solid when dried, but upon addition of a solvent, swells until it reaches an equilibrium value[14]. It is widely understood that the swelling kinetics of a gel are determined by the diffusion of the polymeric network into the solvent, rather than the diffusion of solvent molecules into the network[16]. In the theory of swelling kinetics described by Tanaka and Fillmore[17], the rate of swelling was found to be proportional to the square of the smallest dimension of the gel, as well as its diffusion coefficient. Once swollen, the interactions between the network and the solvent molecules are then responsible for the overall characteristics of the gel[14].

In general, the mechanical properties of a hydrogel depend on several factors, including its constituent monomers, co-monomers and crosslinkers; the density of crosslinking; degree of swelling; and the solvent in which it is immersed[1]. In turn, the degree of swelling depends on the interactions between the polymer and the solvent used, and the density of crosslinking, where the crosslinking density refers to the number of crosslinked monomer units per main chain[18]. In general, the more highly crosslinked a polymeric network is, the stiffer[18] and stronger the material is; and the lower its degree of swelling[1]. Accordingly, the choice and exact composition of co-monomers and crosslinkers, as well as formation conditions, play important roles in the ultimate mechanical properties of a hydrogel[1]. The mechanical behaviour exhibited by hydrogels may be theoretically described by rubber elasticity and the viscoelasticity theory[1].

1.1.2 Gelation

Many types of hydrogel exist, both naturally and synthetically derived[2]. Crosslinking of the hydrogel matrix can occur covalently (chemically crosslinked hydrogels), or as a result of noncovalent interactions, such as hydrogen bonds or electrostatic forces (physically crosslinked hydrogels)[15,19]. Once crosslinked into a network, swelling of the network takes place when it is immersed in a suitable solvent[18].

Physical crosslinking refers to the connection of polymer chains by strong secondary bonds or intermolecular associations[18]. Noncovalent interactions such as hydrogen bonds, van der Waals forces and hydrophobic interactions can all cause the self-assembly of macromolecules into scaffolds with specific structures and functions[2]. Many physically entangled polymer networks are based on naturally derived polysaccharides or proteins[2], such as agarose and gelatin, respectively. Gelation is often thermally driven[2], and such physical gels can be described as thermoreversible, as their bonds can be broken by heating[15]. Alternatively, ionic interactions may drive gelation, as for the polysaccharide alginate, where crosslinking is caused by intra- and inter-chain coordination of divalent cations[20].

In chemical crosslinking, covalent bonds are formed between polymer chains[18]. This can take place during polymerization or after linear polymers have been formed[18]. With chemically crosslinked hydrogels, improved control over the gelation is possible compared to physically crosslinked hydrogels[2]. A conventionally used chemical crosslinking approach is the free radical polymerization of low molecular weight monomers with crosslinking agents[21]. Vinyl monomers or water-soluble polymers with polymerizable groups are frequently used monomers and co-monomers[21]. Free radical polymerization can be performed in bulk, suspension, solution, or emulsion, and typically proceeds when an initiating agent is thermally or photolytically degraded[18]. First, an initiator radical is formed, before it is subsequently added to the monomer. Propagation reactions then take place as monomer radicals are successively added to monomer molecules. Eventually, termination of propagating chains or initiator radicals occurs[18]. An advantage of photoinitiated polymerization is the ability to perform it within a rapid completion

time and with high spatiotemporal control[22]. Photoinitiators convert light absorbed in the spectral range between UV and visible into chemical energy with the formation of reactive intermediates[23]. In general, there are two classes of photoinitiator that undergo photolysis to generate free radicals, which occurs via promotion of the photoinitiator to an excited state and subsequent homolytic bond cleavage. Type I photoinitiators are single molecules that directly undergo bond cleavage after absorbing radiation, whereas type II photoinitiators also require a second molecule, often referred to as a "co-initiator", to produce initiating species[22,23].

Intrinsically, radical polymerization reactions are susceptible to inhibition by molecular oxygen which can result in incomplete or failed polymerization[22]. For photopolymerization, the possible mechanisms for oxygen inhibition include quenching of the excited state of the photoinitiator, or reacting with the initiator radical or propagating radicals, including the propagating polymer chain[22]. When radicals are initially generated, their reactions with pre-dissolved oxygen can have significantly faster rates than initiation or propagation. As a result, at the beginning of polymerization, there is generally an induction period in which radicals produced react with dissolved oxygen. During this period, the concentration of molecular oxygen is reduced to a point at which the rate of polymerization becomes competitive. At this point, polymer chains can propagate. However, at the interface with the surrounding environment, effects of oxygen inhibition remain dominant due to the dynamic absorption and diffusion of oxygen.

There are several strategies by which oxygen inhibition can be reduced. One of the most widely used approaches to prevent diffusion of oxygen from the environment is blanketing the environment with an inert gas such as nitrogen[22]. A liquid or solid barrier, such as a wax or a film, can also be used. Another approach is to increase the irradiation intensity, to yield a higher concentration of initiating radicals to combine with dissolved oxygen, or to increase the photoinitiator concentration, which can also decrease the induction period[22]. Finally, oxygen scavenging molecules can also be added[22].

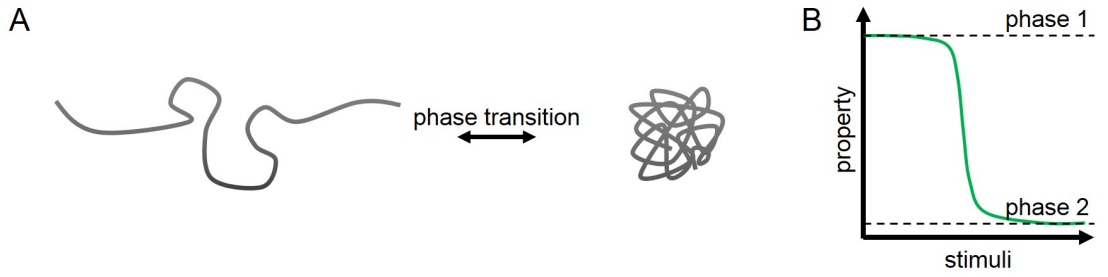

Figure 1.1: (A) Coil-to-globule phase transition of a responsive polymer. **(B)** Phase transitions of responsive polymers and hydrogels occur discontinuously, as a result of infinitesimal environmental changes.

1.1.3 Sensitivity to external stimuli

Although not conventionally considered as responsive materials, there are examples of hydrogels which are sensitive to photodegradation[24], or particular enzymes produced by cells such as matrix metalloproteinases[25], which cause degradation of target domains. However, the work in this thesis focuses on responsive hydrogels, able to undergo enormous changes in volume as a result of infinitesimal changes in environmental conditions **(Figure 1.1)**[14]. These types of hydrogel, which may be natural as well as synthetic[26], undergo a discontinuous phase transition in response to external stimuli such as temperature[27,28], solvent[16], pH[29], electric field[30] and light[31].

Thermoresponsive hydrogels are one of the most widely studied subsets of responsive hydrogels and may undergo a volume phase transition when heated[27,28] or cooled[32]. Hydrogels of the former category contract when heated above the lower critical solution temperature (LCST); whereas hydrogels of the latter category contract when cooled below the upper critical solution temperature (UCST). However, hydrogels rarely show a USCT in aqueous solutions[32]. Typically, the UCST relies on hydrogen bonding or coulomb interactions[33]. A hydrogel with a UCST has been synthesised from an interpenetrating polymer network (IPN) of poly(acrylic acid) (PAAc) and poly(acrylamide(AAm)-co-butyl methacrylate (BMA)[32]. In this example, the transition was hypothesised to be a result of hydrogen-bonded intermolecular complexes between poly(acrylamide) and poly(acrylic acid) at low temperatures, which dissociate at high temperatures. Interestingly, hydrogels

have been prepared that have both LCST and UCST transitions[34]. However, the most comprehensively studied thermoresponsive hydrogels demonstrate a LCST response and are typically formed from poly(*N*-isopropylacrylamide) (PNIPAm) or other alkyl-substituted acrylamides. Of these, PNIPAm was initially identified as an ideal polymer for in vivo applications due to its physiologically relevant LCST, which has been experimentally demonstrated to lie between ca. 30 and 35°C depending on the polymer microstructure[35,36]. This has resulted in extensive study of its physical properties[28,37–39], and demonstrations of its utility in actuating and shape-changing materials[40–42]. Polymerization may proceed via free radical initiation, redox initiation or with the use of ionic initiators[35]. Usually, gelation is performed by free radical polymerization, with the addition of a crosslinking agent (**Section 1.1.2**)[35]. *N,N*-methylenebis(acrylamide) (MBA) is frequently used as a crosslinking agent due to its structural similarity to the *N*-isopropylacrylamide (NIPAm) monomer and established use in the formation of gels for electrophoresis[35].

The nature of the phase transition of PNIPAm has been comprehensively studied[28,37–39]. In solution, the conformation of the polymer results from how it must order itself to hydrogen bond with surrounding water molecules[35]. Due to the hydrophobic effect, water molecules cannot hydrogen bond with nonpolar regions and become ordered around these regions. As a result, upon mixing of polymer molecules and water, there is decreased entropy. However, this is overcome by the enthalpy of hydrogen bond formation between the polar groups of the polymer and water molecules. When the temperature is increased, the entropy increases beyond the enthalpy. At the point at which the free energy change becomes positive (the LCST), phase separation occurs[35]. This conformational change is also known as a coil-to-globule phase transition[43], and is manifested by the replacement of polymer-water contacts with polymer-polymer and water-water contacts[35].

When PNIPAm is crosslinked into a hydrogel, the coil-to-globule transition results in a volume phase transition in which there is a rapid decrease in the volume of the gel[44]. Theories attempting to physically describe the volume phase transition for PNIPAm, which are diverse and incomplete, have been summarised by Schild[35].

As the kinetics of swelling and contraction are governed by diffusion of the polymer network in water, and the rate of these kinetics is inversely proportional to the square of the smaller dimension of the gel[45], the response of PNIPAm is relatively slow[46]. To address this, comb-type PNIPAm hydrogels have been synthesised, in which PNIPAm chains grafted onto crosslinked networks act as hydrophobic nucleation points for collapse[45,47]. Alternatively, macroporous PNIPAm hydrogels have been synthesised, which incorporate pore-forming agents that are extracted from the hydrogel after polymerization[46,48].

Neither the molecular weight of the polymer nor crosslinking density of the hydrogel have been shown to have a significant effect on the LCST of PNIPAm[35]. However, altering the monomer composition can allow the LCST to be tuned. In general, the incorporation of hydrophobic comonomers results in a decreased LCST, whereas the incorporation of hydrophilic comonomers results in an increased LCST[49]. Examples of monomers that have copolymerized with NIPAm to increase the LCST include acrylamide (AAm)[49], acrylic acid (AAc)[41], and poly(ethylene glycol) diacrylate (PEGDA)[9].

1.1.4 Enhancing responsive hydrogels

The integration of certain additives into responsive hydrogels can create novel stimuli-responsive properties. For example, photothermally active nanoparticles, or photo-sensitive molecules such as dyes, can be utilised in conjunction with thermoresponsive polymers to yield light-responsive polymers. Plasmonic nanoparticles such as gold nanoparticles (AuNPs) are widely utilised (see **Chapter 3** for detailed discussion). Approaches to incorporate AuNPs into responsive hydrogels include loading via swelling in a nanoparticle-containing aqueous solution[50–52], chemical modification of the hydrogel matrix with gold-reactive functional groups[53], and simply mixing nanoparticles into the pre-gel before polymerization[9,54,55]. Similarly, dyes have also been mixed into the pre-gel, such as chlorophyllin[31]. Photoactive moieties can also be directly copolymerized, as with the monomer *N*-(4-phenylazophenyl)acrylamide[56].

As hydrogels are typically weak materials, exhibiting poor mechanical strength[1], efforts to improve their physical properties have also been explored. Dispersed inorganic clay has been integrated into PNIPAm hydrogels, resulting in improved toughness, as well as improved transparency and rate of contraction[57]. Another approach to improve the strength of hydrogels is the formation of double network hydrogels, which are typically formed from two sequentially polymerized hydrogels[58]. Hydrogels with superior toughness can be formed from double networks of a chemical gel with a physical gel[59]. When an ionically bonded alginate network was entangled with a covalently bonded polyacrylamide network, a tough double network hydrogel was formed, which was able to stretch to more than to 20 times its original length[59]. Another potentially useful advance to enhance the mechanical properties of hydrogels is the development of hydrogel-elastomer hybrids[60].

1.1.5 Applications

Responsive hydrogels have diverse applications in a number of fields. The use of responsive hydrogels to form complex shape changing structures has formed a basis for suggested applications in biomedical applications and soft robotics, among others[42,61]. Shape change in responsive hydrogels, beyond the types of volumetric contraction discussed in **Section 1.1.3**, relies upon the formation of hydrogels whose composition is heterogeneous. Frequently, this is demonstrated by modulation of swelling or contraction in particular regions **(Figure 1.2** and **Figure 1.3)**. One approach to do this involves attaching a non-responsive hydrogel to a responsive hydrogel[8,9,61]. Upon exposure to the appropriate stimuli, the responsive hydrogel can be shrunk, whilst the non-responsive hydrogel remains inert, causing actuation of the overall structure. Modulation of swelling has also been achieved throughout hydrogel structures by forming gradients in monomer concentration[40] or crosslinking density[41] **(Figure 1.3A)**. In another approach, the incorporation of cellulose fibrils with modulated alignment was used to make biologically inspired structures, in which swelling in particular regions was dependent on the orientation of the fibrils[42,62] **(Figure 1.3B)**. Finally, crosslinking density

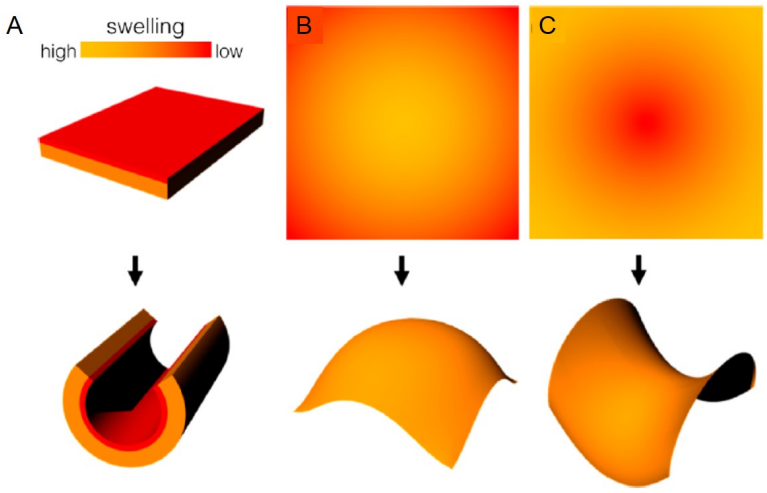

Figure 1.2: (A) Schematic describing the modulation of swelling in different regions of a compositionally heterogeneous hydrogel structure, resulting in **(B-C)** different types of curved surfaces. Reproduced from Jeon et al.[63]

(and therefore swelling) throughout a structure has been modulated by incorporating crosslinkers with different gelation times, and exposing different regions to UV light for different lengths of time **(Figure 1.3C)**.

Of the conceivable applications for responsive hydrogels, biomedical applications are the most fully realised, with many demonstrations of proof-of-principle devices. Self-folding capsules have been fabricated which were designed to encapsulate cells[65] or deliver drugs[66]. Microgrippers have been designed which were also able to carry cargo, in addition to performing in vivo biopsies **(Figure 1.4)**[67]. Drug delivery devices have also been fabricated to produce sustained drug release profiles after adhesion to tissue[68], as well as visible light-induced drug release from a transdermal patch containing light-responsive hydrogel beads[69]. Tissue engineering applications are less widely explored for responsive hydrogels, but a centimetre-scale scaffold designed to stimulate differentiation of dental mesenchymal stem cells was fabricated from PNIPAm with an adhesion-promoting peptide[70]. The contraction of the hydrogel scaffold at 37°C resulted in increased induction of odontogenic transcription factors as well as mineralization, both relevant for tooth differentiation.

Although robotics is frequently discussed as a possible application for shape-changing materials[41,42,61], shape-changing responsive hydrogels may be of limited use

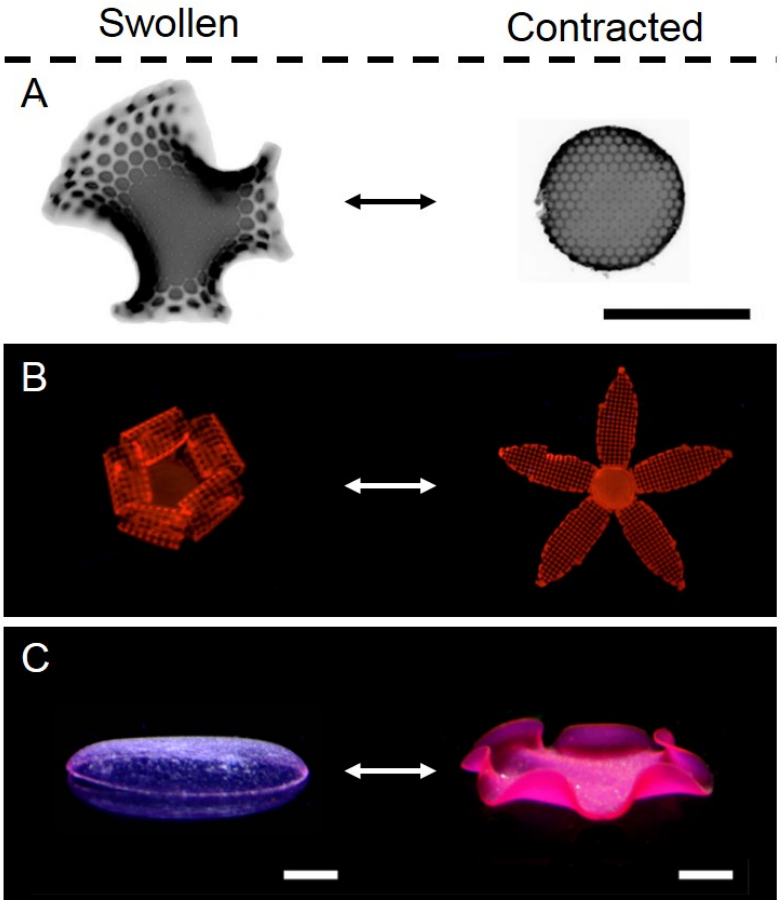

Figure 1.3: **(A-C)** Microscopy images of shape changes of responsive hydrogels. **(A)** Reproduced from Kim et al.[41] Scale bar, 500 µm. **(B)** Reproduced from Gladman et al.[42] No scale bars given in original article; nozzle size given as 250 µm. **(C)** Reproduced from Nojoomi et al.[64] Scale bar, 2 mm.

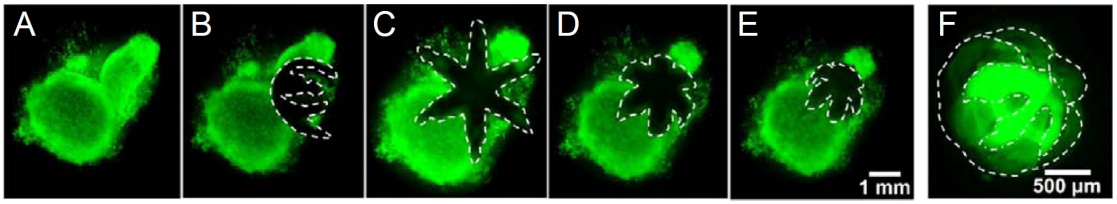

Figure 1.4: **(A-F)** Capture and removal of cells from a clump of fibroblasts. Reproduced from Breger et al.[67]

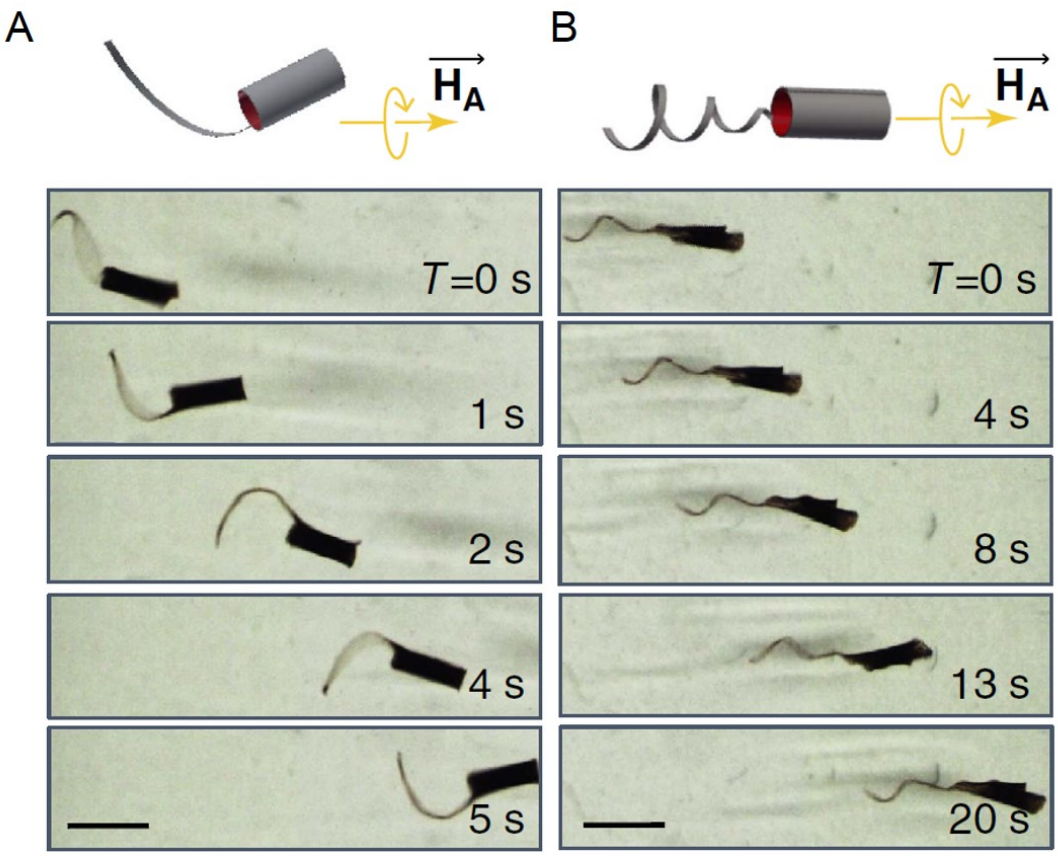

Figure 1.5: (A-B) Two types of soft nanocomposite hydrogel microswimmer, with different modes of swimming controlled by rotating magnetic fields with strength $\mathbf{H}_A$. Reproduced from Huang et al.[9] Scale bars, 2 mm.

in this field due to their mechanical weakness[1] and slow kinetics[46], especially at larger scales. However, there have been a range of developments in this area. For example, millimetre-scale swimmers have been fabricated, able to respond to a variety of stimuli. Electroactive hydrogels have been used to fabricate millimetre-scale robots able to swim[71,72] and walk in response to an electric field[72]. Nanocomposite hydrogels have been used to make swimmers whose motion could be controlled by a rotating magnetic field **(Figure 1.5)**, and whose bodies and resulting motility could be reprogrammed with near infrared (near IR) radiation[9]. Other types of actuators have also been demonstrated, such as centimetre-scale dual-layer thermoresponsive hydrogels that could change shape and be used to grip an object[8], and near IR-responsive actuators and crawlers[73].

Other less developed application areas include sensors[7], responsive optics[11]

and wearable materials[12,13].

1.1.6 Fabrication methods

Importantly, as hydrogels are typically formed by solution polymerization of liquid pre-hydrogels, which collapse under their own weight, there are certain constraints on the techniques used to fabricate them. The simplest approach is the use of a solid mould, such as a tube[17] or capillary[31], in which a pre-gel can be kept until polymerization is complete, before transfer of the hydrogel into water. Similarly, a two-phase approach has been used, in which sub-millimetre-sized spherical droplets of pre-gel are formed with a micropipette in an oil phase[17]. The formation of monodisperse spherical hydrogel particles in high throughput was also automated using a microfluidic device[48]. These types of approach to form gels were widely utilised to examine phase transition properties[17,27,29,48], as well as being investigated for biomedical applications[69,70] and optical applications[11]. As liquid pre-hydrogels are able to mix with one another, hydrogels formed tend to be composed of a single, homogeneous material.

Nonetheless, some compositionally heterogeneous hydrogels have been fabricated in the form of planar sheets, which may take on 3D shapes after formation, or after the phase transition is initiated. For example, a mixer and Hele-Shaw cell were used to program gradients of a high NIPAm concentration pre-gel with a low NIPAm concentration pre-gel in a hydrogel sheet[40]. These gradients were frozen upon polymerization, resulting in a non-uniform gel disk that could wrinkle and buckle. Several other approaches have effectively utilised photopatterning techniques to form hydrogels with heterogeneous compositions[41,75]. In one example, surfaces with different curvatures were generated by using a combination of photomasks and a photoactivatable crosslinker to pattern more densely crosslinked regions **(Figure 1.6A)**[41].

In order to make devices capable of more complex functions, fabrication processes have been developed that allow responsive hydrogels to be adjoined to other types

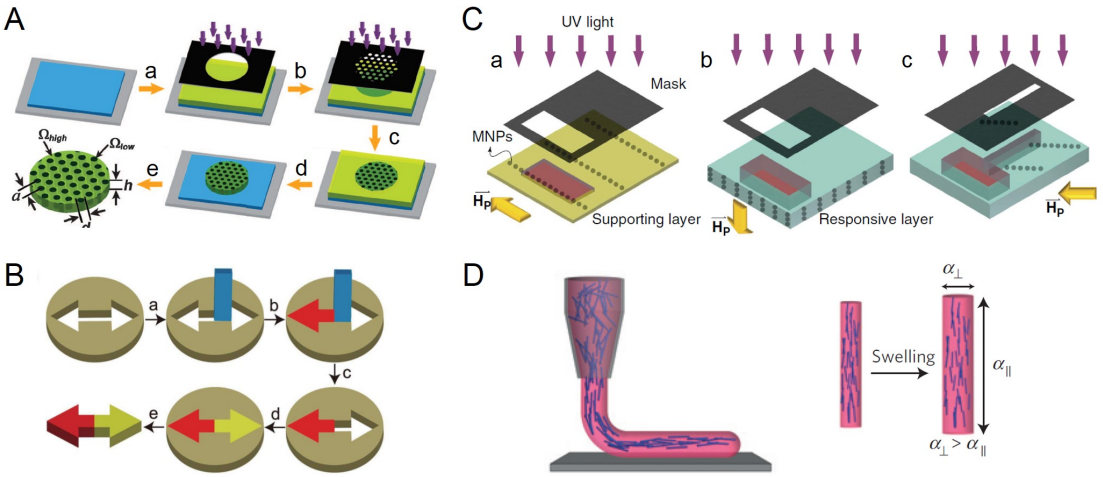

Figure 1.6: Schematics of different fabrication methods for the formation of responsive hydrogels. **(A)** Photolithographic patterning of a PNIPAm sheet crosslinked with a photoactivatable crosslinker, benzophenone, using multiple photomasks. Reproduced from Kim et al.[41] **(B)** Formation of a two-domain dual-pH responsive hydrogel using different regions of a mould. Reproduced from Hu et al.[74] **(C)** Photolithographic formation of a multimaterial nanocomposite hydrogel using three photomasks. Reproduced from Huang et al.[9] **(D)** Extrusion printing of a nanocomposite hydrogel, whose swelling (α) in different directions was modulated by the alignment of nanofibrillar cellulose. Reproduced from Gladman et al.[42]

of hydrogel in layered structures. For cm-scale hydrogels, one example of a multi-material hydrogel was formed from a dual-layer gel slab[8]. To do this, a PNIPAm hydrogel was formed first between two glass slides. Then, a polyacrylamide (PAAm) slab was formed in between the PNIPAm hydrogel and another glass slide, forming an interpenetrating network and adjoining the two hydrogels. Spatially modulated gel structures formed from this technique were able to curl, change shape, or grip objects when heated, due to differential contraction of the PNIPAm hydrogel compared to the PAAm hydrogel. Similarly, a two-domain polyacrylamide-DNA hydrogel was formed in a two-step process with a mould and blocker **(Figure 1.6B)**[74]. Here, one type of pH-responsive hydrogel was formed in one half of the mould, whilst the other half was blocked off. Then, a second type of pH-responsive hydrogel was formed in the other half, allowing it to form an adjoined structure with the first hydrogel. With photolithography, millimetre-scale layered structures have been fabricated[9,61]. To achieve this, an inert hydrogel layer was initially formed with one

photomask, before a responsive hydrogel layer was polymerised on top in sub-regions with multiple photomasks **(Figure 1.6C)**[9,61]. Multi-photon lithography has also been utilised to form multimaterial hydrogels with a resolution of tens of microns[7].

With 3D printing, the pre-hydrogel can be dispensed robotically during fabrication, with high precision and reproducibility in manufacture[2]. Generally, there are two types of 3D printing approach: inkjet, to print liquids; or extrusion printing, to print viscoelastic materials[76]. Both of these approaches have their own challenges. In inkjet or "droplet-on-demand" printing, the ejection of liquid droplets is achieved via thermal or acoustic approaches. A balance must be achieved to deposit sufficiently high concentrations to fabricate the desired material without clogging the nozzle. In contrast, extrusion printing involves the fabrication of continuous filaments of viscoelastic materials using a pressurised flow. The material must be polymerized rapidly after deposition to prevent its collapse. This can be improved via the incorporation of additives to improve rheological properties[42], or via the use of supporting fugitive ink scaffolds[77], or shear-thinning, self-healing hydrogel baths that enable suspension of printed material[78]. As much of the focus in developing these systems lies in bioprinting applications[79], there have been limited examples of their use for responsive hydrogels. In one case, extrusion printing was used to form hydrogel structures, each formed from a single type of nanocomposite hydrogel with modulated swelling, including a nanocomposite PNIPAm **(Figure 1.6D)**[42]. In this case the swelling was modulated by the orientation of nanofibrillar cellulose, whose order was controlled by the nozzle diameter and printing speed. Dispersed inorganic clay was incorporated into the pre-gel[57] as a rheological aid to allow direct extrusion printing[42]. Although methodologies have been developed to enable multimaterial printing of hydrogels[80], opportunities remain to improve the integration of multiple materials[76], especially for responsive hydrogels.

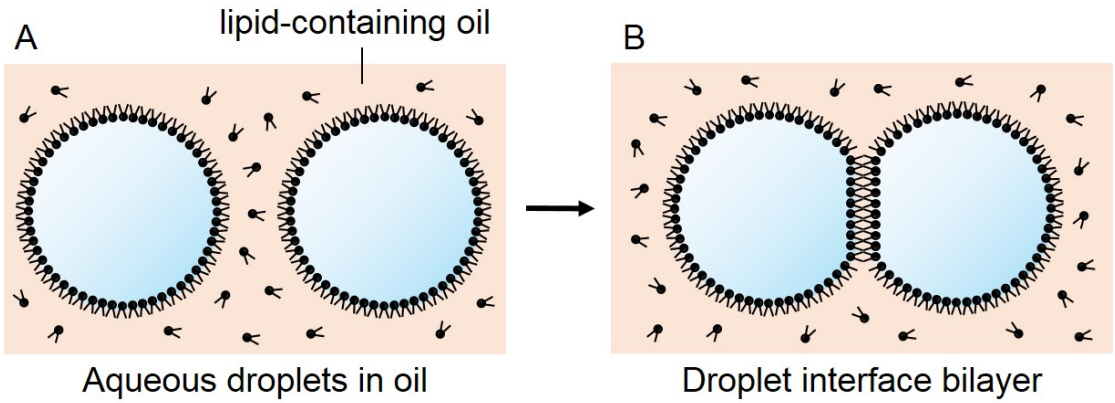

Figure 1.7: **(A)** Aqueous droplets formed in a lipid-containing oil acquire a lipid monolayer coating. **(B)** A droplet interface bilayer (DIB) forms at the interface between them.

1.2 Droplet networks

1.2.1 Droplet interface bilayers

When an aqueous droplet is formed in a lipid-containing oil, the droplet becomes coated with a lipid monolayer **(Figure 1.7A)**. If two such droplets are brought together, a droplet interface bilayer (DIB) can form at their interface[81] **(Figure 1.7B)**. The DIB was originally developed as a technique to study membrane proteins when only small quantities of biological material were available, or if expensive reagents were required, as droplets can be between femtolitre- and microlitre-volume. The lipid bilayer formed can be functionalised with membrane proteins, such as channels, pores and transporters, where they can be electrically interrogated by the insertion of electrodes into the two droplets[81]. A wide variety of lipids can be used to form DIBs[82]. In addition to dissolving the lipid in the oil phase ("lipid-out" formation), the lipid can also be incorporated into the bilayers from vesicles inside the droplets ("lipid-in" formation).

A droplet pair joined by a bilayer exists in a local energy minimum, due to thermodynamic instability towards coalescence into a single droplet[82]. Despite this, their use in a variety of applications is possible due to kinetic stability. Although a thorough understanding of many fundamental properties of DIBs is incomplete, certain factors are known to have an impact on the strength of the bilayer. Some

of the factors known to affect bilayer adhesion include the interactions between phospholipid headgroups and van der Waals forces between their tail groups, as well as the hydrophobic effect[83]. Other factors of known importance include the lipid composition and concentration, the internal contents of the droplets, the external oil phase, and the ambient temperature[82]. It has been assumed that the area of a DIB, as well as the corresponding contact angle between droplets, reflects the strength of the bilayer. These parameters can therefore be used to estimate the bilayer strength.

1.2.2 Fabrication of droplet networks

Interesting possibilities arise when multiple droplets, instead of two, are joined by bilayers[82]. Such an assembly, known as a droplet network, possesses properties unachievable by a droplet pair alone. For example, electronic devices have been assembled from small droplet networks in which different membrane proteins are incorporated. These devices include a battery[84], a light sensor[84], and a full-wave rectifier[85]. With larger droplet networks, tissue-like behaviour has been achieved, including shape change[86] and electrical communication[86], which has also been light-activated[87].

The simplest approach for the assembly of small-scale droplet networks utilises manual droplet formation, for example with a micropipette or syringe, and manipulation either by hand or with a micromanipulator[84]. One of the techniques developed to assist droplet placement in small networks involved the use of a magnetic probe to manipulate droplets containing paramagnetic beads[88]. Networks with up to three layers could be constructed as well as two-layer networks containing up to fourteen droplets. Different chemical and electrical communication pathways were generated within the networks via the use of the α-haemolysin protein pore (αHL). Optical tweezers have also been used to manipulate droplets less than 30 µm in diameter, allowing the construction of a pyramid containing eleven droplets[89]. With these fabrication techniques, 2D and 3D networks have been formed, containing up to tens of droplets, of multiple different types **(Figure 1.8)**.

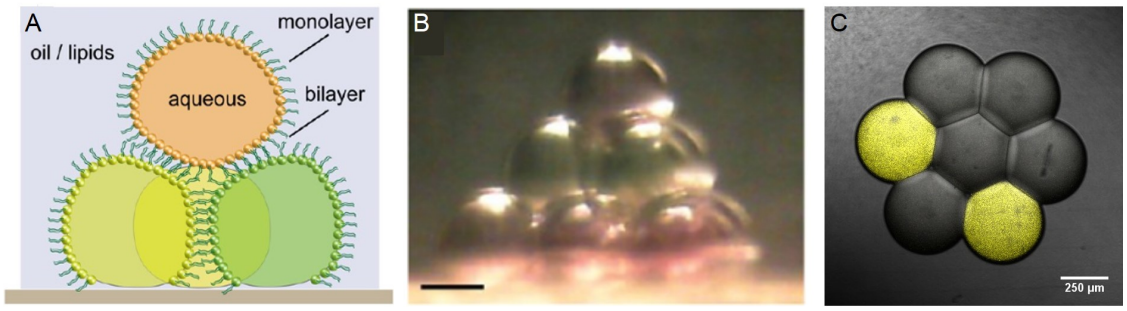

Figure 1.8: **(A)** Schematic of a 3D droplet network comprising 4 droplets. **(B)** Brightfield image of a pyramidal structure comprising 10 droplets over 3 layers. Scale bar, 200 µm. Reproduced from Wauer et al.[88] **(C)** Overlaid brightfield and fluorescence images of a 2D hexagonal droplet network comprising two types of droplet. Reproduced from Booth et al.[90]

For the manufacture of larger networks, or to facilitate the formation of more than a few copies of a particular type of network, automated approaches have been developed. Microfluidic devices have been fabricated, able to produce droplet networks containing thousands of droplets[91]. However, droplet generation is uncontrolled, making patterning difficult; and assembled droplet networks are difficult to extract from the container in which they are formed. To address these issues and enable the formation of large yet precisely patterned droplet networks, a 3D droplet printer was built[86] (see **Section 4.1.2** and **Section 4.1.3** for detailed discussion). With this droplet printer, tens of thousands of picolitre droplets could be precisely patterned into synthetic tissue-like materials, including two types of droplet. By creating osmolarity gradients across droplet networks, a flower-shaped synthetic tissue was fabricated that was able to fold into a hollow ball, as water flowed from regions of low osmolarity into regions with high osmolarity. Furthermore, by patterning this tissue-like material with membrane proteins along a defined pathway, rapid electrical communication was demonstrated. This electrical communication could be externally controlled, with a light-activated in vitro transcription translation system that generated αHL[87].

Synthetic tissues such as these are of interest for possible downstream applications in medicine[82]. For example, a droplet network might be interfaced with a biological tissue for control or repair. However, many examples of functional

droplet networks in the literature so far are constrained to an oil environment[86,87]. Multi-compartment vesicles, and multisomes, are types of droplet network that exist in a bulk aqueous environment[92,93]. Multi-compartment vesicles have been formed via gravity-mediated phase transfer[92], using a two phase system formed from a lipid-containing oil with water below it. Phase transfer takes place as droplet networks formed in a lipid-containing oil are passed via gravity through a lipid monolayer at the water/oil interface, allowing internal bilayers to be kept intact. However, this approach required modification of the density of the droplets via the addition of sucrose, which created an osmotic gradient between the internal phase and external phase after phase transfer. As a result of this, the lifetime of these structures was only ca. 60 minutes. Multi-compartment vesicles have also been formed using a surfactant-assisted microfluidic approach[93]. In compartmentalised structures such as these, communication between compartments has been demonstrated via the insertion of αHL[93], enabling enzymatic reactions to be carried out[94]. In addition, in vitro transcription and translation has been performed within compartments, for the expression of fluorescent proteins[93,95]. However, the arrangement of droplets within these structures is not easily controlled, relying on either the configuration of droplets falling through the water-oil interface, or generated in a microfluidic w/o/w system. Multisomes are a type of droplet network formed within an oil drop in a bulk aqueous environment. These have been formed via manually pipetting nanolitre droplets into an oil drop suspended on a Teflon-coated wire loop[96]. Controlled rupture of the internal compartments was initiated using pH and temperature-sensitive lipids. Microfluidically generated multisomes have also been prepared, containing up to four droplets[97]. In two-droplet multisomes prepared in this way, the membrane-permeant primary amine, ethanolamine, passed through the bilayer in the multisome to react with a membrane-impermeant pyrylium in the second droplet, forming a fluorescent pyridinium salt. Finally, the formation of patterned multisomes has been achieved by 3D droplet printing into a suspended oil drop[86]. These 3D printed multisomes were found to be stable for several weeks. The incorporation of membrane proteins within these 3D printed structures would be a useful advance, as it would allow

their communication with the external environment and between compartments. A further development to aid the translation of these structures for medical applications would be the ability to detach them from the stabilising wire loops.

1.2.3 Use of droplet networks with hydrogels

The use of droplet networks in conjunction with hydrogels was first explored with droplet hydrogel bilayers (DHBs), where a lipid-coated droplet in oil forms a bilayer with a lipid-coated hydrogel immersed in oil[82]. DHBs were initially used to record electrical current and fluorescence simultaneously[98], and have allowed parallelised optical sensing of nucleic acids in a single DHB[99]. In a further development, an array of droplets containing the light-driven proton pump, bacteriorhodopsin (bR), was interfaced with a common hydrogel structure, which allowed shape detection[100].

Another interesting avenue for the use of hydrogels with droplet networks is as a means for stabilisation. One approach to do this uses a hydrogel as an external shell. In one example, a microfluidic device was fabricated which allowed several aqueous droplets to become encapsulated in an oil drop, which itself was encased within an alginate shell[101]. These alginate-encased droplet networks were stable for weeks, in water as well as in air. Similarly, oil drops (50-200 µL) injected into agarose during gelation could themselves be injected with aqueous droplets ($<$ 50 nL) which contained DPhPC liposomes[102]. These aqueous droplets then formed networks within the oil drops.

The incorporation of hydrogels into 3D printed droplet networks was initially investigated as a means to stabilise patterned cell-containing microtissues to allow their phase transfer into water[103]. Although the successful encapsulation of cells into aqueous droplet networks in oil was demonstrated with an aqueous bio-ink[103], Fmoc-dipeptides and agarose were incorporated into the bio-ink to stabilise the patterned structures in advance of phase transfer. The incorporation of gelators into the structure then prevented its coalescence with the aqueous phase (see **Chapter 4**), whilst initial patterning of the structure was retained based on the original positions of droplets in the printed network.

1.2.4 Development of droplet networks for use with responsive hydrogels

Currently, the state-of-the-art fabrication techniques that have been used to form responsive hydrogels are limited to single materials with modulated compositions[40–42], or simple layered[9,61] or dual-material structures[7,74]. To open further avenues for the fabrication of responsive hydrogels, a new method is needed, in which liquid pre-hydrogels are easily patterned such that multi-material hydrogels can be formed, across multiple length scales.

Consequently, droplet networks are a promising means to pattern responsive hydrogels, as they could allow the encapsulation of different aqueous solutions within different bilayer-enclosed compartments. The lipid bilayers between each compartment would prevent the mixing of pre-hydrogels placed adjacent to one another. As a result, pre-hydrogels would not require modification with rheological additives or scaffold materials to enable their fabrication. With droplet networks, the bottom-up assembly of a variety of structures would be possible, as each droplet could act as a 3D pixel, or voxel, rather than extruded filaments, planar sheets, or large moulded blocks.

1.3 Summary of thesis work

In this thesis, the development of a novel method to fabricate multi-material responsive hydrogels utilising patterned droplet networks is outlined. **Chapter 2** describes the use of nanolitre pre-gel droplets to assemble droplet networks, which were photopolymerized to form micron-to-millimetre-scale hydrogel structures able to change shape in response to temperature. **Chapter 3** elaborates the use of this technique to form nanocomposite responsive hydrogels, capable of light-activated shape change, and magnetically controlled movement. The adaptation of the 3D droplet printer to generate responsive hydrogels from picolitre pre-gel droplet networks is then described in **Chapter 4**. Finally, future developments of the technique, and possible applications, are outlined in **Chapter 5**.

2

Templating multi-material responsive hydrogels with droplet networks

This chapter describes the development of a novel method to fabricate patterned and responsive multi-material hydrogel structures using droplet networks. With this method, a variety of 2D and 3D geometries using pre-hydrogel droplets connected by lipid bilayers can be formed. These droplet compartments have been used to pattern the pre-gels, resulting in multi-material hydrogel structures after photopolymerization **(Figure 2.1)**. With the monomer *N*-isopropylacrylamide (NIPAm), multimaterial thermoresponsive poly(*N*-isopropylacrylamide) (PNIPAm) hydrogel structures, capable of shape change in an aqueous environment, were fabricated.

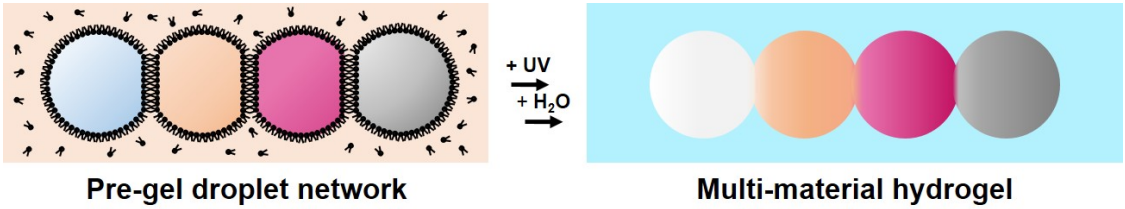

Figure 2.1: Schematic of droplet-network-templated multi-responsive hydrogel structures. Different pre-gels are encapsulated in individual compartments of a droplet network in oil, resulting in a multi-material PNIPAm hydrogel after photopolymerization, which can be transferred into water.

2.1 Introduction

Fabrication methods for responsive hydrogels rely primarily on photolithography[61] and extrusion printing[42], which generate planar structures[42,61]. As a result, examples of patterning have been limited to layering on top of sub-regions of these planar sheets[61], which may restrict the construction of functional devices[2] (see **Section 1.1.6** and **Section 1.2.4**).

Droplet networks allow high resolution patterning of aqueous droplets, which may also contain gelators and biomolecules (see **Section 1.2**). These gelators can form physically crosslinked hydrogels within droplet networks. This has allowed the fabrication of highly patterned, cell-containing microtissues formed from agarose[103] and, in unpublished work from Dr Linna Zhou in the Bayley group, Matrigel®. Droplet interface bilayer (DIB) networks have also been assembled from pre-formed agarose objects[104], and encapsulated within agarose and alginate to improve the mechanical stability of droplets within[101,102]. However, the possible candidate hydrogels for incorporation could be expanded to include chemically crosslinked hydrogels, and furthermore, responsive hydrogels (see **Section 1.1.2** and **Section 1.1.3**). With the latter, the hydrogel becomes a functional component itself, as opposed to simply a scaffold material with embedded functional components. To date, chemically crosslinked hydrogels have only been incorporated into lipid-encapsulated compartments in efforts to improve the robustness of bilayers joining the compartments[105]. In this example, a pre-gel containing a crosslinking monomer, poly(ethylene glycol) dimethacrylate (PEG-DMA), and a free radical photoinitiator, Irgacure 2959, was mixed 1:1 with a solution containing 1 mg mL^{-1} DPhPC vesicles and used to form two neighbouring aqueous droplets in oil. Photopolymerization of these compartments could be performed before or after lipid-in[106] bilayer formation. Finally, although the use of two phases for the polymerization of responsive hydrogels dates initially to the formation of spherical PNIPAm hydrogel droplets in mineral oil[28], no responsive hydrogels have been incorporated into droplet networks as yet.

Consequently, as droplet networks can be patterned, they are a promising means to fabricate multi-material responsive hydrogels. Unlike previous methods (see

Section 1.2.4), each droplet could act as a 3D pixel, or voxel, opening up avenues to create 3D patterned multi-material structures, as opposed to extruded filaments, gel sheets, or large moulded blocks. However, to use droplet networks to form multi-material responsive hydrogels, several requirements would need to be met. Firstly, to allow the formation of aqueous droplets in oil, the pre-gel used would need to be based on water-soluble components. These components would also not destabilise the lipid bilayers, which are crucial for the formation and stability of networks. Additionally, the process of polymerization would need to take place in situ, following droplet network formation. For example, the use of a chemical initiator such as APS and TMEDA would be unsuitable, as gelation would begin before droplet formation, complicating the assembly of networks, particularly if large or patterned. Finally, the chosen method would allow pre-gel formulations to be easily screened, to simplify development. Since droplet networks produced by 3D droplet printers have to date only contained up to 2 different types of droplet (see **Section 1.2.2** and **Section 4.1.2**)[86,87,107], a manual assembly method was chosen. Such methods, which allow networks comprising multiple different droplet types to be easily assembled, include the use of pipettes[84] or Hamilton syringes[87] to produce droplets.

To address these requirements for templating and patterning responsive hydrogels, a Hamilton syringe was initially chosen to form nanolitre aqueous-based pre-gel droplets, before bringing them together to form droplet networks. This would allow screening of pre-gels both as individual droplets, and as droplet networks connected by DIBs. The hydrogel used to develop the technique was PNIPAm, one of the most widely used and well characterised thermoresponsive polymers (see **Section 1.1.3**). PNIPAm undergoes a coil to globule phase transition when heated above its lower critical solution temperature (LCST). When crosslinked into a hydrogel and heated above the LCST, it expels water and contracts. This contraction can be characterised by a shrinkage or swelling ratio. As an example, a shrinkage ratio was obtained by dividing the diameter of a gel disk during contraction by its diameter whilst fully swollen[40]. A second approach defined an areal swelling ratio as the

area of the fully swollen film (and subsequently, during contraction), divided by the area of the film in its dry, as-crosslinked state[41].

A major reason for choosing this polymer was that the characteristics of the phase transition have been tuned in several studies[9,40,41]. This has been done by incorporating additional components, or modifying structural properties of the hydrogel (see **Section 1.1.2** and **Section 1.1.6**). For example, the LCST of PNIPAm can be increased by the addition of hydrophilic co-monomers and crosslinkers[9,41], and the shrinkage ratio can be modified by changing the crosslinking density[41]. Furthermore, the incorporation of nanoparticles into PNIPAm hydrogels allows stimuli other than temperature to be harnessed to induce its volume transition (see **Chapter 3**)[63]. PNIPAm hydrogels are formed from a pre-gel containing the water-soluble monomer, NIPAm, with a crosslinker such as methylene bis(acrylamide) (MBA), which can be photopolymerized under UV light with the use of an appropriate photoinitiator. It was hypothesised that droplets in oil could be formed from an aqueous NIPAm-based pre-gel, and photopolymerized once assembled into the desired droplet network structure.

2.2 Formation of responsive hydrogels from droplet networks

This chapter demonstrates the use of droplet networks as a useful fabrication method for responsive hydrogels. NIPAm pre-gel droplets in oil were assembled into networks, which were subsequently photopolymerized. This resulted in rupture of the bilayers and yielded thermoresponsive PNIPAm hydrogel structures with one, two and three-dimensional geometries, which could be transferred from oil into an aqueous environment. These PNIPAm structures reversibly contracted when heated to 42°C, which is above the LCST of PNIPAm. Furthermore, by encapsulating different NIPAm pre-gels in different lipid-enclosed compartments, multi-material, patterned PNIPAm hydrogel structures were formed. Next, the hydrophilic crosslinker poly(ethylene glycol) diacrylamide (PEGDAAm) was used to produce modified PNIPAm hydrogels. These PEGDAAm-PNIPAm hydrogels showed a PEGDAAm

concentration-dependent increase in LCST, and decreased contraction upon heating above the LCST. By patterning PEGDAAm-PNIPAm in certain droplet-templated domains, multi-material structures were fabricated, which were capable of shape changes beyond isotropic contraction. Due to differential contraction in PNIPAm hydrogel regions compared to PEGDAAm-PNIPAm regions, this allowed us to design structures capable of complex conformational changes such as curling.

2.2.1 Formation of PNIPAm hydrogel droplets

Droplets of a **standard NIPAm pre-gel** containing 1.34 M NIPAm monomer, 13.1 mM methylene bis(acrylamide) crosslinker, and 13.1 mM α-ketoglutaric acid photoinitiator were formed **(Figure 2.2A)** in a **standard lipid-in-oil**, consisting of a 1:1 v/v mixture of hexadecane and silicone oil AR20 in which 1.2 mM 1,2-diphytanoyl-sn-glycero-3-phosphocholine (DPhPC) was dissolved. This pre-gel and lipid-in-oil were used throughout this thesis, unless otherwise stated. All pre-gels used in each Figure are listed in **Table 6.3**. The combination of hexadecane and silicone oil with DPhPC remains widely used for the formation of stable DIBs (see **Section 1.2.1**)[86,87,90,96], and was chosen to facilitate later formation of droplet networks.

Once formed, droplets in oil were isolated in individual wells of a micromachined poly(methyl methacrylate) well array. The well array containing the NIPAm pre-gel droplets was placed in a sealed chamber through which nitrogen was flowed to purge the surrounding environment of oxygen **(Figure 2.3)**. If the chamber was insufficiently purged and there was still oxygen present in the surrounding

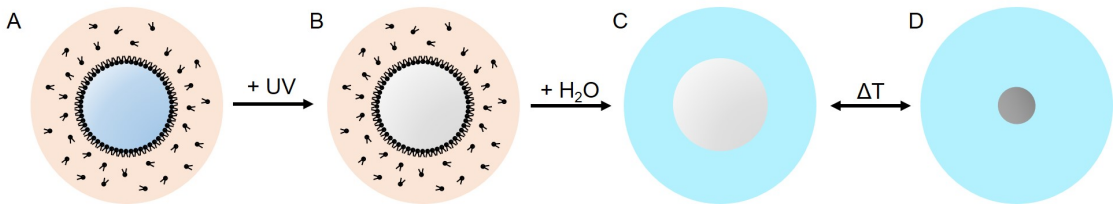

Figure 2.2: Schematic showing **(A)** formation of a single NIPAm pre-gel droplet, before **(B)** its gelation to form a PNIPAm hydrogel droplet, and **(C)** phase transfer into an aqueous environment. **(D)** Reversible heat-induced contraction of the PNIPAm droplet.

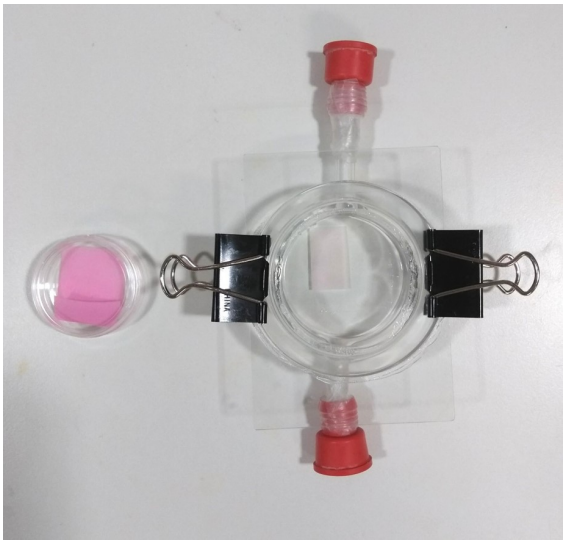

Figure 2.3: Photograph of sealed chamber through with nitrogen was flushed, to create an inert environment during polymerization. Anaerobic indicator strips show the presence of oxygen outside the chamber (pink); and no oxygen, within the chamber after purging for 45 minutes (white).

environment, gelation was inhibited due to termination of propagating chains and quenching of free radicals[22] (see **Section 1.1.2**). However, in the work presented in this thesis, a 45 minute period of purging was typically sufficient such that when the chamber was irradiated with UV light, hydrogel formation took place via a free radical polymerization **(Figure 2.2A-B, 2.4)**. UV irradiation was typically performed for 30 minutes, although this could be reduced to 1 minute without affecting gelation. As the free radical polymerization is exothermic[108], during photopolymerization, the temperature may be expected to increase, possibly above the LCST of PNIPAm. However, it is unknown what possible effect this may have on the resulting structure and ultimately, its overall properties.

Successfully polymerized PNIPAm hydrogel droplets **(Figure 2.5A)** were able to reversibly contract upon heating above the LCST of PNIPAm, reported in the literature to lie between 30 and 35°C[35] (see **Section 1.1.3**). Henceforth, unless otherwise stated, the structures fabricated in this thesis were heated to 42°C, which was above the reported LCST. Similarly, heating was performed on a heat plate, and the assumed temperature was the temperature given on the sensor of the heat plate. After heating a PNIPAm droplet above the LCST, the hydrogel matrix uniformly

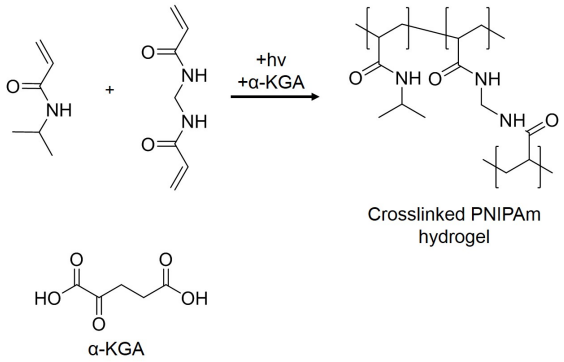

Figure 2.4: Scheme depicting photopolymerization of NIPAm and MBA, using α-KGA as the photoinitiator. Illumination with UV light initiates formation of a crosslinked PNIPAm hydrogel.

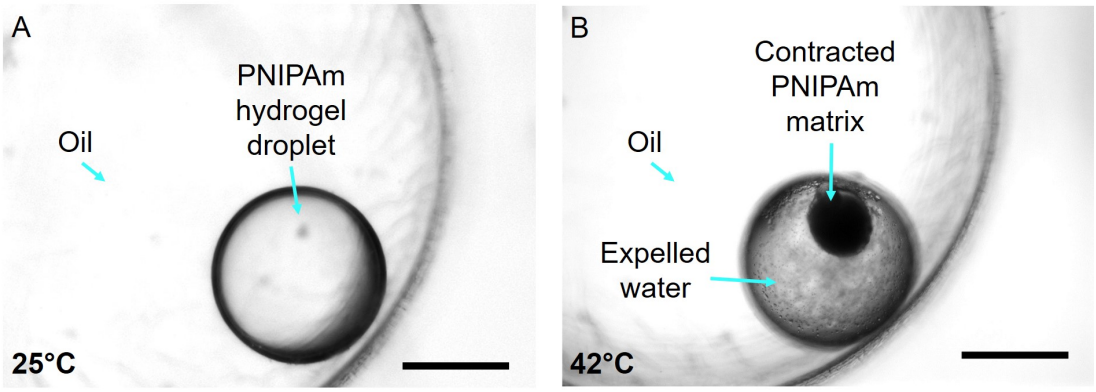

Figure 2.5: Brightfield microscopy images of contraction of a PNIPAm hydrogel droplet in oil **(A)** before and **(B)** after heating to 42°C, with water expelled as a single droplet from the contracted PNIPAm matrix. Scale bars, 250 µm. See **Section 6.4.7**.

contracted, expelling water **(Figure 2.5)**. This mostly happened in the form of a large single droplet, within which would be the collapsed PNIPAm hydrogel matrix. Interestingly, water could also be expelled from the hydrogel matrix in multiple smaller droplets **(Figure 2.6)**. In either case, the contracted hydrogel droplet was visible as a spherical object with a different refractive index from expelled water. Once cooled below the LCST to room temperature, the PNIPAm droplets re-swelled by taking up the previously expelled water.

These hydrogel droplets could be transferred, using the capillary action of a gel loading tip, into an aqueous environment, where they swelled **(Figure 2.2C)**. Once fully swollen in water, the individual PNIPAm droplets became transparent and were difficult to see. To aid visualisation in water, 0.1 mM of the fluorescent crosslinker

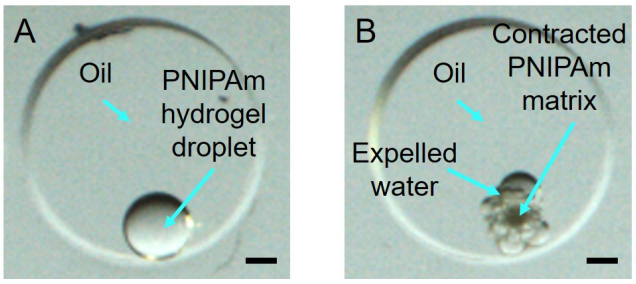

Figure 2.6: Brightfield microscopy images of contraction of a PNIPAm hydrogel droplet in oil **(A)** before and **(B)** after heating to 42°C, with water expelled as multiple smaller droplets from the contracted PNIPAm matrix. Scale bars, 250 µm.

ethidium bromide bis(acrylamide) (EBBA), was additionally incorporated to the **standard NIPAm pre-gel**. The location of the droplets was then more easily identified using fluorescence microscopy **(Figure 2.7A)**. Droplets were also imaged using the brightfield phase contrast mode. As in oil, when heated above the LCST, the PNIPAm droplets uniformly contracted **(Figure 2.2D, Figure 2.7)**, and reswelled once cooled below the LCST. A MATLAB script was written to extract the radii of the droplets from a timelapse of the images during contraction and reswelling **(Figure 2.8, Methods 6.5.7)**. No significant difference was observed in the rate of contraction of the individual droplets. The kinetics of this process have been shown to be limited by the rate at which water can diffuse in and out of the polymeric network (see **Section 1.1.3**)[16,48]. It is noted that since the response rate is inversely proportional to the square of the smallest linear dimension of a gel[17,45,47,109], it is expected that larger PNIPAm gels will contract and reswell at a slower rate than smaller PNIPAm gels.

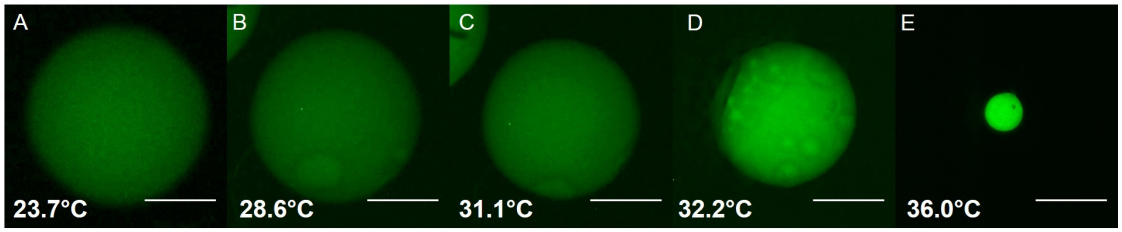

Figure 2.7: (A-E) Fluorescence microscopy images of an EBBA-PNIPAm droplet contracting in water as it is heated above the LCST. Scale bars, 250 µm. See **Section 6.5.10**.

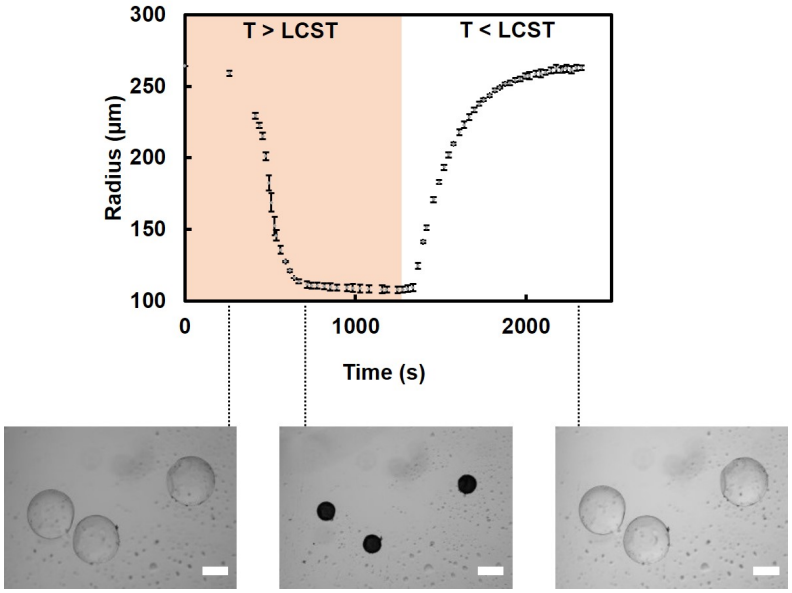

Figure 2.8: Radii of individual, non-connected PNIPAm droplets during contraction, whilst heating to 42°C, and reswelling, whilst cooling to room temperature. Data were extracted from brightfield microscopy images (examples shown below graph). Scale bars, 250 µm. Error bars represent one standard deviation about the mean radius. See **Section 6.5.7** and **Section 6.5.13**.

Due to the contraction in volume of the EBBA-PNIPAm droplets, the brightness of the droplets increased during heating. It was hypothesised that this could be a result of the increase in density of fluorescent ethidium bromide moieties as the droplets contracted (see **Section 2.2.5** for detailed discussion). This increase in the functional density of chemical moieties in a hydrogel, as a result of the volume transition, has previously been used to reveal a message written in a fluorescent monomer, methacryloxyethyl thiocarbamoyl rhodamine B[7]. Additionally, it has been proposed that the enhanced fluorescence of ethidium bromide whilst bound to nucleic acid is a result of a reduction in quenching by water molecules[110].

2.2.2 Formation of continuous hydrogel structures across droplet interface bilayers

Since individual NIPAm pre-gel droplets could be polymerized in oil, to then form higher order structures it was first necessary to ensure stable lipid bilayers could be formed between droplets. This would enable the formation of pre-gel droplet

networks. Once polymerized, the droplets would also need to be connected to one another to achieve a shape change across the entire structure. Methods to form continuous hydrogel structures from 3D printed hydrogel-containing droplet networks have been developed to allow transfer into water, without disintegration of the structure. In one approach, after initially patterning agarose within 3D printed droplet networks, the physically crosslinked droplets encapsulated within the network were wrapped in a thin coating of agarose to form a continuous structure[103]. In unpublished work from Dr Ravinash Krishna Kumar and Dr Linna Zhou of the Bayley group, gelation of physically crosslinked hydrogels has been shown to take place across the lipid bilayers. Both methods allow the patterned structures to retain designed shapes, although require multiple intermediate steps for the formation of a continuous hydrogel.

Initially, droplet pairs were formed by rolling together two **standard NIPAm pre-gel** droplets individually formed in the same well of a well array **(Figure 2.9A)**. DIBs could be formed by tilting the well array, so the droplets rolled together under the influence of gravity. This method was preferred to pushing the droplets together, which was more likely to result in coalescence of the droplets. Nonetheless, gently pushing a pair of droplets together with a gel-loading pipette tip could facilitate the formation of a bilayer that was reluctant to form. In general, after coming into contact, droplets adhered to one another within 1-3 s as has previously been observed[86], forming a bilayer at their interface **(Figure 2.9B, Figure 2.10A)**. Droplets joined by a DIB are at a thermodynamically unstable local energy minimum[82]. It was therefore important to handle droplets with care during formation, as mechanical force, static shock, extremely imbalanced components, or an overly high ambient temperature were observed to result in coalescence.

Subsequently, gelation was performed via UV irradiation in a chamber purged of oxygen, as for individual droplets. In general, continuous PNIPAm hydrogel structures were formed, which retained the shape of the pre-gel droplet pair after polymerization was complete **(Figure 2.9C, Figure 2.10B)**. Upon heating above the LCST, rather than contracting as two individual droplets, two adjoined hydrogel

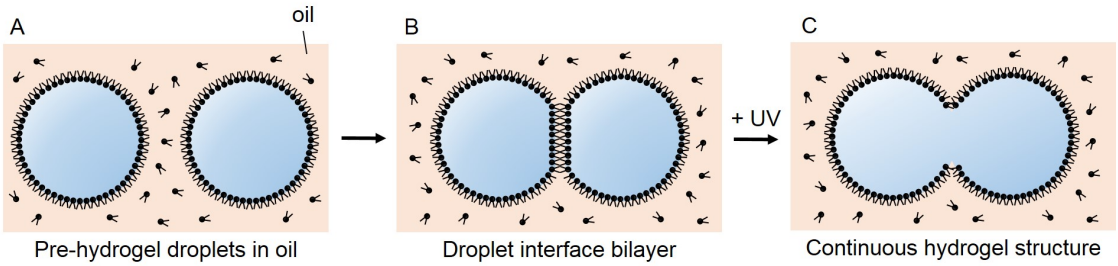

Figure 2.9: Schematic of the fabrication process for a hydrogel structure templated by a droplet pair. **(A)** Pre-gel droplets formed in lipid-in-oil acquire a lipid monolayer coating. **(B)** When the two droplets are brought together, a lipid bilayer forms at the interface between them. **(C)** In situ photopolymerization results in the rupture of the bilayer, and formation of a continuous hydrogel structure.

droplets shrunk as a single structure **(Figure 2.11A-B)**. Infrequently, distinct polymerization of two droplets was also possible, where the polymerization did not occur through the bilayer. This would result in discrete hydrogel droplets still connected by a bilayer. When heated in oil above the LCST, each individually polymerized droplet of the pair contracted as two separate hydrogel droplets, within their own lipid-enclosed compartments **(Figure 2.11C-D)**. Conversely, coalescence could occur during purging. If coalescence occurred towards the beginning of gelation, this would result a single hydrogel droplet, rather than a droplet pair-shaped structure (see **Section 3.3.2**).

To explain this non-intuitive through-bilayer polymerization, it is noted that the monomer and crosslinker are bilayer-permeable[111]. Thus, it was hypothesised that during polymerization, growing polymer chains extend into the bilayer, resulting in its rupture. To confirm rupture of the bilayer, a bilayer-impermeable fluorescent dye, ATTO-488, was added to the **standard NIPAm pre-gel** to a final concentration

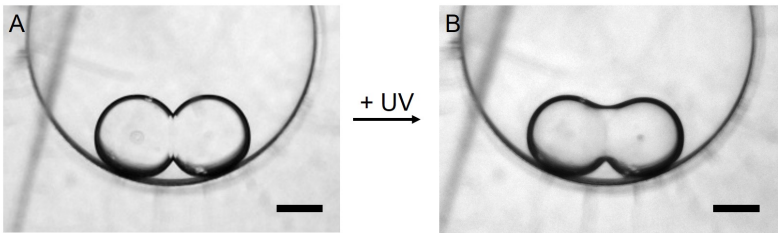

Figure 2.10: Brightfield microscopy images of a droplet pair **(A)** before and **(B)** after gelation. Scale bars, 250 µm. See **Section 6.4.4**.

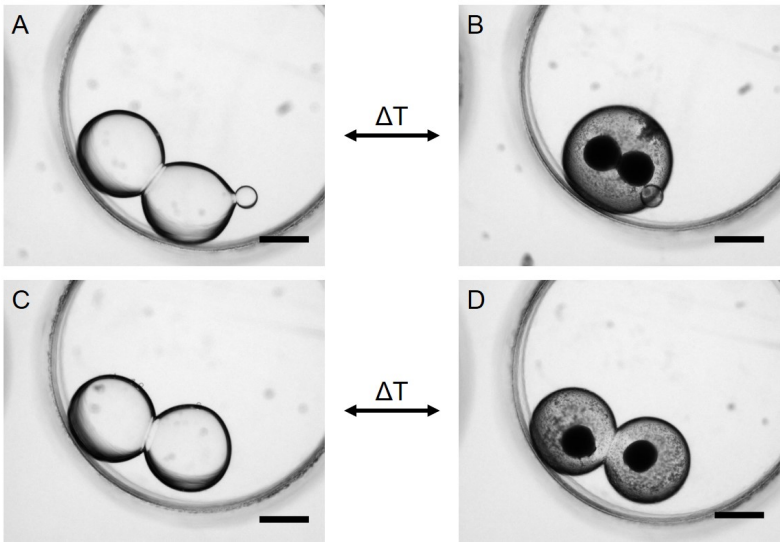

Figure 2.11: Brightfield microscopy images of a droplet pair for which **(A)** through-bilayer polymerization took place, resulting in **(B)** shrinkage as a single structure. **(C)** When polymerization does not proceed across the bilayer, **(D)** the PNIPAm hydrogel droplets contract separately within their own lipid-enclosed compartments. Scale bars, 250 µm. See **Section 6.4.7**.

of 1 µm. This ATTO-488-containing NIPAm was used to form a droplet pair with a **standard NIPAm pre-gel** droplet **(Figure 2.12A)**, in a lipid-in-oil that contained 1.2 mM DPhPC, with 0.01 mol % of a lipid with a fluorescently labelled headgroup, Texas Red®-1,2-dihexadecanoyl-sn-glycero-3-phosphoethanolamine (TR-DHPE). TR-DHPE was used to indicate the presence of lipid at oil-water interfaces and at the bilayer. After polymerization, the ATTO-488 dye had transferred to the region which had originally contained no dye **(Figure 2.12B)**, indicating that the bilayer had ruptured during polymerization.

It was hypothesized that the linkage of each droplet region by PNIPAm chains would facilitate the intact transfer of these structures into an aqueous environment. Furthermore, the physical connection between droplets is essential for cooperative shape change **(Figure 2.11)**. As there were no bilayers left in these polymerized structures, an alternate approach was developed for the phase transfer of these structures, compared to those used for droplet networks (see **Section 1.2.2**), where the bilayers must be kept intact so that the compartments do not fuse. First, the lipid-in-oil was exchanged for a lipid-free oil, to dilute the lipids in the oil, thus

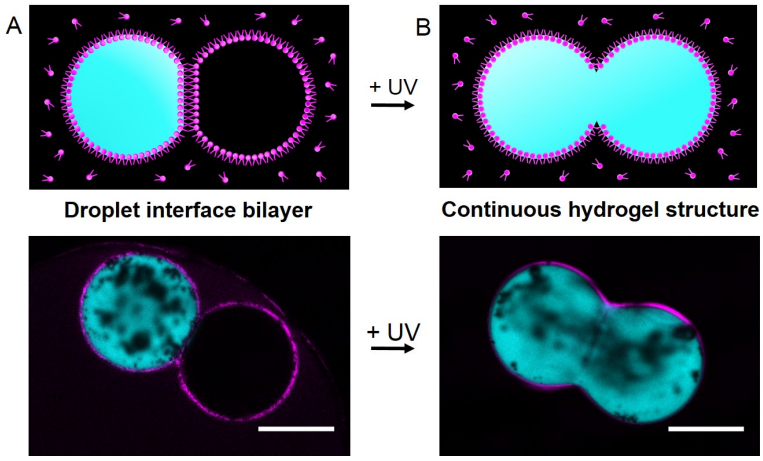

Figure 2.12: Schematic and fluorescence microscopy images of a droplet pair before and after photopolymerization. **(A)** The droplet pair was formed from a NIPAm pre-gel droplet and a NIPAm pre-gel droplet which contained a bilayer-impermeable dye, ATTO-488. The ATTO-488 remained localised in one droplet whilst the bilayer was intact. **(B)** However, following polymerization, the dye diffused into the other droplet, indicating bilayer rupture. Scale bars, 250 µm. See **Section 6.5.2** and **Section 6.5.6**.

preventing the formation of any lipid-enclosed aqueous droplets in downstream steps. Then, the oil was removed and slowly replaced with water. Multiple washing steps were performed to remove as much oil as possible from the surrounding environment. The PNIPAm structures were then transferred by micropipette to a water-containing glass cuvette for imaging **(Figure 2.13A)**, where they swelled. To prevent breakage of polymer chains connecting each droplet region, it was important to handle transfer of these structures with care. As with individual droplets, these droplet network-templated hydrogel structures reversibly contracted upon heating above the LCST in an aqueous environment. This contraction was also uniform, with the shape of the contracted hydrogel resembling that of a droplet pair **(Figure 2.13B)**, as in oil.

2.2.3 Optimisation of the NIPAm pre-gel

Having formed PNIPAm hydrogels from single droplets (see **Section 2.2.1**) and droplet pair-templated structures (see **Section 2.2.2**), it was then important to optimise the amount of contraction the hydrogel exhibited from its fully swollen state, by varying the concentrations of its components. To characterise contraction for PNIPAm hydrogel droplets, the shrinkage ratio was obtained by dividing the

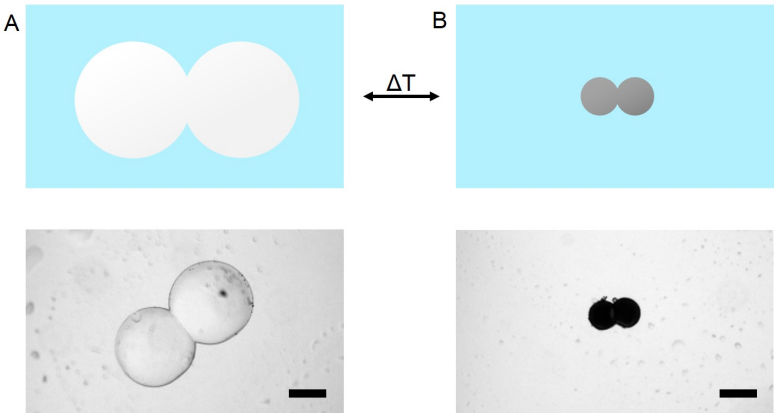

Figure 2.13: Droplet pair-templated structure after **(A)** phase transfer into water and **(B)** heating above the LSCT to 42°C. Scale bars, 250 µm. See **Section 6.4.5**.

radii of a droplet during contraction with its radii whilst fully swollen. The term 'shrinkage ratio'[40] was chosen, rather than 'swelling ratio'[41], as the initial state of the droplets used to determine the ratio in the experiments performed in this thesis was when the droplets were fully swollen in water. Characteristics relating to the phase transition behaviour, such as the shrinkage ratio, affect the eventual shape-change behaviour of PNIPAm structures[40,41] (see **Section 1.1.5**). By varying the monomer, crosslinker and photoinitiator concentrations in the NIPAm pre-gel, a range of shrinkage ratios could be identified.

Effect of NIPAm monomer concentration

For PNIPAm hydrogels, it has been reported that the NIPAm monomer concentration affects the shrinkage ratio[40]. For example, hydrogels polymerized with a low concentration of NIPAm monomer shrink to a greater degree than hydrogels polymerized with a high concentration of NIPAm monomer[40]. To test whether droplet-templated PNIPAm hydrogels would show this expected behaviour, single NIPAm pre-gel droplets were formed, containing different NIPAm concentrations (0.8 - 1.5 M), but constant MBA and α-KGA concentrations (20 mM, 13.1 mM, respectively). It is noted that as the MBA concentration is kept the same, the ratio of crosslinker to monomer is expected to decrease, as is the crosslinking density. These single NIPAm droplets also contained a fluorescent crosslinker,

EBBA, to aid visualisation (see **Section 2.2.1**). It is noted that the incorporation of a fluorescent crosslinker may increase the crosslinking density, but at the low concentration used (0.1 mM), this effect should be negligible. These EBBA-NIPAm pre-gel droplets were formed in oil, photopolymerized and phase transferred into an aqueous environment, as previously described (see **Section 2.2.1**). At least 3 droplets of each NIPAm concentration were imaged in water, before and after heating to 42°C. This experiment, including imaging and droplet radii extraction using the previously described MATLAB script (see **Section 2.2.1**), was performed by Joshua Sauer, a Doctoral Training Centre rotation student at the University of Oxford. The shrinkage ratio was then calculated from the radii of droplets after fully contracting, normalized to their initial radius. Interestingly, the shrinkage ratio was dependent on the concentration of NIPAm **(Figure 2.14A)**, despite the hypothesised decrease in crosslinking density. For 1.5 M, the highest concentration of NIPAm used, the shrinkage ratio was at a maximum of 0.34 ± 0.01. This was the highest concentration used, as the NIPAm and MBA stock solutions were dissolved close to their maximum solubility. It was found that for droplets containing 0.8 M NIPAm, the lowest concentration used, the shrinkage ratio was as low as 0.21 ± 0.01. Below this concentration of NIPAm, single droplets did not form a crosslinked matrix that was stable enough to be transferred into water. Similarly, when a lower concentration (13.1 mM) of crosslinker was used with concentrations below 1 M NIPAm, single droplets did not crosslink. Also, when this concentration of MBA was used with higher concentrations of NIPAm, there was a high variability in shrinkage ratio.

Furthermore, the radius of droplets before heating above the LCST was higher on average for low NIPAm concentration droplets than for high NIPAm concentrations **(Figure 2.14B)**. Since all droplets formed had an initial volume of 50 nL, the degree of swelling upon immersion in water was therefore higher for low NIPAm concentrations than for high NIPAm concentrations. Consequently, the dependence of the shrinkage ratio on NIPAm concentration was more due to differences in the initial amount of swelling, as opposed to the final radius after the droplets

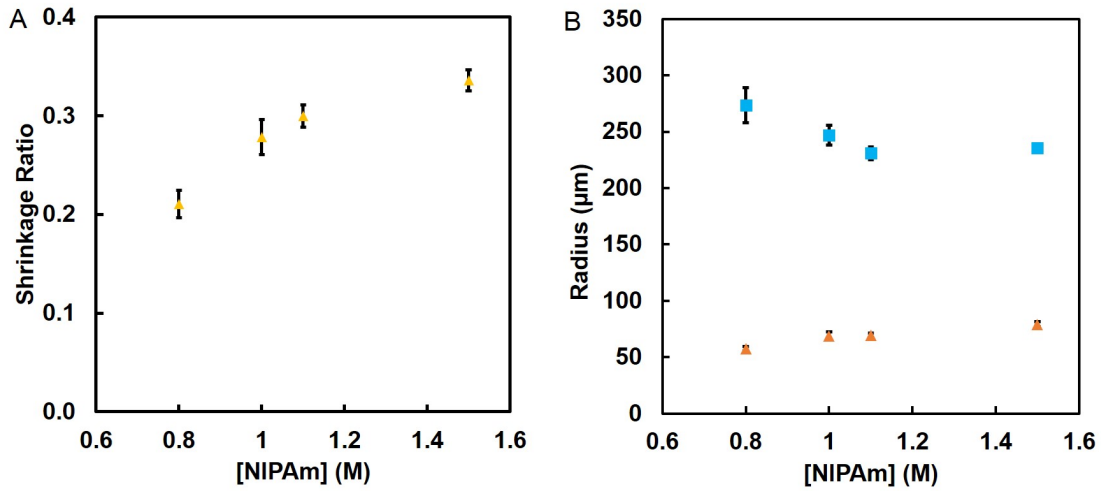

Figure 2.14: **(A)** Shrinkage ratio of EBBA-PNIPAm hydrogel droplets containing different concentrations of NIPAm monomer. Higher concentrations of NIPAm resulted in less shrinkage upon heating. The MBA and α-KGA concentrations were kept constant at 20 mM and 13.1 mM respectively. **(B)** Radii of EBBA-PNIPAm droplets before (blue squares) and after (orange triangles) heating to 42°C. Error bars indicate one standard deviation about the mean shrinkage ratio and radii, respectively. See **Section 6.4.7** and **Section 6.5.13**.

had been heated above the LSCT. Additionally, the variability was higher for the measurements of the radius for lower concentrations of NIPAm, likely a result of the formation of a more loosely crosslinked hydrogel matrix.

Effect of MBA crosslinker concentration

Crosslinking density is also known to affect the swelling of PNIPAm hydrogels[1], and has been modulated throughout gel sheets to produce 2D shape-changing structures[41]. Crosslinking density is dependent on the concentration of crosslinker[1]. To investigate the effect of the crosslinker concentration, and therefore crosslinking density, single NIPAm pre-gel droplets were formed, whilst the concentration of MBA was varied (10 – 25 mM). The concentrations of NIPAm monomer, α-KGA photoinitiator, and EBBA for visualisation, were kept constant (1.34 M and 13.1 mM respectively). These droplets were formed and analysed using the same method as that used to investigate the effect of varying NIPAm concentration. It was found that the shrinkage ratio was also dependent on the MBA concentration **(Figure 2.15A)**. For the lowest concentration of MBA used, the shrinkage ratio was as low

as 0.24 ± 0.04. Conversely, for the highest concentration of MBA used, the shrinkage ratio was at a maximum of 0.35 ± 0.01. As when varying the NIPAm concentration, the radius of the droplets after swelling upon immersion in water was higher for low MBA concentration droplets **(Figure 2.15B)**, suggesting the dependence of the shrinkage ratio on MBA concentration was a result of the initial degree of swelling, as there was little variation in the droplet radii after heating above the LCST. Similarly, the variability was higher for lower MBA concentration droplets, again indicating the formation of a more loosely crosslinked hydrogel matrix.

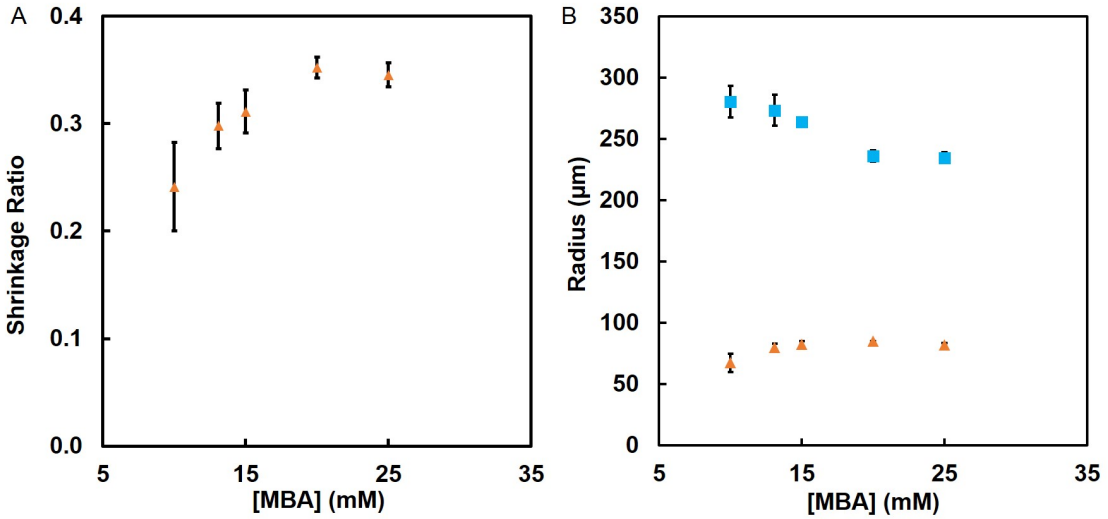

Figure 2.15: **(A)** Shrinkage ratio of EBBA-PNIPAm hydrogel droplets containing different concentrations of MBA crosslinker. Higher concentrations of MBA resulted in less shrinkage upon heating. The NIPAm and α-KGA concentrations were kept constant at 1.34 M and 13.1 mM respectively. **(B)** Radii of EBBA-PNIPAm droplets before (blue squares) and after (orange triangles) heating to 42°C. Error bars indicate one standard deviation about the mean shrinkage ratio and radii, respectively. See **Section 6.4.7** and **Section 6.5.13**.

Effect of α-KGA photoinitiator concentration

The optimal concentration of photoinitiator used for photopolymerization is dependent on the presence of oxygen as well as many other factors (see **Section 1.1.2**), and affects the rate of photopolymerization[23]. This relationship between the polymerization conditions and the optimal photoinitiator concentration is not fully understood[112]. Nevertheless, it was important to use the optimal concentration of

α-KGA photoinitiator, as too low a concentration may result in a poorly polymerized gel droplet. As for NIPAm and MBA variation studies, single PNIPAm droplets were formed, this time varying the α-KGA concentration (10 - 100 mM) whilst keeping the NIPAm and MBA at constant concentrations (1.34 M and 13.1 mM, respectively). These droplets were phase transferred and analysed as previously described. For the concentrations used, there was little dependence of the shrinkage ratio on α-KGA concentration, within error **(Figure 2.16A)**. Similarly, there was no dependence of radius before or after heating on α-KGA concentration **(Figure 2.16B)**.

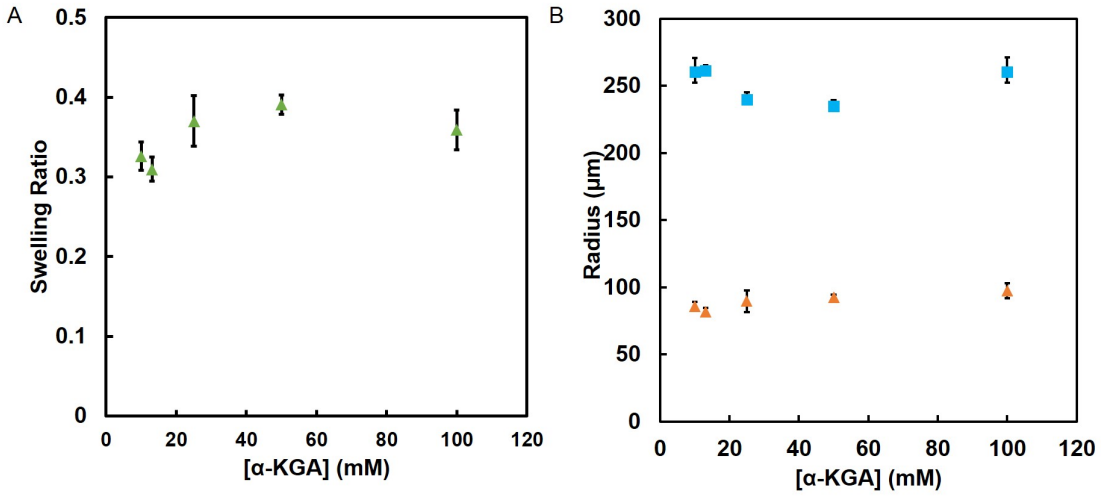

Figure 2.16: **(A)** Shrinkage ratio of EBBA-PNIPAm hydrogel droplets containing different concentrations of α-KGA photoinitiator. The NIPAm and MBA concentrations were kept constant at 1.34 M and 13.1 mM respectively. **(B)** Radii of EBBA-PNIPAm droplets before (blue squares) and after (orange triangles) heating to 42°C. Error bars indicate one standard deviation about the mean shrinkage ratio and radii, respectively. See **Section 6.4.7** and **Section 6.5.13**.

For further experiments, unless otherwise stated, concentrations of NIPAm, MBA and α-KGA chosen were 1.34 M, 13.1 mM and 13.1 mM respectively, which resulted in a shrinkage ratio of 0.31 $\pm$ 0.01.

2.2.4 Templating linear, triangular and pyramidal geometries

To demonstrate the versatility of droplet-templating to fabricate differently shaped responsive hydrogels, small NIPAm pre-gel droplet networks with different geome-

tries were assembled. Unlike previous methods, which produce extruded filaments, gel sheets, or large moulded blocks (see **Section 1.1.6**), droplet networks can be arranged in 3D (see **Section 1.2**)[88], enabling the formation of multi-material structures with 3D patterning. These networks were assembled manually, either by rolling droplets containing the **standard NIPAm pre-gel** into place until they adhered to one another, or by manipulation using a gel-loading pipette tip.

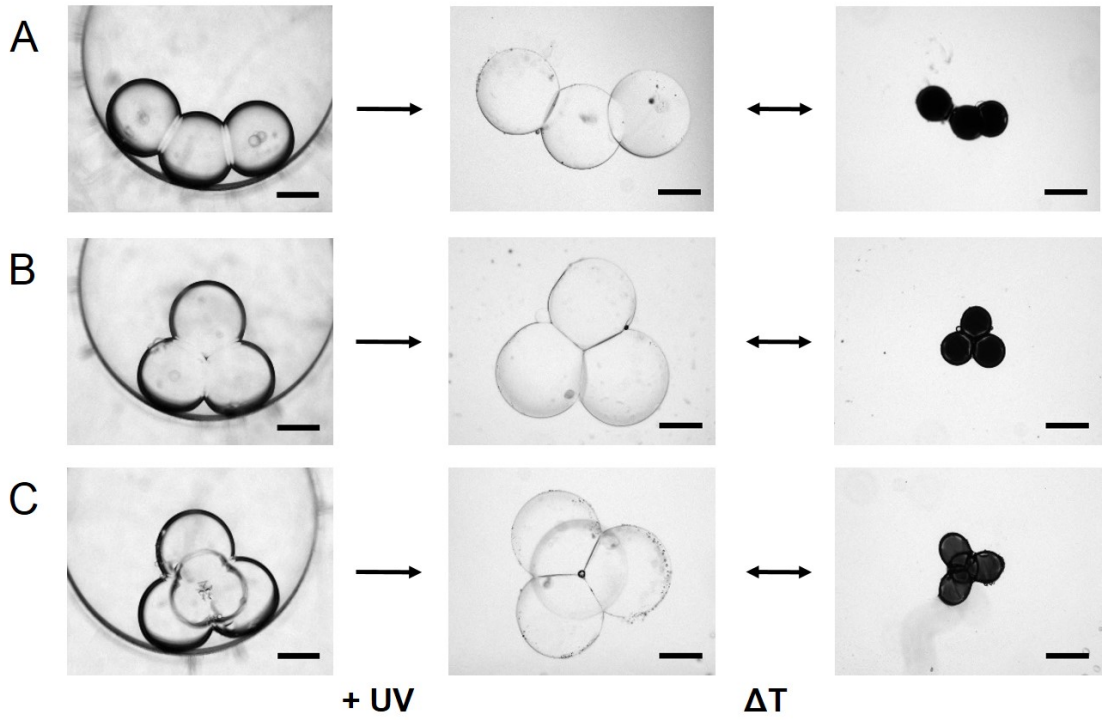

Figure 2.17: (A) Brightfield images of a **standard NIPAm pre-gel** droplet chain in oil, which was photopolymerized to form a continuous hydrogel structure. This was then transferred into water and demonstrated reversible isotropic contraction when heated to 42°C. Triangular **(B)** and pyramidal **(C)** structures were also fabricated and demonstrated similar temperature-controlled contraction. Scale bars, 250 µm. See **Section 6.5.5** and **6.5.8**.

Capillary action could be used to draw a droplet into the narrow end of the tip, and by applying pressure to the wide end of a tip, it could be ejected at a desired location. The **standard lipid-in-oil** was also used to form these structures, for optimal bilayer stability (see **Section 2.2.1**). Due to the fluidity of the DPhPC bilayers, it was possible to move and pull apart bilayers whilst manipulating droplets. For example, by applying a shearing force to the bilayer with the narrow end of a

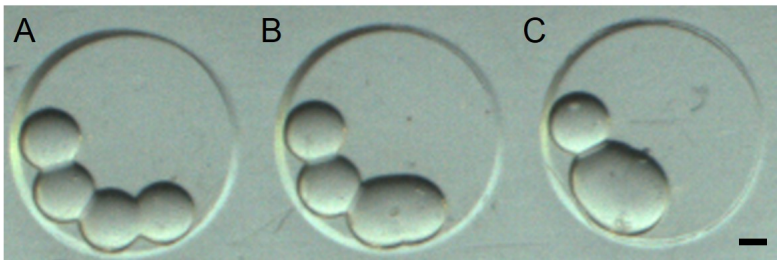

Figure 2.18: Three hydrogel structures formed from the same pre-gel, with simultaneous UV irradiation. **(A)**, successful polymerization. **(B)** Coalescence of two droplets during polymerization. **(C)** Coalescence of three droplets during polymerization. Scale bar, 250 µm.

gel-loading pipette tip, it could be pulled apart. Furthermore, a linear chain of three droplets such as depicted in **Figure 2.17A**, could be transformed into a triangular droplet network such as that depicted in **Figure 2.17B**, by rotating an end droplet around to form a bilayer with the droplet at the opposite end, in addition to its bilayer with the middle droplet. To form the pyramidal structure **(Figure 2.17C**), a triangular structure composed of three droplets was first made. A fourth droplet placed on top of the pyramid using a gel-loading pipette tip formed bilayers with each of the three bottom droplets. These linear, triangular and pyramidal pre-gel droplet networks **(Figure 2.17, left column)** were photopolymerized as before (see **Section 2.2.1**) and subsequently transferred into an aqueous environment **(Figure 2.17, middle column)**. These structures underwent a reversible, isotropic contraction upon heating **(Figure 2.17, right column)**. As observed with the droplet pair (see **Section 2.2.2**), the reversibly shrinking hydrogel structures resembled the initial droplet networks. Coalescence of droplets was detrimental to network formation, as it resulted in malformed structures **(Figure 2.18)**.

It was important to confirm that these droplet network-templated PNIPAm hydrogel structures behaved as expected from literature studies of bulk gels[57] and microgels[28,38], whereby a reversible and reproducible volume transition took place. To do this, brightfield images were taken of water-swollen structures before heating, fully contracted structures after heating above the LCST, and then structures that had fully re-swollen once cooled, comprising one heating and cooling cycle. Heating and cooling cycles with these corresponding images were performed multiple times,

and across different days. The radii of the droplets comprising each structure were extracted using a MATLAB script. The radii of each droplet comprising each structure at each time point during the cycles was analysed to extract the shrinkage ratio. No significant difference was found in the shrinkage ratio at either temperature over each of the heating and cooling cycles **(Figure 2.19)**.

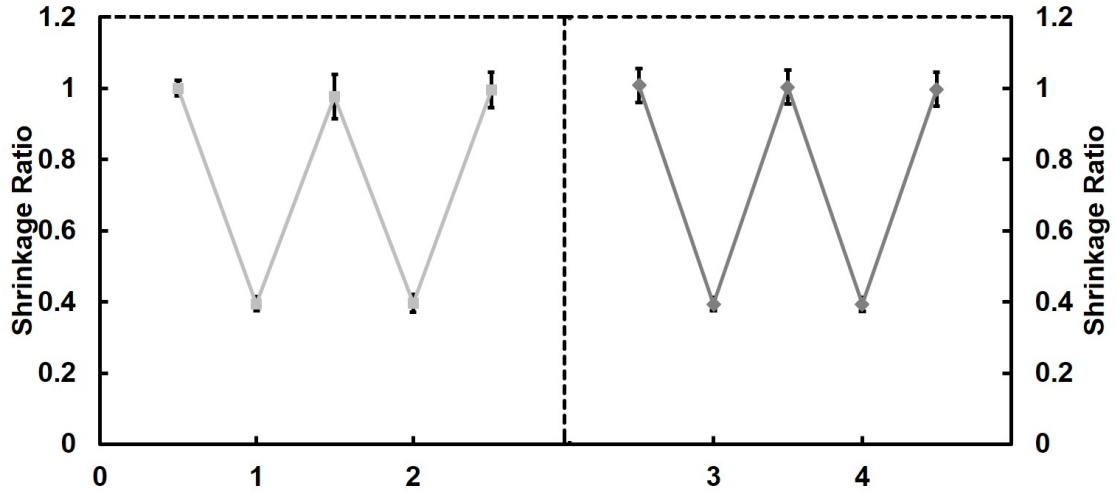

Figure 2.19: Heating and cooling cycles were performed multiple times for the droplet pair-, chain- and triangle-templated structures. At each temperature, the radius of each of the droplets comprising each structure was measured and normalised to its initial radius, resulting in the shrinkage ratio. The break in the x axis indicates that two cycles were performed on each of two different days. Error bars indicated one standard deviation about the mean shrinkage ratio. See **Section 6.5.8**.

2.2.5 Patterning of hydrogel structures

It was hypothesised that encapsulating different bilayer-impermeable pre-gels within each lipid-coated compartment would allow the formation of patterned multimaterial PNIPAm structures. To demonstrate this initially, two NIPAm pre-gel droplet types were used to form 19-droplet hexagonal structures, with and without the fluorescent crosslinker EBBA **(Figure 2.20)**. Both types of droplet contained the concentrations of NIPAm, MBA and α-KGA used in the **standard NIPAm pre-gel**; the fluorescent NIPAm droplets also contained 0.1 mM EBBA, as previously used (see **Section 2.2.1**). The hexagonal droplet networks were assembled from these two droplet types in a PMMA well array containing 2 mm diameter wells

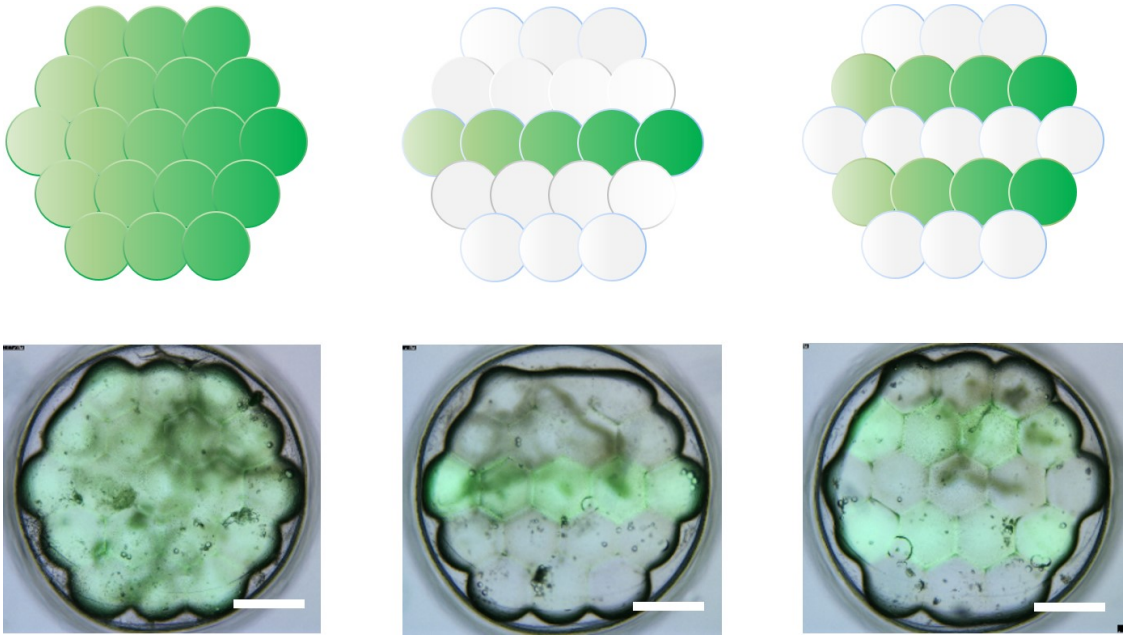

Figure 2.20: Overlaid brightfield and fluorescence microscopy images of hexagonal hydrogel structures patterned with a fluorescent crosslinker. Scale bars, 500 µm. See **Section 6.5.1** and **Section 6.5.5**.

by Dr David Lunn, a postdoctoral researcher in the Bayley group. By completely filling the wells with droplets, hexagonal structures were formed, as the fluid bilayers rearranged for optimal packing of the droplets within the constrained circular wall of the well. EBBA-NIPAm and NIPAm droplets could be positioned such that fluorescent patterns were visible within the hexagon. Gelation was performed as previously described, and resulted in multimaterial hydrogel structures. A variety of patterned multimaterial PNIPAm structures could be made using this technique **(Figure 2.20)**.

Interestingly, upon heating, these structures did not contract as much as expected (see **Section 2.2.3**) **(Figure 2.21)**. To quantify this, a volumetric shrinkage ratio was used. To determine this, first, the image analysis software FIJI was used to measure the area of the structure, and the diameter of a single droplet. The volume was then approximated by multiplying the extracted area by the height of the structure, which was approximated to be roughly equal to the diameter of a single droplet within the structure **(Table 2.1)**, assuming that the surface of the structure was flat. The volumetric shrinkage ratio was also calculated for the single PNIPAm

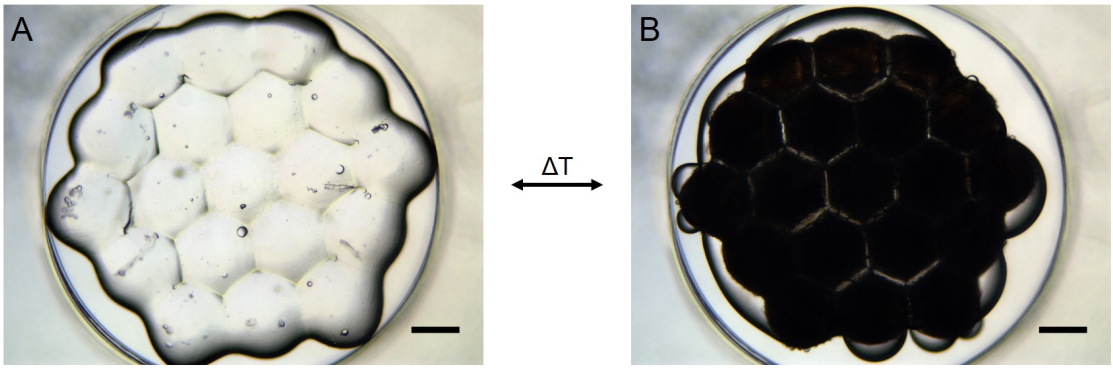

Figure 2.21: Brightfield images of a hexagonal hydrogel structure in oil, **(A)** after gelation and **(B)** after heating to 42°C. Scale bars, 250 µm. See **Section 6.4.7**.

	Swollen structure	Contracted structure
Area	2.7 x 10^6 µm^2	2.1 x 10^6 µm^2
Height	460 µm	415 µm
Volume	1.2 x 10^9 µm^3	8.7 x 10^8 µm^3

Table 2.1: Approximate measurements of swollen and contracted structure in oil (see **Figure 2.21**), with a 1.34 M NIPAm-containing pre-gel.

droplets monitored in **Figure 2.8**, also formed with the **standard NIPAm pre-gel**. This value was calculated from the radius before and after heating, again, assuming that the droplet was spherical. Interestingly, for the hexagonal structure, the volumetric shrinkage ratio was found to be ~0.73, which was significantly higher than ~0.07, the volumetric shrinkage ratio calculated for single droplets (distinct from the shrinkage ratio which was calculated from the radii before and after heating, 0.31 ± 0.01). As discussed in **Section 2.2.1**, larger PNIPAm gels are expected to respond at a slower rate than smaller gels. Accordingly, one possibility is that due to the larger size of this gel compared to a single droplet, it did not reach its fully contracted state within the time frame of the experiment (20 minutes of heating). However, as mentioned in **Section 2.2.1**, response rate is inversely proportional to the square of the smallest linear dimension, which should be the same for the single droplet and the single-droplet-thick hexagonal structure.

Another possibility involves the observation that smaller droplets experience oxygen inhibition to a greater degree (see **Chapter 4**), which may be due to their higher surface-to-volume ratio. Hence, the disparity in volumetric shrinkage ratios

may have been due to the lower surface-to-volume ratio of the hexagonal structures compared to single droplets, causing increased crosslinking in the larger structures. Consequently, the next EBBA-PNIPAm hydrogel structures were made from a pre-gel containing a lower concentration of NIPAm (see **Section 2.2.3**), in order to achieve a lower volumetric shrinkage ratio. These structures were formed with a pre-gel containing 0.72 M NIPAm, with 7.1 mM MBA and 7.1 mM α-KGA **(Figure 2.22A)**, and were photopolymerized to form a continuous hydrogel structure. This low concentration of monomer and crosslinker would not have resulted in successfully crosslinked single 50 nL droplets (see **Section 2.2.3**), confirming the hypothesis of improved crosslinking in these larger hexagonal structures. Upon heating, the structure exhibited an increased fluorescence upon heating, as fluorescent moieties increased in density **(Figure 2.22B)**.

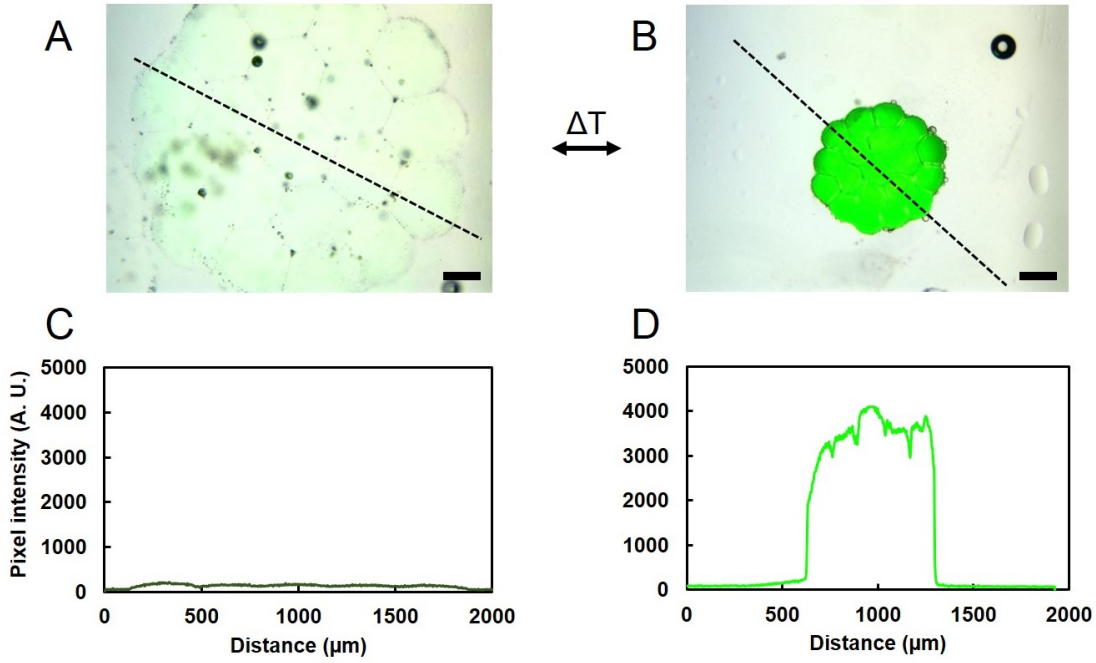

Figure 2.22: Fluorescence microscopy images of hexagonal hydrogel structures patterned with a fluorescent crosslinker **(A)** after phase transfer and **(B)** after heating to 42°C. The corresponding pixel intensity plot profiles (along the black dashed line) are plotted in **(C)** and **(D)** respectively. The fluorescence signal increases upon temperature-induced contraction. Scale bars, 250 μm. See **6.4.7**.

The mean pixel intensity of the structure, calculated using FIJI was found to increase upon contraction of the structure **(Table 2.2)**. However, due to the change

	Swollen structure	Contracted structure
Area	3.1 x 10^6 µm^2	5.4 x 10^5 µm^2
Mean pixel intensity	137	3180
Height	540 µm	230 µm
Volume	1.7 x 10^9 µm^3	1.2 x 10^8 µm^3

Table 2.2: Approximate measurements of swollen and contracted structure in water, with a 0.72 M NIPAm-containing pre-gel.

in opacity of the structure upon contraction, it was likely that transmission of fluorescence through the structure was reduced. A comparison between the fluorescence before and after heating would therefore not be representative. Measurements of the structure's dimensions were also made using FIJI **(Table 2.2)**. From these data, the volumetric shrinkage ratio for this structure was calculated to be ~0.07, which was the same as the previously determined value for a single droplet formed from the **standard NIPAm pre-gel**, ~0.07. This proved a further indication of the problem of oxygen inhibition for smaller PNIPAm structures, compared to larger structures, and will be discussed in detail in **Chapter 4**.

2.3 Modulation of shrinkage in droplet pairs with PEGDAAm

To create non-uniform shape changes in PNIPAm hydrogel structures, it was necessary to modulate their temperature-induced contraction in certain regions. This strategy, where some regions contract to a greater degree than others, has been previously utilised to create complex shape changes for hydrogel sheets (see **Section 1.1.5**). One approach to do this utilises different amounts of crosslinking density in different areas to control the amount of temperature-induced contraction[41]. Initially, droplet pairs were formed containing NIPAm pre-gels with different concentrations of MBA crosslinker in each droplet (see **Section 2.2.3**), to modulate the amount of contraction upon heating above the LCST. Although MBA is bilayer-permeable[111], it was hypothesised that the time taken for its concentration in each droplet to equilibrate would be within the timescale of the experiments. However, after

gelation and heating, rather than differentially contracting, the droplets contracted to the same degree. This indicated that although the pre-gel droplets had originally contained different amounts of MBA, during the time taken to purge the well arrays with N_2 and UV irradiate the droplets, the concentration of MBA had indeed equilibrated.

A second approach was to form an 'inert' droplet type, which incorporated a hydrophilic co-monomer that would increase the LCST of PNIPAm. Hence, when this droplet type was heated to 42°C, it would not contract to the same extent as PNIPAm without the co-monomer. As poly(ethylene glycol) diacrylate (PEGDA) has been used previously to increase the LCST of PNIPAm above physiological temperature, to 42°C[9], it was hypothesised that a similarly hydrophilic, PEG-containing crosslinker, poly(ethylene glycol) diacrylamide (PEGDAAm), could also be used to increase the LCST. A range of concentrations of PEGDAAm (0 – 7 mM) were screened, which were used in addition to MBA (13.1 mM), with the same concentrations of NIPAm and α-KGA as previously used (1.34 M and 13.1 mM, respectively). The EBBA fluorescent crosslinker was also incorporated (0.1 mM) to aid visualisation. These PEGDAAm-EBBA-NIPAm pre-gel droplets were formed in oil and photopolymerized as for PNIPAm droplets (see **Section 2.2.1**). These droplets were transferred into 200 µL of water and imaged at different temperatures. The temperature was measured in parallel using a probe, in a 200 µL volume of water which was simultaneously being heated with the plate and did not contain a sample. The droplets were imaged, and their shrinkage ratios were calculated as previously described (see **Section 2.2.3**) at temperatures between 24.2°C and 57.8°C **(Figure 2.23)**. As expected, for hydrogel droplets containing no PEGDAAm, a sharp transition in the shrinkage ratio was observed above 32°C. This behaviour was also observed for hydrogel droplets containing a low concentration of 1 mM PEGDAAm. However, this transition became more continuous rather than sharp for intermediate and higher concentrations of PEGDAAm.

Due to this more continuous transition, at 36°C, a temperature just above the literature value of the PNIPAm LCST (see **Section 1.1.3**), the shrinkage ratio

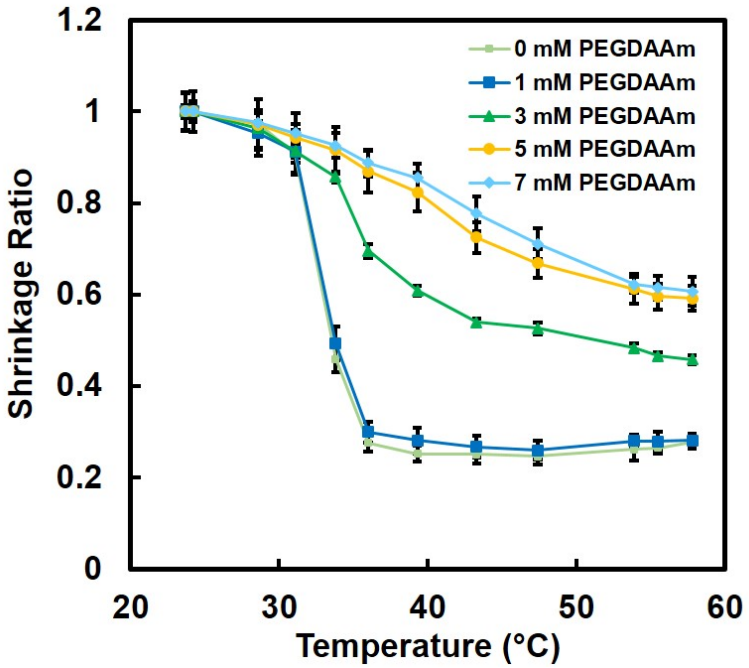

Figure 2.23: Temperature dependence of the shrinkage ratio of PEGDAAm-PNIPAm droplets with different concentrations of PEGDAAm. For all concentrations, the mean radius of at least 3 droplets was taken. Error bars indicate one standard deviation about the mean radius. See **Section 6.5.3** and **Section 6.5.10**.

of the maximum concentration of PEGDAAm used, 7 mM, was 0.89 ± 0.03. At this temperature, the PNIPAm droplets without PEGDAAm had already almost completely contracted, with a shrinkage ratio of 0.28 ± 0.02. At the highest temperature (57.8°C), for the highest concentration of PEGDAAm (7 mM) the shrinkage ratio decreased further from its value at 36°C, to 0.61 ± 0.03. However, at a PEGDAAm concentration of 1 mM, the final shrinkage ratio, at 0.28 ± 0.01, was the same as that of PNIPAm with no PEGDAAm, and had not decreased further.

Importantly, it was necessary to establish whether PEGDAAm could be encapsulated inside a single droplet in a droplet network and not diffuse across the bilayer, and therefore be used to increase the LCST only in a particular region. Due to the hydrophilicity and size of the molecule, it was expected that it would be bilayer-impermeable. As a result, only the droplet in which PEGDAAm was originally incorporated would remain 'inert' at the chosen temperature. A droplet pair comprising one NIPAm droplet and one PEGDAAm-NIPAm droplet were photopolymerized, with a PEGDAAm concentration of 8 mM. Both droplets had

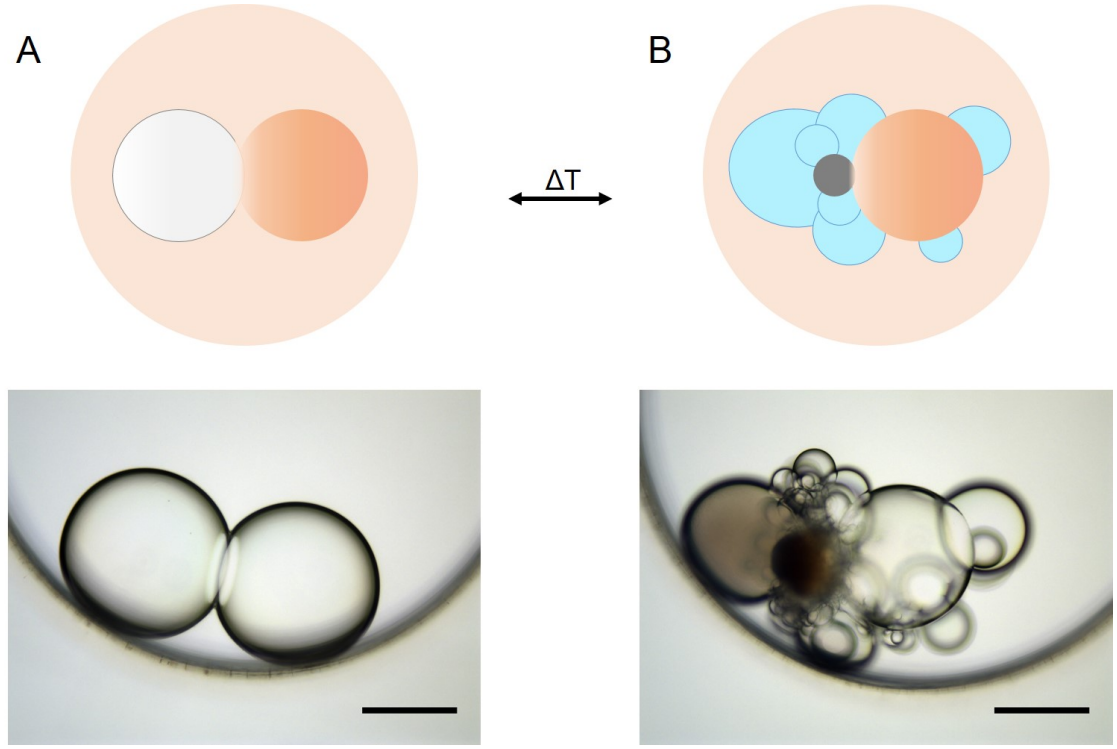

Figure 2.24: (A) A droplet-templated hydrogel structure composed of PNIPAm and PEGDAAm-PNIPAm. **(B)** Upon heating, the PEGDAAm-PNIPAm region contracts to a lesser degree than the PNIPAm region. Scale bars, 250 µm. See **Section 6.5.11**.

a NIPAm concentration of 1.34 M, and MBA and α-KGA concentrations of 13.1 mM. After gelation, this hydrogel structure was heated to 42°C. In this case, the temperature was taken to be the value given by the plate sensor, rather than measuring the temperature of the oil with the probe. Crucially, the PNIPAm region contracted to a greater degree than the PEGDAAm-PNIPAm region **(Figure 2.24)**.

Next, the hydrogel structure was transferred into an aqueous environment **(Figure 2.25)**. Again, the plate was heated to 42°C, although as the heat capacity of water is lower than that of oil, it is likely that the actual temperature of the hydrogel structure is lower. Nonetheless, the PEGDAAm-PNIPAm region again contracted to a lesser degree than the PNIPAm region. This confirmed that the PEGDAAm crosslinker did not cross the bilayer, and could be used to create differential contraction in higher order structures.

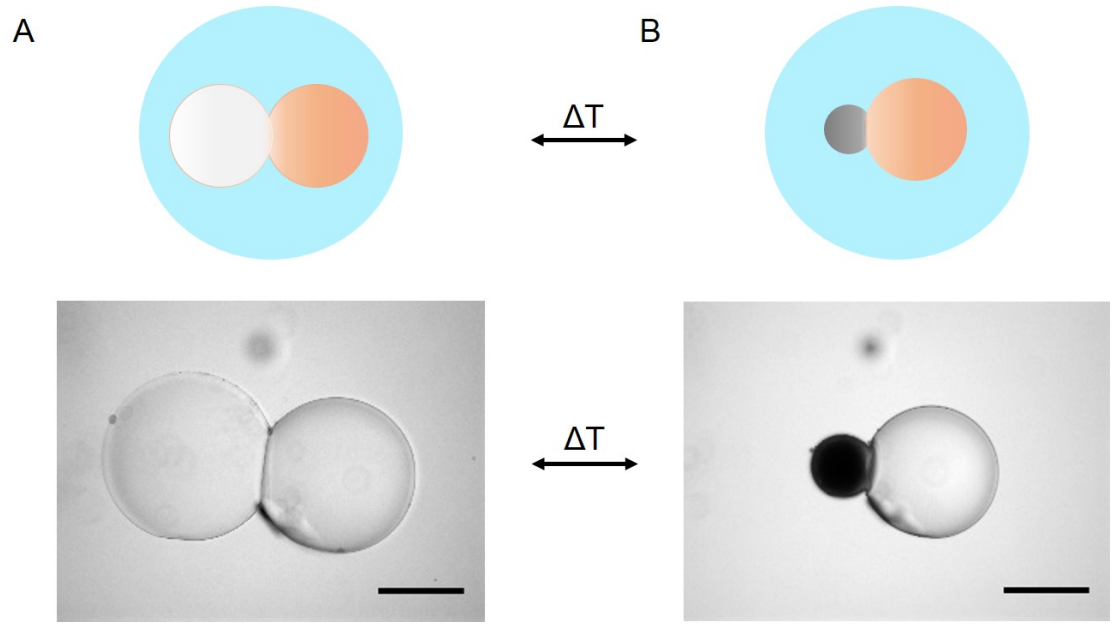

Figure 2.25: A droplet templated hydrogel structure composed of PNIPAm (white circle) and PEGDAAm-NIPAm (orange circle). When heated, the PEGDAAm-PNIPAm contracts to a lesser degree than the PNIPAm droplet (dark grey circle). Scale bars, 250 µm.

2.4 Self-folding structures

To create structures able to undergo more complex temperature-induced conformational changes than with two droplets (see **Section 2.3**), larger droplet networks were assembled from up to 39 droplets and photopolymerized, to form patterned, multimaterial hydrogels. The pre-gels used for these experiments were a PEGDAAm-NIPAm pre-gel (the **standard NIPAm pre-gel**, with an additional 8 mM PEGDAAM), and the **standard NIPAm pre-gel**. These droplet networks were formed in a PMMA well array with square wells of side length 8 mm. Each droplet was rolled to the bottom edge, which was flat, therefore enabling the formation of linear assemblies of droplets. Upon encountering a droplet on either side, it would adhere to them and form a bilayer within 1-3 s. A parallel double strip composed of 29 droplets was formed, from a chain of PEGDAAm-NIPAm droplets and a chain of NIPAm droplets adhered to one another **(Figure 2.26A)**. The droplet network was kept in place against the bottom edge of the well array, which was tilted at the opposite end. This ensured that there was no rotation

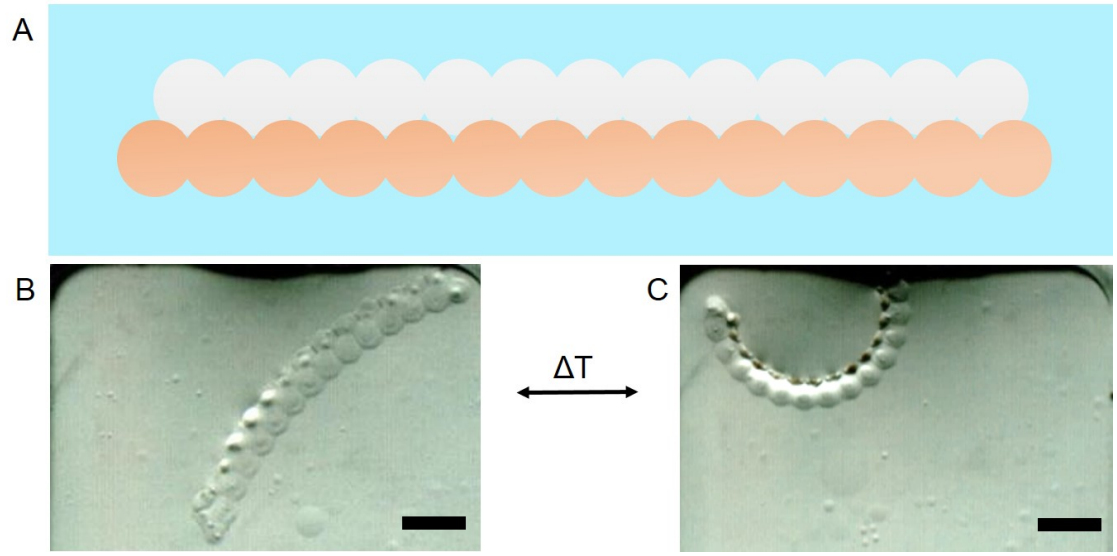

Figure 2.26: Reversible curling of a PEGDAAm-PNIPAm/PNIPAm structure formed from NIPAm (grey droplets) and PEGDAAm-NIPAm (orange droplets). Scale bars, 1 mm. See **Section 6.4.5**, **Section 6.5.5** and **Section 6.5.11**.

or other movements of the constituent droplets.

Following gelation and transfer to an aqueous environment **(Figure 2.26B)**, this structure showed an intrinsic curvature, as the PNIPAm region swelled more in water. This appeared to be due to a slight increase in volume of the PNIPAm-only hydrogel region compared to the PEGDAAm-PNIPAm region. The addition of PEGDA as a co-monomer has been used to reduce swelling of a PNIPAm-based hydrogel upon immersion in water after formation[9]. Thus, it was hypothesised that the volume change observed, and resulting curvature, was due to a difference in swelling between the two types of hydrogel as water moved throughout the entire hydrogel structure. Upon heating to 42°C, the structure underwent a reversible curling motion, as the PEGDAAm-PNIPAm region contracted to a lesser degree than the PNIPAm region **(Figure 2.26C)**.

Following the formation of the single curling structure, a more complex double curling structure was fabricated. This was formed from two parallel chains of droplets, in which each chain was made up from half PEGDAAm-NIPAm droplets and from half NIPAm droplets **(Figure 2.27A)**. Following gelation and transfer to an aqueous environment **(Figure 2.27B)**, this structure underwent a reversible

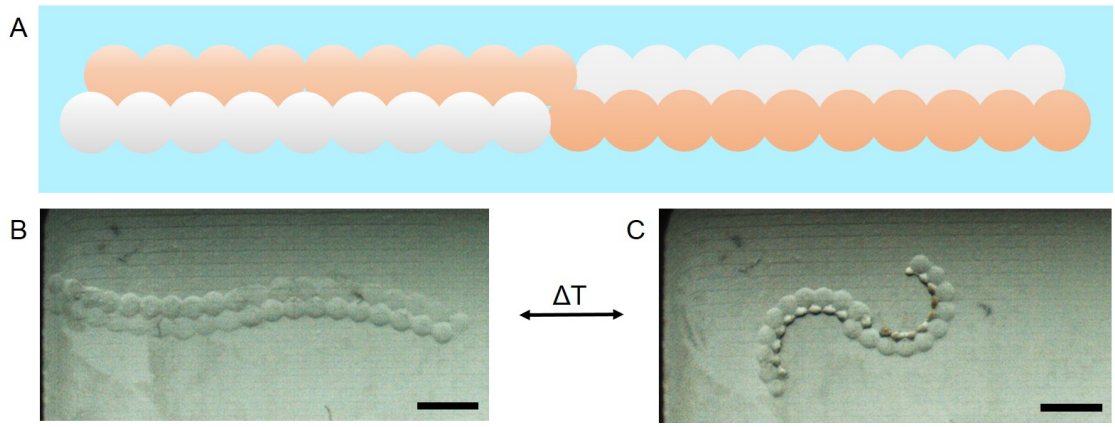

Figure 2.27: Reversible curling of a PEGDAAm-PNIPAm/PNIPAm structure formed from PNIPAm (grey droplets) and PEGDAAm-PNIPAm (orange droplets). Scale bars, 1 mm.

double curling motion upon heating above the LCST, as the PEGDAAm-PNIPAm region again contracted to a lesser degree than the PNIPAm region **(Figure 2.27C)**. To quantify the temperature-dependent curvature of this type of structure, a MATLAB script was written, and used to analyse four halves of two different structures (see **Section 6.5.14**). Firstly, points were selected along the PNIPAm domain of the structure, taken at the centre of each droplet-templated section. Then, a circle fitting function was used to estimate the radius of curvature (R), with which the curvature ($\frac{1}{R}$) could be determined. Again, due to the difference in swelling of the two types of hydrogel, at room temperature, there was a slight intrinsic negative curvature **(Figure 2.28)**. This changed to a high positive curvature upon heating above the LCST, and returned to the slight negative curvature after heating.

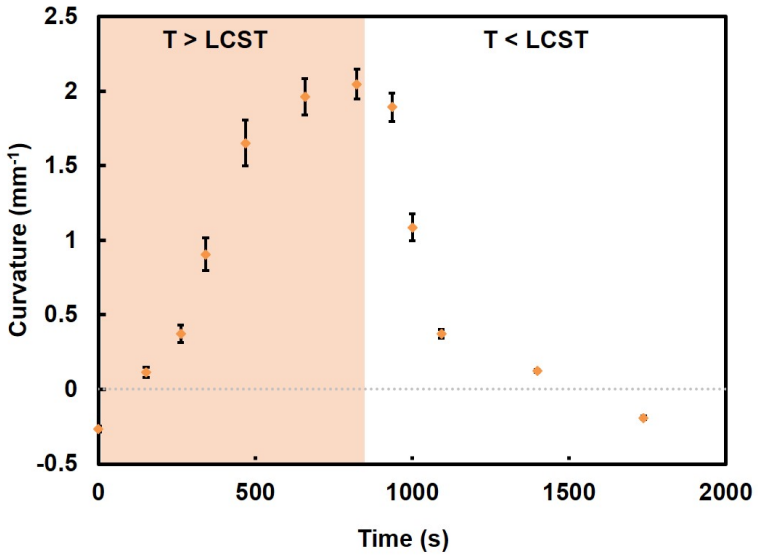

Figure 2.28: Kinetics of curvature of three **Figure 2.27**-type structures during heating (pale orange) and cooling (white). Error bars represent one standard deviation about the mean curvature. See **Section 6.5.14**.

2.5 Conclusion

This chapter has described the development of a novel method to fabricate multi-material responsive hydrogel structures templated by droplet networks. Droplet networks with one-, two- and three-dimensional geometries were used to template PNIPAm hydrogel structures capable of reversible temperature-induced contraction. When the bilayer-impermeable hydrophilic crosslinker, PEGDAAm, was encapsulated in different compartments, patterned, multi-material PNIPAm hydrogel structures were formed. These patterned, multi-material hydrogel structures underwent pre-programmed, temperature-induced curling.

3

Incorporation of functional additives into droplet-templated hydrogels

This chapter outlines the incorporation of functional components into the droplet-templated PNIPAm hydrogels whose fabrication was described in **Chapter 2**. These components add additional functionality, including control of shape change using light and magnetic control of movement. To achieve this, it was important to further optimise the previously developed method of droplet-templating hydrogels with respect to these additional components. Firstly, for shape control by light, the fabrication method needed to be made compatible with the addition of gold nanoparticles. This would allow us to fabricate multi-responsive hydrogels, capable of two types of shape change, as a result of heating or illumination. Secondly, for magnetic control of movement, the method had to be made compatible with the addition of magnetic beads. By also utilising a mechanism for dual temperature control, this would allow the fabrication of a magnetically controlled gripper-like device.

Acknowledgement of collaboration

Unless otherwise stated in the text, all work in this chapter was performed by the author. The practical and intellectual input of Dr David Lunn is acknowledged. Initial syntheses and optimisation studies for the use of gold nanoparticles were

performed by Dr David Lunn, with help from George Klemperer (a Doctoral Training Centre rotation student at the University of Oxford).

3.1 Introduction

Incorporation of additives such as nanoparticles to responsive hydrogels can result in composite materials with novel functionality or improved properties, such as enhanced mechanical performance (see **Section 1.1.4**). Such functional additives have been shown to respond to different wavelengths of light[55], magnetic fields[9] or a chemical stimulus[113]. These added stimuli-responsive properties may then facilitate a means for the composite hydrogel to change shape, or add the ability for locomotion.

3.1.1 Shape change in composite hydrogels

Responsive hydrogels can be prepared with incorporated additives that allow stimulation via secondary mechanisms. Frequently, for thermoresponsive hydrogels such as PNIPAm, this is realised by photothermal heating[63], both for many types of inorganic nanomaterials or for photosensitive moieties such as chromophores[56,114]. Such materials are able to absorb light and re-emit it as heat, causing a thermoresponsive hydrogel to become light-responsive. Shape change can then be initiated remotely and with the high spatiotemporal control offered by light[63]. In contrast to the use of temperature, which requires the entire surrounding environment to be heated, focused light can allow photothermal activation of regions with a diameter of tens of microns. To augment pre-existing shape change capabilities of stimuli-responsive hydrogels, such as PNIPAm, functional materials such as magnetic nanoparticles[115], graphene-based nanomaterials[73] and gold nanoparticles (AuNPs)[54,55] have been incorporated into hydrogels.

Plasmonic nanoparticles are widely used for the photothermal heating of thermoresponsive hydrogels. Plasmons are the quantised collective oscillations of free electrons in metals[116]. These free electrons can be described in the form of a cloud, analogous to a plasma, whose oscillations occur about a lattice of positive ions[116]. At the surface of a metal, there exist certain modes of these plasmons, known

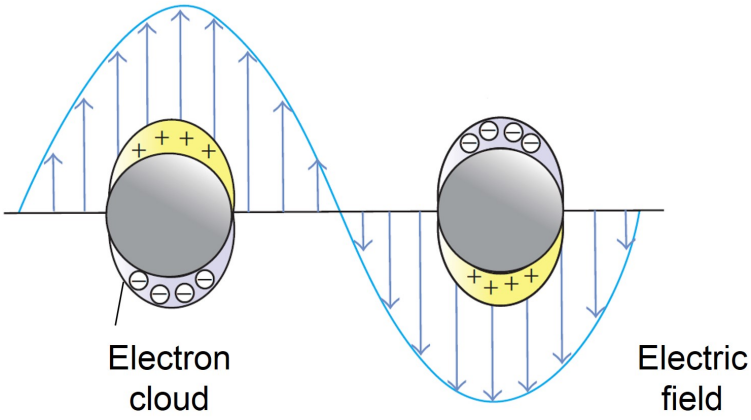

Figure 3.1: Schematic of surface plasmons, the oscillations of the free electron cloud at the surface of a metallic nanoparticle. Reproduced from Zielinska-Jurek et al.[119] Exciting the plasmons at their resonant frequency results in surface plasmon resonance.

as surface plasmons, which can be excited by electromagnetic radiation, resulting in displacements of the cloud from equilibrium[116]. For plasmonic nanoparticles, these surface plasmons can only be excited by electromagnetic radiation whose frequency is in resonance with the oscillation frequency[116] **(Figure 3.1)**. In the extinction spectra of a nanoparticle dispersion, peaks appear in regions where incident light is able to excite the surface plasmons, due to resonance[117]. This phenomenon is known as surface plasmon resonance (SPR). The excitation resulting from SPR is efficiently and rapidly converted into heat[118], resulting in a local temperature increase. Consequently, the advantage of using plasmonic heating to drive shape change in thermoresponsive hydrogels lies not only in its precision, and the possibility of remote activation, but also the increase in speed, e.g. from minutes[48] to seconds[54] for hydrogel sheets.

Furthermore, numerous shape changes can be realised from the same structure, depending on which regions are photothermally activated. For instance, multiple arbitrary deformations could be generated from poly(*N*-isopropylacrylamide-co-acrylic acid) hydrogel sheets with incorporated AuNPs by patterning the light source to illuminate defined regions[54] **(Figure 3.2)**. Due to the varying properties of the wide range of plasmonic nanoparticles, different wavelengths of light can be used for photoactivation, including within the visible spectrum[54] and near

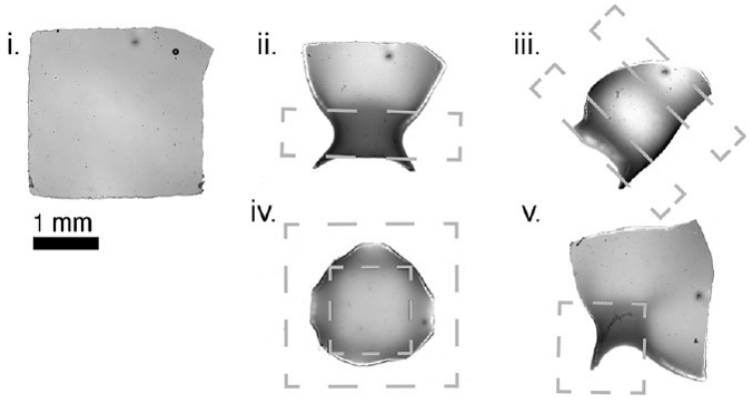

Figure 3.2: Multiple arbitrary deformations of a PNIPAm-based hydrogel sheet containing AuNPs. Reproduced from Hauser et al.[54]

infrared[9,55]. Another advantage of the use of plasmonic nanoparticles is that additional chemical modification of the hydrogel is not required, such as for the incorporation of polymerizable azobenzene moieties[56].

For AuNPs, SPR peaks appear in the visible regime to infrared. The wavelength at which the peak appears is known as the λ_{max}. The intensity, width, location and number of peaks depend on the size and shape of the nanoparticle[117]. As a result, these aspects of the nanoparticle can be tuned, such that the wavelength of light resonant with the SPR peak is compatible with use for living tissue[120]. This, coupled with the precise spatiotemporal control available to light, has allowed mechanical manipulation of single cells, with a gold nanorod-containing PNIPAm hydrogel with embedded microstructures that could be activated by near infrared radiation[55].

3.1.2 Locomotion in composite hydrogels

Since responsive hydrogels lack intrinsic capabilities for locomotion, the incorporation of components allowing movement is essential. For systems ranging from the micron to millimetre scale, different mechanisms are available, whether biological, chemical or physical in nature[121]. Motion may be driven by integration with a motile microorganism, via conversion of chemical fuels in the surrounding environment, as well as remotely via thermal, optical, acoustic or magnetic energy sources[121]. Of these, magnetic control is a particularly attractive option for miniaturised

soft robotic systems, as remote actuation in confined spaces can be achieved[122]. Magnetic control is also highly suitable for in vivo applications as a result of its biocompatibility at clinically usable field strengths[123]. Of the many examples of magnetically directed micro-robotic devices that exist, several have been designed for in vivo applications[67,73,124].

Magnetic locomotion mechanisms range from the simple guiding of a magnetically active structure using an external magnet[67], to the use of sophisticated rotating fields for the oscillation of implanted ferrofluid droplets[125], or biologically inspired flagella-like propulsion[9]. As in the latter example, hinging upon recent advances in magnetic field control[126], rapid shape-shifting structures[122] and soft robots with multimodal gait[127] have been formed. These devices are capable of complex 3D shape changes and multiple types of locomotion, respectively, owing to advanced fabrication approaches integrating programmed magnetization of specific domains[122].

Typically, such materials rely on the incorporation of magnetic nanoparticles[9,122] or microparticles[127]. As with plasmonic nanoparticles, an additional advantage of magnetic nanoparticles or microparticles is that they can also be embedded within, rather than chemically attached to a scaffold material to yield magnetically controllable composite materials.

3.2 Developing patterned multi-responsive hydrogels

As patterning of composite hydrogels has so far been limited to layering of gel sheets using photolithographic methods[9], droplet-templating was a promising means by which to form multi-material, multi-responsive hydrogels incorporating functional components. AuNPs were chosen to achieve light-responsive shape change, as the most widely studied photothermal system[54,55]. For locomotion, magnetic control was chosen, due to the suitability of magnetic fields for control in confined spaces, as well as biocompatibility.

This chapter outlines the incorporation of functional additives into droplet-templated responsive hydrogels. Firstly, the incorporation of AuNPs into PNIPAm

hydrogels (AuNP-PNIPAm) for photothermally controlled shape change is described. This required the synthesis of stable AuNPs that remained photothermally active after gelation, and were also reproducibly usable to induce contraction within the hydrogel structures. Photothermal contraction of the AuNP-PNIPAm structures took place within seconds, and separate domains of the structures could be individually activated. Multi-material structures were also fabricated, comprising AuNP-PNIPAm and PNIPAm domains. These structures could be made to undergo one type of conformational change when irradiated with green light, and another upon heating. 3D patterned structures could also be fabricated, comprising AuNP-PNIPAm, PEGDAAm-PNIPAm, and PNIPAm. Secondly, the incorporation of magnetic beads into PNIPAm structures is described. Magnetic bead-containing PNIPAm could be spatially controlled using a magnetic field. In addition, this magnetically controllable PNIPAm was incorporated into a dual temperature-controlled structure. This structure could be shrunk at 60°C, allowing it to be magnetically moved through channels it was initially too large to traverse, whilst at 35°C, it could be curled in a gripping motion.

3.3 Formation of photothermally controlled PNIPAm hydrogels

For the successful incorporation into PNIPAm hydrogels, AuNPs with a high stability and a good photothermal response when embedded into the hydrogel matrix would be required **(Figure 3.3)**. The AuNPs used would need to be compatible with the polymerization of the PNIPAm hydrogel. For example, they should not hinder polymerization; and still be active after gelation.

3.3.1 Synthesis of stabilised AuNPs

For initial experiments incorporating AuNPs into PNIPAm hydrogels, a synthesis utilising Bunte salts as ligand precursors[128] was performed by George Klemperer. This synthesis is reported to yield nanoparticles around 20 nm in size (hereafter described as Bunte-AuNPs), although with a high polydispersity in diameter. As a

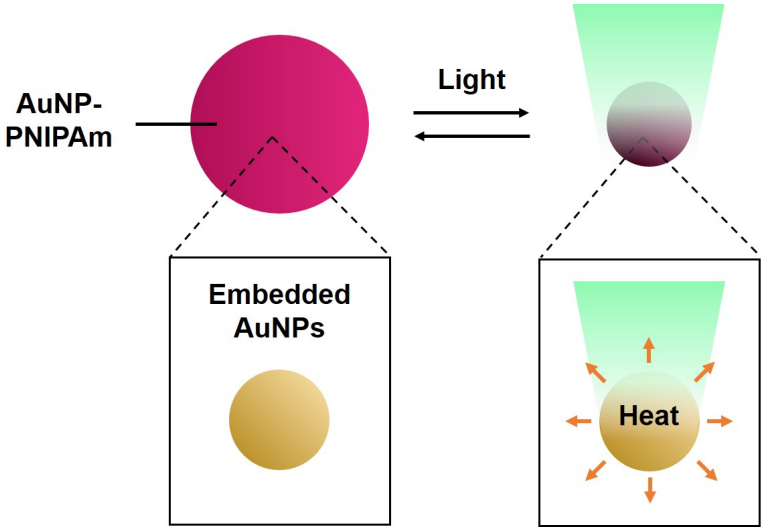

Figure 3.3: Schematic representation of PNIPAm structures containing embedded AuNPs (AuNP-PNIPAm) contracting when illuminated with green light (~λ = 530 nm).

result, smaller nanoparticles can be removed via centrifugation and decanting. After the synthesis was complete, a maroon solution was produced, indicating the presence of nanoparticles greater than 5 nm in diameter. To stabilise the nanoparticles, a poly(ethylene glycol) methyl ether thiol, M_n = 800, (PEG_{800}-SH) was added, before the solution was centrifuged and washed to remove excess PEG_{800}-SH and smaller nanoparticles. Thiol-terminated poly(ethylene glycol) is widely used to stabilise AuNPs due to its solubility in water, and for biomedical applications, biocompatibility and anti-fouling properties[129]. The resulting solution was purple, with a measured λ_{max} of 530 nm.

The incorporation of these nanoparticles into PNIPAm structures was tested by George Klemperer as follows. Initially, a **standard NIPAm pre-gel** was prepared and added to the collected Bunte-AuNPs (final concentration ca. 10 mg mL^{-1}). All pre-gels used in this chapter are listed in **Table 6.4**. The AuNP-NIPAm pre-gel was used to form three-droplet chains and subsequently purged and photopolymerized as previously described. After gelation, the hydrogel structure retained the same 3-droplet chain shape as the AuNP-NIPAm droplet network **(Figure 3.4A)**. The light response was tested with the hydrogel structure kept in oil. Upon illumination of the entire structure with green light, with a λ_{max} of 576 nm, the AuNP-PNIPAm structure was photothermally heated above the LCST. Water was expelled in the

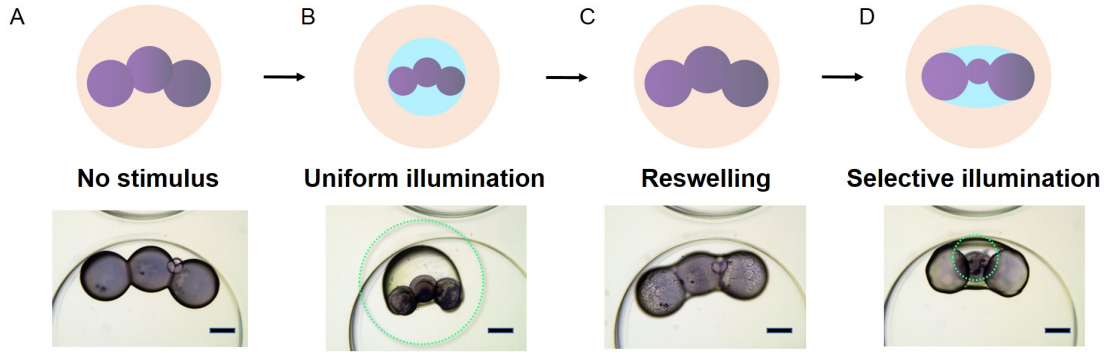

Figure 3.4: Fabrication of AuNP-PNIPAm with Bunte-AuNPs. **(A)** After gelation, the hydrogel structure retained the linear 3-droplet chain of the droplet network. **(B)** Illumination of the entire structure with green light resulted in full contraction. **(C)** The structure reswelled to its original shape, with some evidence of aggregation. **(D)** Selective illumination of a single droplet-region resulted in only that region contracting. Green circle indicates illuminated region. Scale bars, 250 µm. See **Section 6.6.1** and **Section 6.6.9**.

form of a single droplet, and the AuNP-PNIPAm hydrogel contracted into the centre of the droplet **(Figure 3.4B)**. Interestingly, although the hydrogel originally had a smooth, purple appearance, once it had contracted, patterns were visible on its surface, which may have indicated aggregation of the nanoparticles. Similar patterns remained visible as the hydrogel structure was cooled down again and reswelled **(Figure 3.4C)**. By using an aperture diaphragm to restrict the amount of light impinging on the structure, a single droplet-templated region of the structure could be selectively contracted **(Figure 3.4D)**. Similarly, aggregation patterns were visible on the surface of the contracted droplet.

Importantly, repeated illumination attempts yielded a decreased ability of the structure to photothermally contract. Consequently, a different approach was required to afford longer term stability of the AuNPs. The widely utilised citrate reduction procedure was then used for gold nanoparticle synthesis, and was performed by Dr David Lunn based on a conventional protocol[130]. Assuming a complete synthesis reaction due to the excess of reducing agent used, the final concentration of AuNPs in the dispersion was taken to be approximately 0.4 mg mL^{-1}, based on the concentrations of starting material.

UV-vis spectroscopy was performed on the AuNP suspension after dilution to

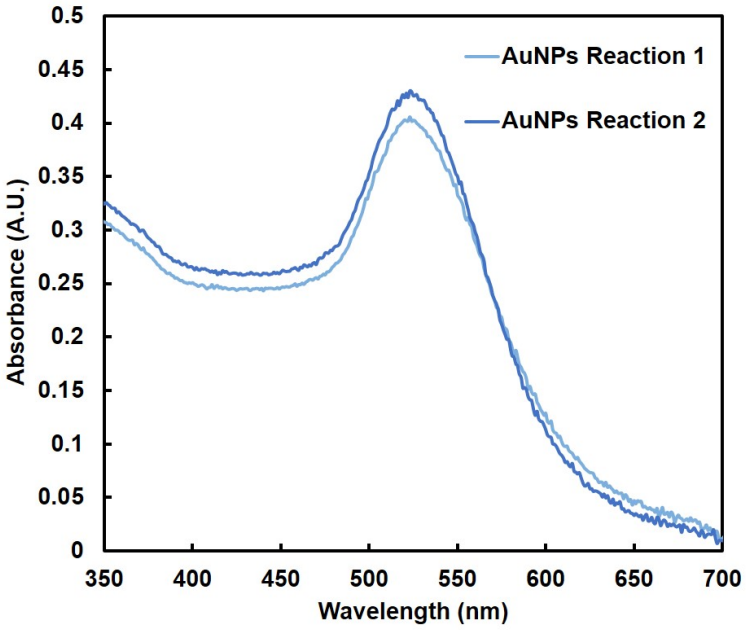

Figure 3.5: UV-Vis spectra of two different syntheses of AuNPs, synthesised by the citrate reduction method. See **Section 6.6.3**.

approximately 0.04 mg mL^{-1} for two different synthesis reactions. The λ_{max} for each was found to be ~525 nm **(Figure 3.5)**.

Next, stabilisation was performed, again utilising the PEG$_{800}$-SH. In the initial tests using the Bunte-AuNPs, the nanoparticles aggregated due to a lack of stability, which may have caused the decreased photothermal activation efficacy over time. To maximise stability of the citrate reduction procedure-synthesised AuNPs, a screen of different PEG$_{800}$-SH concentrations was performed to ascertain how much would result in thorough coverage, and stable nanoparticles as a result. Incubation was performed for at least an hour. Purification was then performed by washing the nanoparticles with water, then collection by centrifugation, and subsequent removal of the supernatant using a micropipette. To prevent aggregation, which was observed as film formation during purification steps, high equivalents were required (16 mg, 90 equivalents PEG$_{800}$-SH for 0.2 mg AuNPs). If lower equivalents of PEG$_{800}$-SH were used, aggregation was observed as a red-purple film on the sides of the Eppendorf in which the reaction was performed. However, with the excess that was used, a minimum amount of film formation was then observed. To investigate the stability of the AuNPs after functionalization with the PEG$_{800}$-SH, UV-Vis spectroscopy

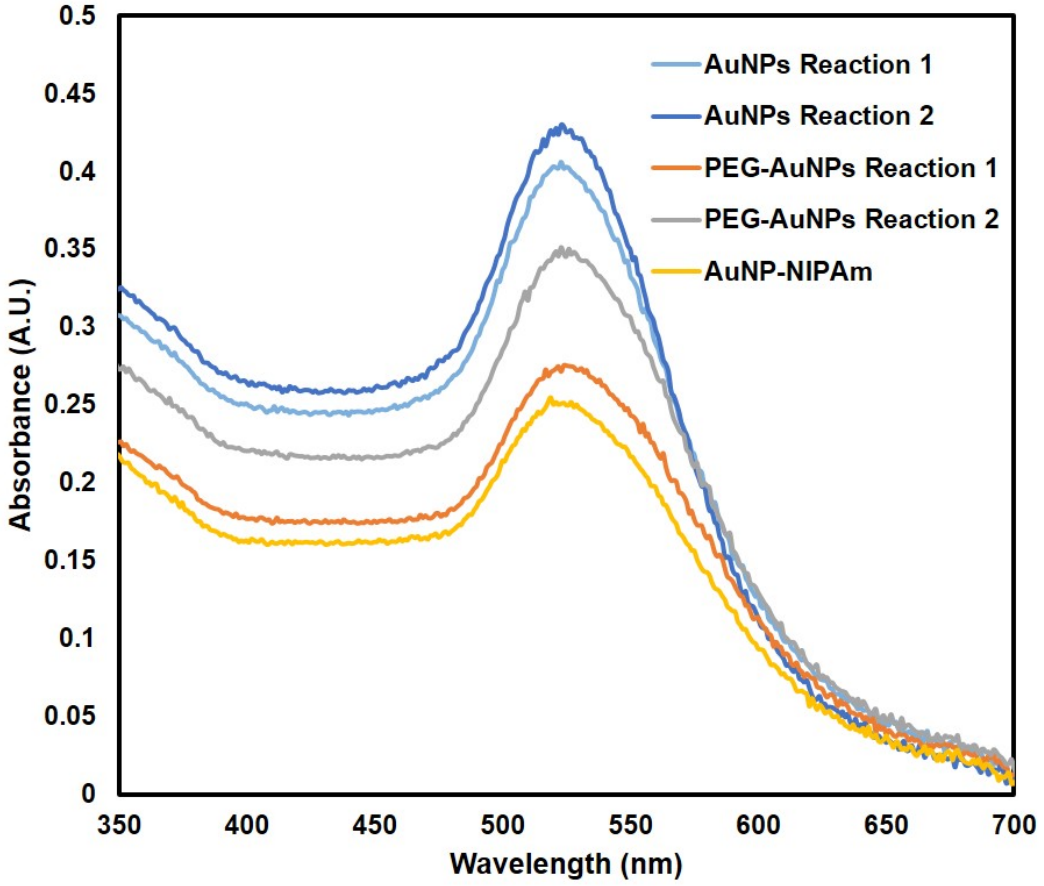

Figure 3.6: UV-Vis absorption spectra of two syntheses of AuNPs (blue traces), both syntheses of AuNPs after functionalization with PEG800-SH (orange and grey trace), and NIPAm containing PEG-AuNPs synthesised in reaction 1 (AuNP-NIPAm) (yellow trace). The absorption maxima of each sample is the same; different peak heights relate to differing concentrations of AuNPs. See **6.6.3**.

was performed on the PEG-stabilised nanoparticles, as well as PEG-stabilised nanoparticles to which the **standard NIPAm pre-gel** had been added **(Figure 3.6)**. When comparing the spectra of PEG-stabilised AuNPs and AuNP-NIPAm to spectra of two reactions of synthesised AuNPs, there was not a significant shift in the λ_{max}, indicating that the nanoparticles were not aggregating. Furthermore, there was no visible colour change of the AuNP dispersion from the initial wine red colour upon addition of the NIPAm pre-gel, suggestive of negligible particle aggregation.

Importantly, the repeated washing and supernatant removal steps resulted in a different final volume of dispersed AuNPs each time the PEG_{800}-SH stabilization was performed. This final volume was typically between 10 and 20 µL. The concentration

of AuNPs in this dispersion would therefore be variable upon each stabilization. As in literature results, this is a limitation in the use of AuNPs in general, due to the assumptions of yields and concentrations that are made.

3.3.2 Use of stabilised AuNPs to form AuNP-PNIPAm

As in **Section 3.3.1**, a pre-gel was made by adding the **standard NIPAm pre-gel** (90 µL) to the PEG-stabilised AuNPs (ca. 10-20 µL). To ensure multi-material PNIPAm hydrogel structures with and without AuNPs could be formed, droplet pairs were formed from a droplet of the **standard NIPAm pre-gel** and a droplet of the AuNP-containing NIPAm pre-gel **(Figure 3.7A)**. The appearance of this droplet pair was as a transparent droplet next to a deep red coloured droplet. Batches of stabilised nanoparticles that had higher concentrations would result in darker red droplets. Purging and photopolymerization was then performed as previously described.

In initial efforts, the shape of the droplet pair was not retained, likely due to coalescence during polymerization. If coalescence occurred prior to polymerization, for example during droplet pair assembly, then the resulting fused single droplet would have an overall pink colour due to diffusion of AuNPs into the NIPAm droplet. However, if coalescence occurred during polymerization, the resulting structure would have specific regions with a red appearance **(Figure 3.7B)**. The irradiated pair shown was made by Dr David Lunn. This specific region

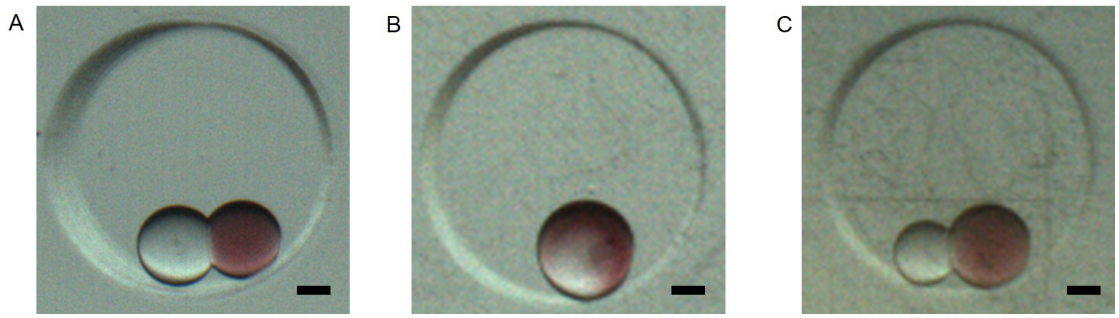

Figure 3.7: (A) A droplet pair consisting of a NIPAm droplet and an AuNP-NIPAm droplet. **(B)** Coalescence during polymerization of a NIPAm/AuNP-NIPAm droplet pair. **(C)** Different sized droplets resulting from different α-KGA concentrations. Scale bars, 250 µm.

formed a crescent shape around the transparent PNIPAm. It was hypothesised that although the NIPAm pre-gel had successfully crosslinked, the AuNP-NIPAm polymerization had been hindered, possibly due to absorption of UV light by the AuNPs. Thus, bilayer rupture occurred due to differing rates of polymerization, as a well-crosslinked PNIPAm hydrogel was formed, whilst the AuNP-NIPAm remained a more fluid pre-gel.

One way to counteract the reduced rate of polymerization in the AuNP-NIPAm droplet was to add an excess of α-KGA photoinitiator into this droplet (see **Section 1.1.2**)[22], whilst keeping the concentration of α-KGA in the NIPAm droplet the same. For the pair shown, formed by Dr David Lunn, although gelation appeared to be successful, there was a change in size of the droplets **(Figure 3.7C)**. This was likely due to an osmotic imbalance resulting from the different concentration of α-KGA in each droplet. An alternative approach was to use a different photoinitiator without charged groups. Like α-KGA, this photoinitiator would need to be water-soluble and compatible with droplet interface bilayers. One such photoinitiator, Irgacure 2959, has been widely utilised in the formation of hydrogels[42]. Multiple NIPAm and AuNP-NIPAm pre-gel droplet pairs were formed, in which the NIPAm-only droplet contained a constant concentration of Irgacure 2959, which replaced α-KGA (0.1 wt %, 4.5 mM Irgacure 2959; 1.34 M NIPAm, 13.1 mM MBA). As before, 90 µL of the NIPAm pre-gel solution was added to ca. 10-20 µL PEG-stabilised AuNPs to form the AuNP-NIPAm pre-gel. A range of different Irgacure 2959 concentrations were tested in the AuNP-NIPAm droplet. These were purged and photopolymerized as previously described.

From these droplet pairs, the shape of the resulting hydrogel structures differed depending on the Irgacure 2959 concentration. It was hypothesised that the shape of the structure depended at which point bilayer rupture occurred during polymerization. For example, with symmetric, PNIPAm-only hydrogels templated by droplet pairs (see **Section 2.2.2**), bilayer rupture occurred towards the end of polymerization, once the hydrogel matrix in each droplet was almost fully gelled, and at this point polymerization continued across the bilayer, linking the two

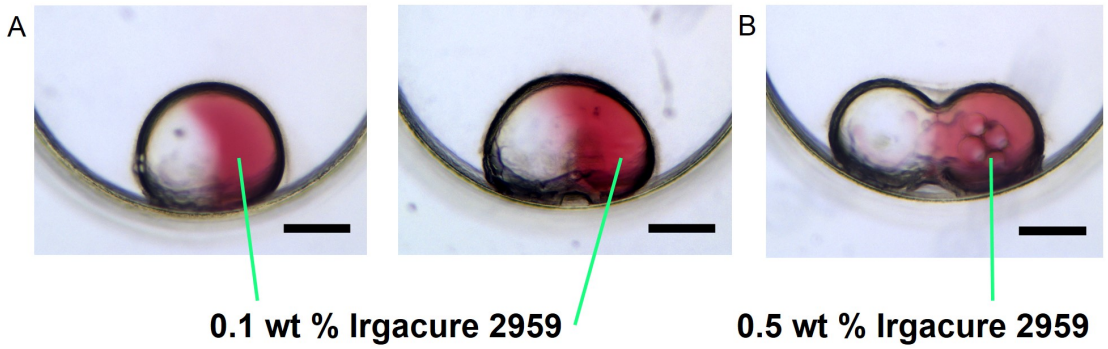

Figure 3.8: Optimization of Irgacure 2959 concentration. **(A)** Two examples of droplet pair-templated structures in which the Irgacure 2959 concentration was balanced. The shape retention was typically poor. **(B)** When the concentration of Irgacure 2959 was higher in the AuNP-NIPAm droplet, the shape retention was improved. Scale bars, 250 µm.

droplets. By contrast, when one droplet was formed from AuNP-NIPAm, and the same concentration of Irgacure 2959 was used as in the NIPAm-only droplet (0.1 wt %, 4.5 mM), the resulting structure had an almost spherical shape in some cases **(Figure 3.8A)**. Greater definition of the red-coloured AuNP-containing region suggested improved crosslinking in comparison to the experiments utilising α-KGA only. When the Irgacure 2959 concentration was increased in the AuNP-NIPAm droplet (0.5 wt %, 22.5 mM), the retention of the droplet shape was significantly improved **(Figure 3.8B)**. This concentration of Irgacure 2959 was used hereafter for the AuNP-NIPAm pre-gel. The distinction between the two droplets in the location where the bilayer had been was clearly visible, with a slight colour gradient, indicating some mixing of the two hydrogels at the interface. However, there was no further diffusion of the AuNPs after gelation was complete.

3.3.3 Photothermal response of AuNP-PNIPAm-containing structures

The photothermal response was then tested with a hydrogel structure kept in oil **(Figure 3.9A)**. Illumination of the structure caused photothermal heating of the AuNP-PNIPAm region above the LCST of PNIPAm **(Figure 3.9B)**. This resulted in contraction of the AuNP-PNIPAm region, but not the PNIPAm only region.

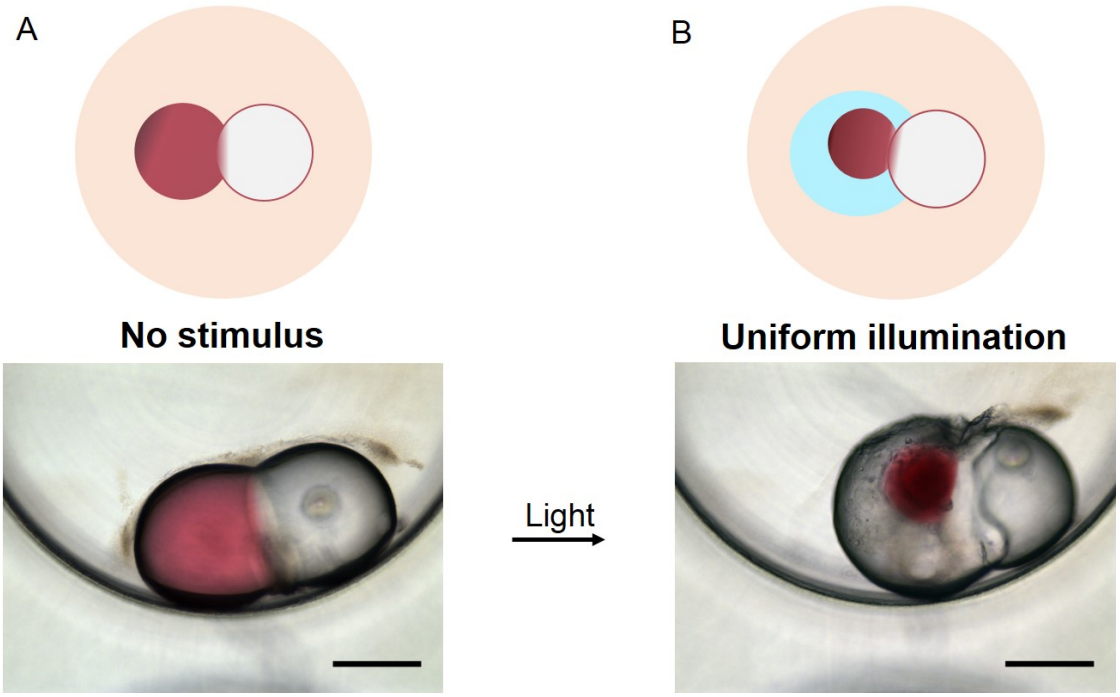

Figure 3.9: Photothermally controlled differential contraction in a droplet pair in oil. (A) Droplet pair-templated AuNP-PNIPAm (red droplet) and PNIPAm (white droplet) structure in oil. (B) After illumination with green light, only the AuNP-PNIPAm droplet shrunk. After illumination, the hydrogel structure re-swelled with the expelled water. Scale bars, 250 µm. See **Section 6.6.9**.

Water was expelled in the form of a single droplet from the AuNP-PNIPAm side of the structure.

Phase transfer of the AuNP-PNIPAm and PNIPAm hydrogel structures was then conducted using the approach that was described in **Section 2.2.2**. The hydrogel structure swelled further, but retained the droplet pair shape that had been observed in oil **(Figure 3.10A)**. For successful photothermal activation of the structure in water, it was necessary to use the light source at the highest shutter intensity. This was measured using a light meter and found to have a maximum irradiation intensity of 50 mW. Additionally, the structure could only be activated in a ca. 15 µL minimum amount of water, likely due to surrounding water acting as a heat sink for the locally generated heat. Contraction of the AuNP-PNIPAm droplet occurred after only several seconds of illumination **(Figure 3.10B)**, significantly faster than the diffusion-limited contraction when the entire surrounding environment was heated above the LCST. The local heating of the AuNP-PNIPAm was enough to

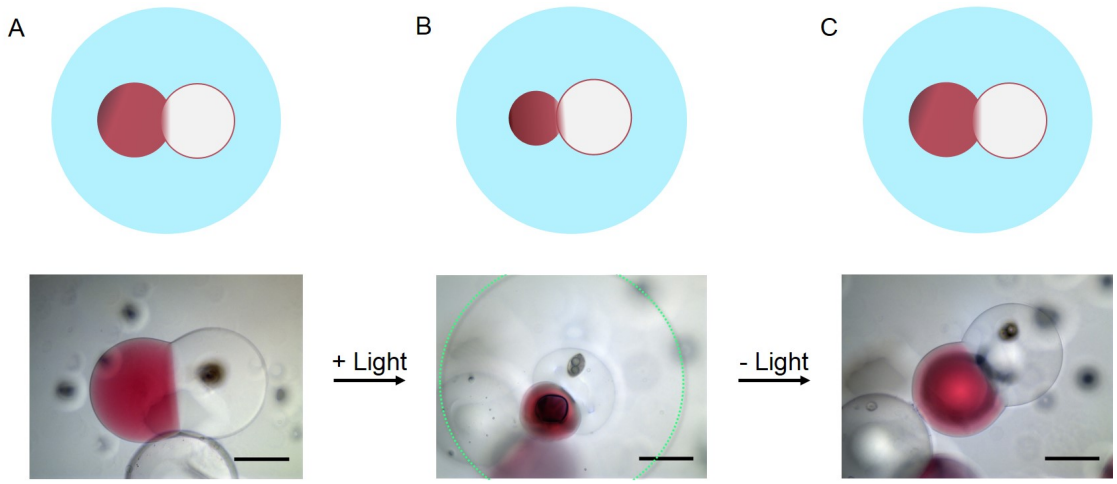

Figure 3.10: Photothermally controlled differential contraction in a droplet pair in water. **(A)** Droplet pair templated AuNP-PNIPAm (red droplet) and PNIPAm (white droplet) structure in water. **(B)** After illumination with green light, only the AuNP-PNIPAm droplet shrunk. **(C)** After reswelling, the structure returned to its original shape. Scale bars, 250 µm.

additionally cause a small amount of contraction of the PNIPAm droplet at the interface. Re-swelling of the hydrogel structure then occurred within seconds to a minute **(Figure 3.10A-C)**, and was dependent on the volume of surrounding water, and the concentration of AuNPs. Unlike the Bunte-AuNPs, the PEG-stabilised AuNPs did not show visible signs of aggregation after heating or photothermal activation. Additionally, photothermal activation could be repeated multiple times.

With these stabilised nanoparticles, having confirmed that photothermal activation of AuNP-PNIPAm in water was possible, it was then necessary to demonstrate selective contraction of the hydrogel, as for the Bunte-AuNP-containing PNIPAm. As before, a chain was formed from three AuNP-NIPAm pre-gel droplets in oil (90 µL of a solution containing 1.34 M NIPAm, 13.1 mM MBA, 0.5 wt % Irgacure 2959; ca. 10-20 µL of PEG-stabilised AuNPs), which was purged with N_2, photopolymerized and transferred into water **(Figure 3.11A)**. The same conditions were used for photothermal activation as for **Figure 3.10**, with a high shutter intensity for the light source on the inverted microscope, and a minimum amount of water. Initially, as for **Figure 3.4**, the entire structure was illuminated. Within seconds, this resulted in a uniform contraction of the whole structure **(Figure 3.11B)**.

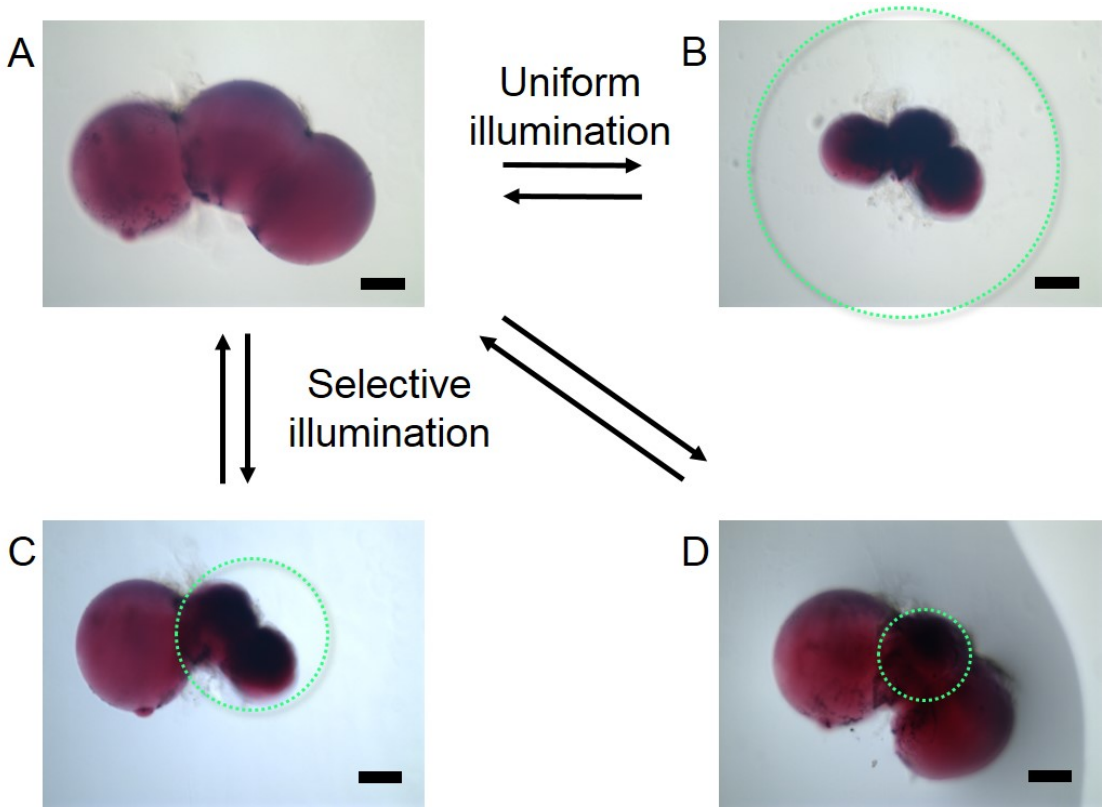

Figure 3.11: Selective photothermally activated contraction of a AuNP-PNIPAm hydrogel structure templated by a droplet chain, using an aperture-restricted green light source. **(A)** The structure is initially fully swollen after phase transfer. **(B)** After illuminating the entire structure with green light, the entire structure contracts. After re-swelling, **(C)** two droplets are illuminated, resulting in their contraction. **(D)** One droplet is illuminated, resulting in its contraction. Green circle represents area of illumination. Scale bars, 250 µm.

Then, the aperture diaphragm on the light source was restricted such that only two of the droplets were illuminated. This resulted in only two of the droplets contracting **(Figure 3.11C)**. Finally, the aperture was decreased such that only one of the droplets was illuminated. As a result, one droplet contracted, with a slight contraction exhibited by a second droplet **(Figure 3.11D)**. The structure shown in **Figure 3.11** was kept and remained stable over several months, with little to no visible leakage of AuNPs.

3.3.4 Light- and temperature-controlled folding of a AuNP-PNIPAm and PNIPAm hydrogel structure

A structure fabricated from AuNP-PNIPAm as well as PNIPAm would be capable of light-controlled curling, in addition to temperature-controlled contraction. To make this structure, a micromachined PMMA well array containing four 4 mm diameter wells was used. In these larger wells, it was possible to make a double chain formed from eleven droplets. As with larger structures formed from NIPAm and PEGDAAm-NIPAm droplets (see **Section 2.4**), these droplet networks were formed by rolling droplets from the top of the well to the bottom. Due to the curvature of well, once a droplet rolled into position next to another droplet, a bilayer would form within seconds. After forming a chain of five NIPAm pre-gel (1.34 M NIPAm, 13.1 mM MBA, 0.1 wt % Irgacure 2959) droplets on the bottom, six AuNP-NIPAm pre-gel (90 µL of 1.34 M NIPAm, 13.1 mM MBA, 0.5 wt % Irgacure 2959; ca. 10-20 µL PEG-stabilised AuNPs) droplets were added. The first AuNP-NIPAm droplet was ejected at the centre of the top edge of the well, and rolled directly in between the two central droplets. Droplets were then added either side, building the structure outwards from the centre. This was crucial in order that the droplet network was packed correctly and as a result, formed the desired structure. It was important for each droplet that was added to form bilayers with the right droplets. Although it was possible to pull apart or rearrange bilayers, applying too much mechanical force to the droplet networks might result in coalescence. Droplets could also be removed from the network with capillary action. However, in some cases, this could also cause coalescence.

After assembly of the droplet network, it was purged with N_2, photopolymerized, and phase transferred. The resulting structure was a hydrogel comprised of a layer of PNIPAm and a layer of AuNP-PNIPAm **(Figure 3.12**, centre). This structure was fabricated by Dr David Lunn. In the regions patterned with PNIPAm, the resulting hydrogel structure was well defined, retaining the shape of the droplet network. The AuNP-PNIPAm region of the structure was observed to have a less well retained shape with respect to the original droplet network, perhaps indicating bilayer rupture

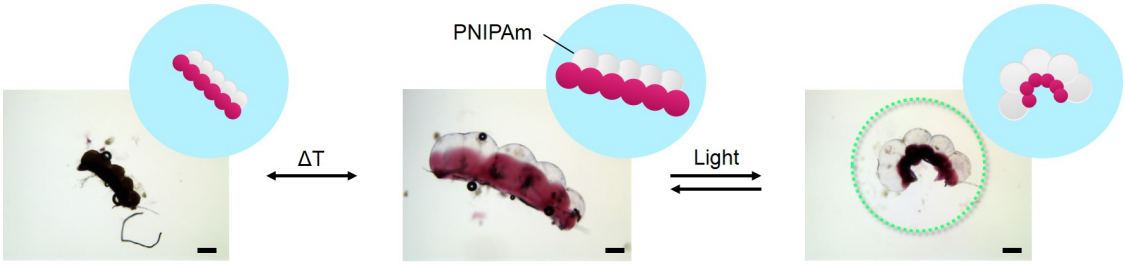

Figure 3.12: Two modes of deformation of a PNIPAm (white circles) and AuNP-PNIPAm (red circles) structure (centre), which isotropically contracts when heated (left), or curls when irradiated with green light (right). Scale bars, 250 µm. See **Section 6.6.8**.

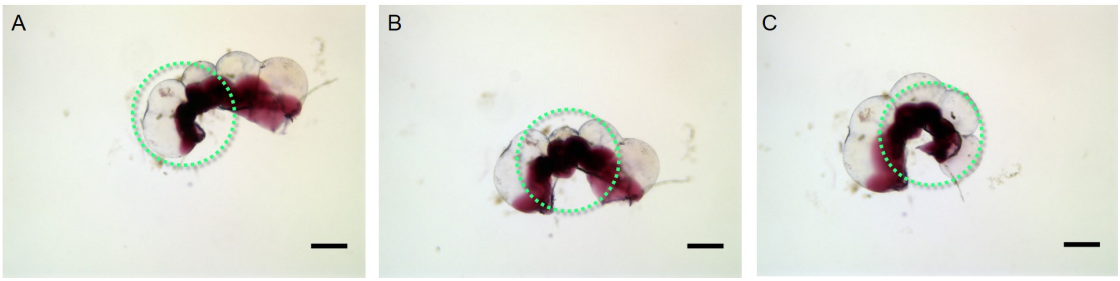

Figure 3.13: Selective contraction of the AuNP-PNIPAm and PNIPAm structure. **(A)** When the one end is illuminated, it curls only at that end. **(B)** Illumination at the centre results in the two ends being brought together. **(C)** When the opposite end is illuminated, it curls at that end. Scale bars, 250 µm.

before full gelation of the AuNP-PNIPAm region (see **Section 3.3.2**). Importantly, however, the definition between the AuNP-PNIPAm region and PNIPAm region was still clearly visible. When the structure was heated, it underwent an isotropic contraction **(Figure 3.12**, left). Photothermal contraction was then performed, resulting in the curling of the structure within seconds, as the AuNP-PNIPAm region contracted **(Figure 3.12**, right). There was some slight contraction of the PNIPAm region, due to excess heat generated by the excitation of the nanoparticles.

Using the diaphragm to restrict the aperture of the light source, three arbitrarily chosen regions of the structure could be contracted. This resulted in just the curling of one end of the structure **(Figure 3.13A)**, or the centre of the structure **(Figure 3.13B)**, or the curling of the opposite end of the structure **(Figure 3.13C)**.

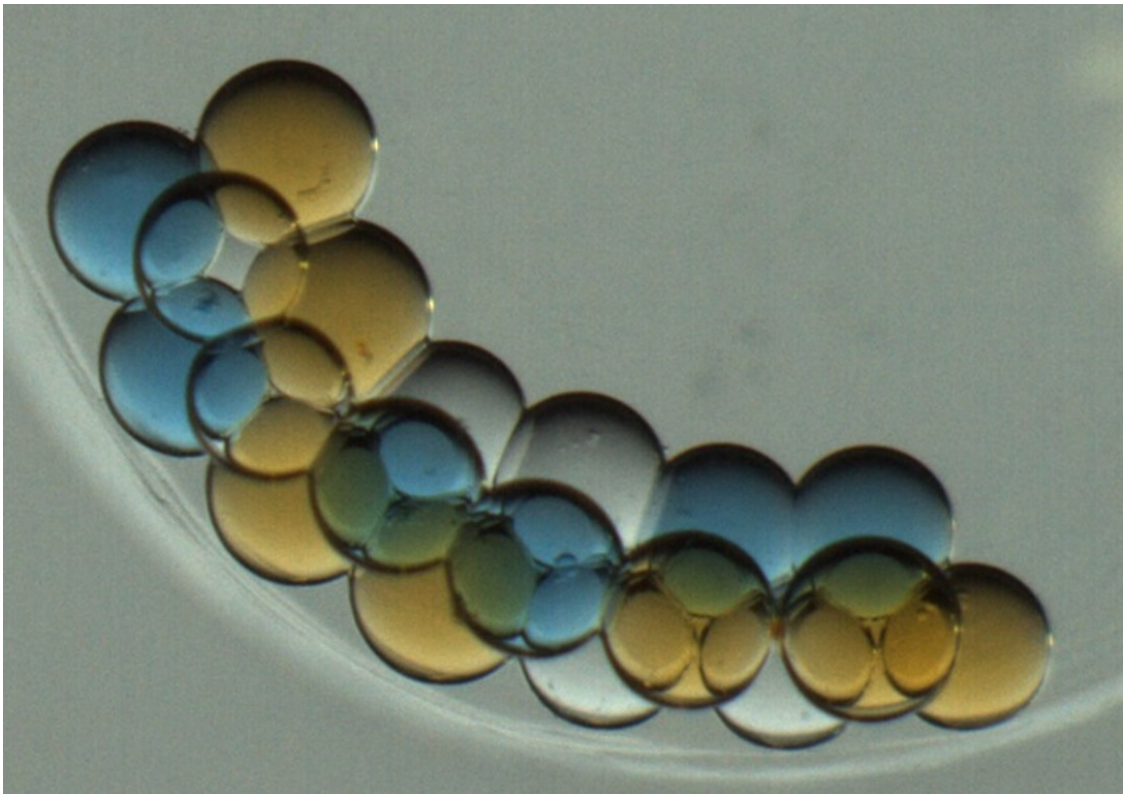

Figure 3.14: 3D patterned droplet network containing a NIPAm pre-gel (clear), as well as an orange G-containing NIPAm pre-gel (orange) and a xylene cyanol-containing pre-gel (blue). All droplets were approximately 50 nL. See **Section 6.6.8**.

3.3.5 Photothermally activated shape change of a 3D patterned AuNP-PNIPAm and PNIPAm structure

As a consequence of the voxel-like patterning possible with droplet networks, three droplet types could be patterned in 3D. To demonstrate this, a PEGDAAm-containing NIPAm pre-gel, the AuNP-containing NIPAm pre-gel used in **Section 3.3.3-3.3.4**, and **the standard NIPAm pre-gel** were used to create a patterned 3D droplet network. With these three droplet types, light and temperature might both be used to induce two different non-uniform responses.

To initially test the formation of a three-droplet type structure, different coloured NIPAm pre-gels were made by incorporating dyes, orange G and xylene cyanol. A 2D droplet network was constructed by rolling from the top edge of the circular 4 mm-diameter well (see **Section 3.3.4**). Then, droplets were positioned on the top by ejecting them from a gel-loading pipette tip (see **Section 2.2.4**) (**Figure 3.14**).

Due to these additional components, differing bilayer formation in this network resulted in poor packing in some regions (see **Section 1.2.1**). Nonetheless, having demonstrated formation of such a 3D patterned droplet network, NIPAm, AuNP-NIPAm and PEGDAAm-NIPAm were used instead. Once a 3D patterned droplet network was constructed from these three droplet types, it was purged with N_2 and photopolymerized. However, for complex networks such as these, containing several regions with polymerization-hindering nanoparticles, the typical process of polymerization was not reproducible. One possible problem was oxygen infiltration, and to ensure that the oxygen was reduced to a minimum level, anaerobic strips were placed in the purging chamber. These strips, saturated with resazurin in an aqueous buffer, are used to indicate the presence of oxygen in culture vessels for anaerobic bacteria, and turn pink in the presence of oxygen or white in an anaerobic environment. Despite this, there remained a slightly reduced efficacy of polymerization in AuNP-containing regions. Another challenge was the differences in AuNP concentration between each batch of stabilised AuNPs. Although UV-Vis can be used to determine the concentration, this could not be done due to the µL volumes of stabilised nanoparticles obtained. The concentrations at these volumes were too high to measure with the NanoDrop spectrophotometer, and experiments with dilutions did not yield reproducible concentration measurements. Overall, achieving a good fidelity of the droplet network-templated shape for these large structures was not reproducible.

However, it was possible to form a smaller 3D patterned shape, consisting of regions formed from NIPAm pre-gel and PEGDAAm-NIPAm, with light-responsive regions formed from AuNP-NIPAm **(Figure 3.15A)**. Three parallel adjoining chains of these droplet types were assembled into a triangular prism-shaped network **(Figure 3.15B)**. With the oxygen reduction strategy in place, this structure was purged for 1.5 hours and then photopolymerized as previously. After gelation was complete and the structure was phase transferred, the structure underwent a pre-programmed curling when irradiated with green light. This curling motion took place across each of the layers of the structure containing the AuNPs **(Figure 3.15C)**.

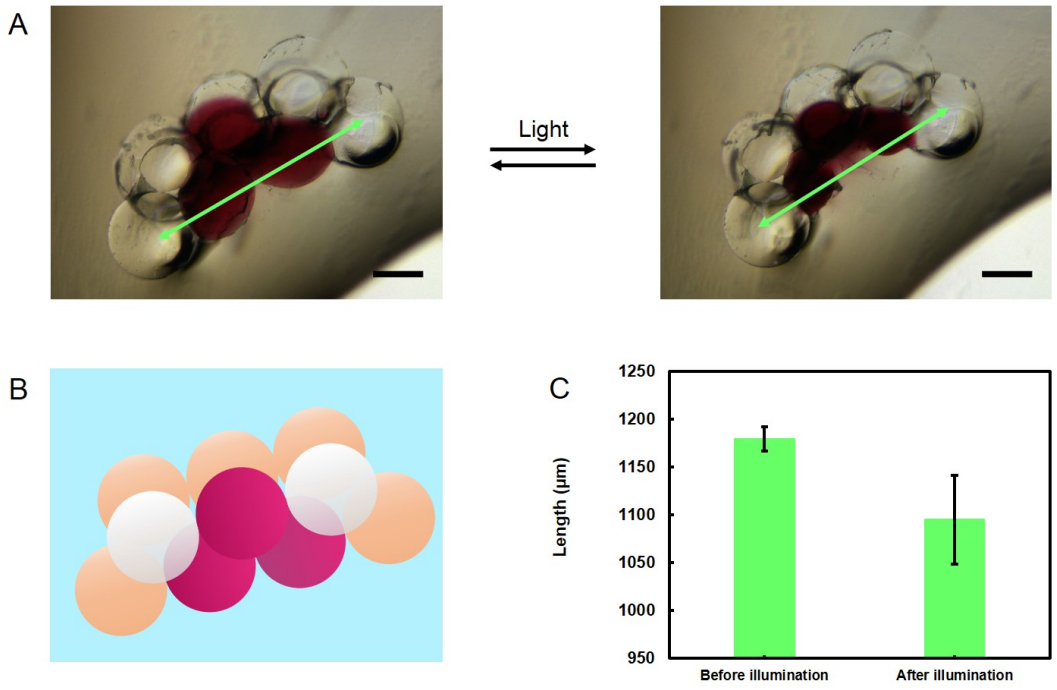

Figure 3.15: Photothermally activated shape change of a 3D patterned, multi-material, droplet-templated PNIPAm structure. **(A)** 3D patterned structure with a central AuNP-PNIPAm (red region) segment. Upon illumination with green light, it undergoes a reversible inwards 3D curling motion across one of the supporting layers, and the top layer. Scale bars, 250 µm. **(B)** Schematic of droplet network patterning, with white circles indicating PNIPAm, red circles indicating AuNP-PNIPAm, and orange circles indicating PEGDAAm-PNIPAm. **(C)** Quantification of difference in length of between the terminal PEGDAAm-PNIPAm regions upon illumination, represented in image by green arrow. The mean was calculated from this length, measured for three different structures, before and after illumination. Error bars indicate one standard deviation about the mean distance.

3.4 Formation of magnetically controlled PNIPAm hydrogels

3.4.1 Incorporation of magnetic beads into PNIPAm hydrogel structures

Next, to allow magnetically controlled locomotion, a magnetically responsive component would need to be incorporated into the droplets. One approach to do this, as with AuNPs, would be to embed magnetic particles into the hydrogel matrix. Our strategy was to use magnetic beads, which have also been used to assemble droplet networks[88]. Similarly as for AuNPs, the **standard NIPAm**

pre-gel was used to dilute the magnetic beads (10 µL pre-gel with 1 µL magnetic bead suspension, hereafter known as the **magnetic NIPAm pre-gel**) prior to droplet formation. Separation of the beads from the pre-gel would occur within seconds as they sunk to the bottom. Due to the inhomogeneity of the magnetic bead-containing NIPAm pre-gel, it was not possible to reproducibly form droplets with the same quantity of magnetic beads each time, which could be observed upon droplet formation. In addition, the beads would visibly sink to the bottom of the droplet upon formation **(Figure 3.16A)**. However, after purging and photopolymerization, the rupture of the bilayer was visible, whilst the droplet pair shape was retained **(Figure 3.16B)**, indicating successful polymerization. In addition, the magnetic beads remained localised on one side of the structure.

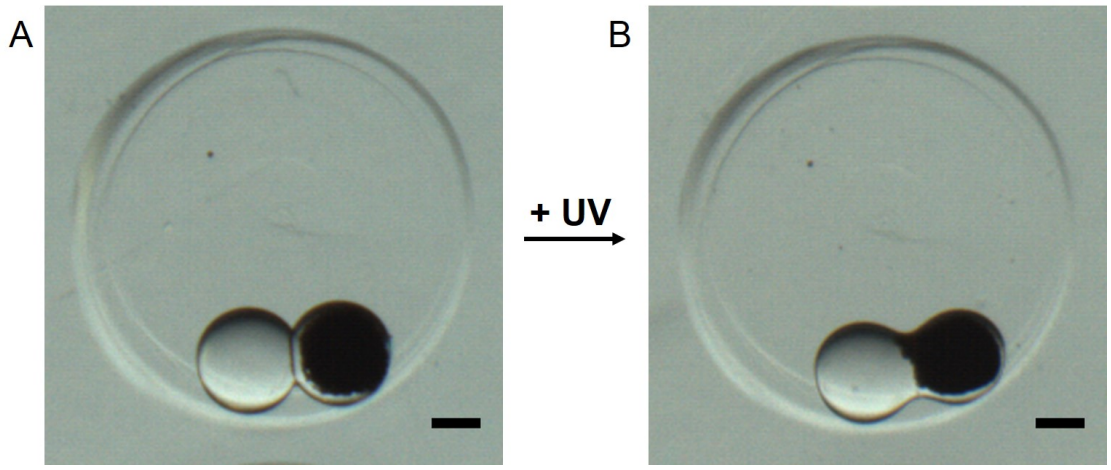

Figure 3.16: Droplet pair containing **standard NIPAm pre-gel**, and magnetic bead-containing NIPAm pre-gel, **(A)** before and **(B)** after gelation. Scale bars, 250 µm.

The structure was then transferred into an aqueous environment using the same procedure as has been utilised previously **(Figure 3.17A)**. It was observed that not all of the beads had become embedded into the hydrogel matrix, as there was visible diffusion of black material into the surrounding water. This is likely a result of reduced polymerization in some regions due to light scattering by the beads. However, upon heating to 40°C, above the LCST of PNIPAm, the entire structure contracted **(Figure 3.17B)**.

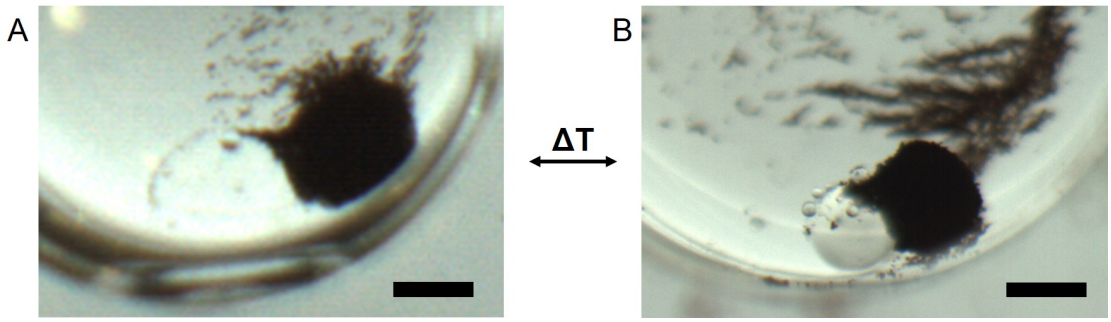

Figure 3.17: (A) Image taken during phase transfer and **B** heating to 40°C of a PNIPAm and magnetic bead-containing PNIPAm structure. Scale bars, 250 µm.

Importantly, it was necessary to ensure that the amount of beads present in the structures was sufficient that they could be magnetically controlled. To test this, a stack of twenty adjoined 5 mm^3 neodymium (Nd) magnets was brought in proximity to the structures. If there were sufficient beads trapped in the hydrogel, the structures could be moved out of the wells and around in the surrounding water with the Nd magnets.

3.4.2 Reversibly shrinking gripper-like device

By patterning responsive hydrogels with droplet networks, a structure could be made that could controllably change shape in two ways, as well as undergo controlled locomotion. Previously, grippers have been fabricated that are able to move through twisting passages designed to mimic in vivo environments[67,131]. These structures require a constantly applied magnetic field in order to remain in a desired location. Here, a device was designed that could shrink and curl depending on the temperature, allowing it to perform different functions in different situations. This device could also be moved using a magnet, before being released in its desired location, where it remained trapped after its shape change.

Dual-temperature-mediated shrinking or curling was achieved by modulation of the LCST in different regions of the structure using different concentrations of PEGDAAm (see **Section 2.3**). A double strip was designed, with two types of the temperature-responsive PNIPAm hydrogel shown in **Section 2.3**, and a magnetic handle incorporated at one end of the structure, using the **magnetic PNIPAm**

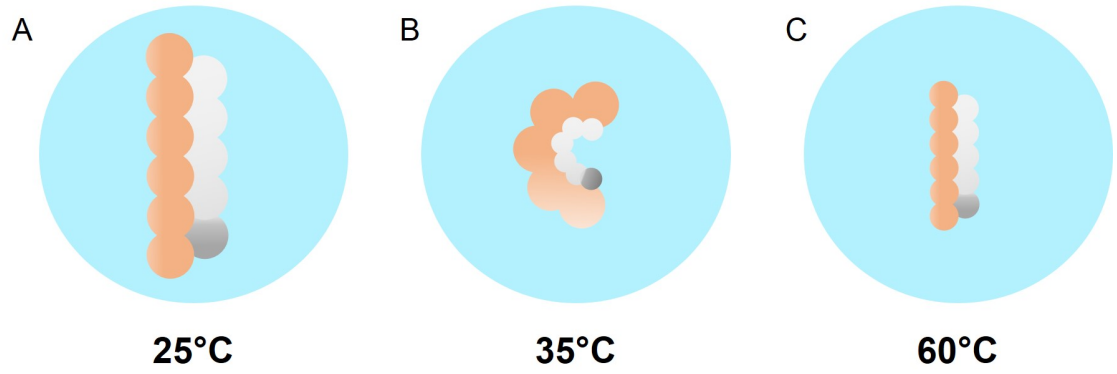

Figure 3.18: Schematic representation of the dual temperature control of the device. **(A)** The PNIPAm and PEGDAAm-PNIPAm regions are both fully swollen below the LCST. **(B)** At 35°C, just above the LCST, the PNIPAm contracts substantially more than the PEGDAAm-PNIPAm, resulting in a high curvature. **(C)** At 60°C, the PEGDAAm-PNIPAm is able to contract to a greater degree, resulting in a decreased curvature.

hydrogel (see **Section 3.4.1**) **(Figure 3.18A)**. At 35°C, it was able to curl due to differential contraction of the two droplet types (see **Section 2.3**) **(Figure 3.18B)**. For the strain-producing region, on the inner side of the strip, a PNIPAm hydrogel was used which contained 0.5 mM PEGDAAm (with 1.34 M NIPAm, 13.1 mM MBA and 13.1 mM α-KGA). This would reach a shrinkage ratio smaller than that experimentally demonstrated for 1 mM PEGDAAm, which was 0.30 ± 0.02 at 36°C **(Figure 2.23)**. For the outer region, an intermediate concentration of PEGDAAm was chosen, 3.5 mM (with 1.34 M NIPAm, 13.1 mM MBA and 13.1 mM α-KGA). which would result in a higher shrinkage ratio than that measured for 3 mM, ca. 0.7 ± 0.02 **(Figure 2.23)**. This would produce a high curvature. However, upon increasing the temperature to 60°C, a slightly higher final shrinkage ratio would be achieved than that measured for 3 mM, 0.45 ± 0.01 **(Figure 2.23)**. This would result in an almost fully contracted device **(Figure 3.18C)**.

To fabricate this device, a droplet network was assembled in a PMMA well array containing lipid-in-oil, in a similar strategy to the light- and temperature-responsive curling device **(Section 3.3.4)**. A chain of six 3.5 mM PEGDAAm-containing NIPAm droplets, was assembled by rolling droplets from the top edge of the 4 mm diameter circular well. Four 0.5 mM PEGDAAm-containing NIPAm droplets were rolled into place from the top, beginning between the two central droplets and

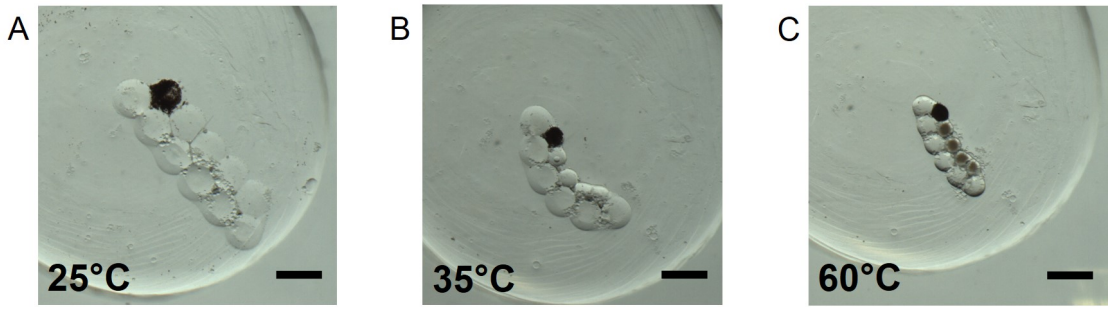

Figure 3.19: Brightfield images of the curling structure at **(A)** 25°C, **(B)** 35°C and **(C)** 60°C. Scale bars, 500 µm. See **Section 6.4.7**.

building outwards. Finally, a **magnetic NIPAm pre-gel** droplet was added to one end. As discussed in **Section 3.4.1**, in forming this magnetic bead-containing NIPAm droplet, it was important to ensure the droplet contained a sufficient quantity of magnetic beads so that the structure could be moved once fabricated. These structures were purged with N_2 and polymerized, before removing the oil and adding water **(Figure 3.19A)**.

With these multi-material hydrogel devices, it was first necessary to show that the desired shape changes would take place at each of the given temperatures. The structures were heated through a relevant temperature range, from below the experimentally determined LCST, to 60°C, where all droplets should have reached a minimum size. Once the plate sensor reported the desired temperature, it was held constant for 30 minutes for the surrounding environment to equilibrate.

As expected, the structure reached a maximum curvature at 35°C **(Figure 3.19B**. Upon heating further, there was a decrease in curvature. At 60°C, there was a low final curvature as the structure underwent almost complete contraction **(Figure 3.19C)**. The curvature was quantified using the same approach as for PEGDAAm-PNIPAm and PNIPAm structures **(Figure 3.20)** (see **Section 2.4**). An initial sharp increase in curvature was observed at the LCST of PNIPAm, which decreased steadily with increasing temperature as the 3.5 mM PEGDAAm-containing PNIPAm region contracted further.

To form a moveable gripping structure, it was necessary to demonstrate the combined functions of dual temperature control with magnetic control **(Figure**

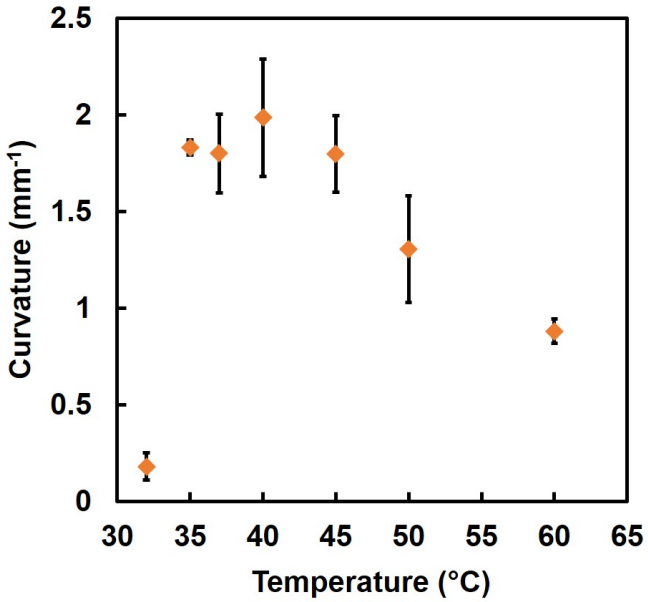

Figure 3.20: Temperature dependence of the curvature of the shape-morphing device. Error bars indicate one standard deviation about the mean. See **Section 6.5.14**.

3.21). The designed structure **(1)** could be uniformly contracted to a smaller version of its original shape when heated, allowing it to move through a narrow channel it could not before **(2)**. When cooled, it could re-swell, and subsequently remain in the second chamber. Here, it could curl via cooling to 35°C **(3)**. Only when heat-contracted to 60°C a second time **(4)** would it be able to move through to the final chamber **(5)**.

The container in which the experiment was conducted consisted of three interconnected chambers, micromachined into a PMMA container **(Figure 3.22)**. Initially, it was important to test the manoeuvrability of the hydrogel devices within this container with the magnets. After fabrication and phase transfer of a structure, it was moved into the experiment container. By holding neodymium magnets above the surface of the container, in close proximity to the device (see **Section 3.4.1**), the structure could be manipulated according to the lateral motion of the magnet.

It was then possible to test the combined dual temperature control, with the heat stage, and magnetic control, with neodymium magnets **(Figure 3.22)**. Due to the low volume of water filling the chambers, measures were taken to counteract evaporation during heating. These included covering the chamber between points

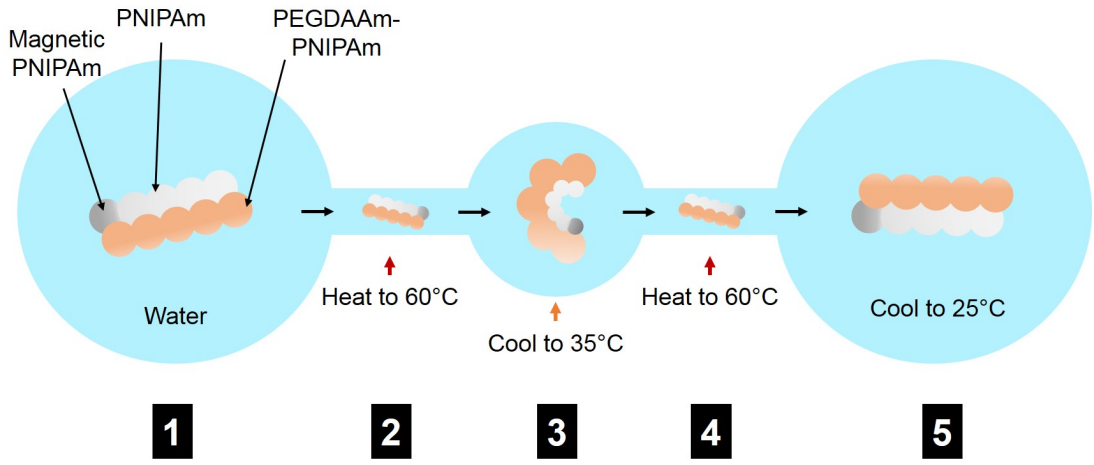

Figure 3.21: **(1)** Initially, the device is trapped in a chamber. **(2)** After heating to 60°C, it fully contracts and can be pulled through a narrow channel with a magnetic field. **(3)** Once in the central chamber, it is cooled to 35°C, where it undergoes a curling motion. **(4)** It is only able to escape to the final chamber after fully contracting, when heated to 60°C again, and pulled through with a magnetic field. **(5)** Once in the final chamber, it is cooled to room temperature and returns to its original size and shape.

at which imaging was performed, as well as keeping a 200 µL reservoir of water at the same temperature to top up the chambers when needed. For each change in temperature, 30 minutes were allowed for the heating and shape change to take place. Firstly, the temperature of the heat stage was changed to 60°C, allowing a contracted device with low curvature to be moved with the magnet through the narrow, straight channel connecting the first and second chamber **(2)**. Once in the second chamber, the temperature was reduced to 35°C to allow curling of the device **(3)**. Then, the temperature was raised to 60°C, enabling the hydrogel to shrink and straighten, and be magnetically moved through the second channel **(4)**, into the final chamber. Here, it was cooled to room temperature, where it transitioned through its curled state and fully reswelled to its original dimensions **(5)**.

At each stage, the curvature was analysed using the previously described MATLAB script (see **Section 2.4**). Interestingly, the curvature at 40°C was slightly higher than in **Figure 3.19**, likely due to slight detachments between the 3.5 mM PEGDAAm-containing PNIPAm regions, visible in the high curvature image in the central chamber. These fissures (indicated by orange arrows) were

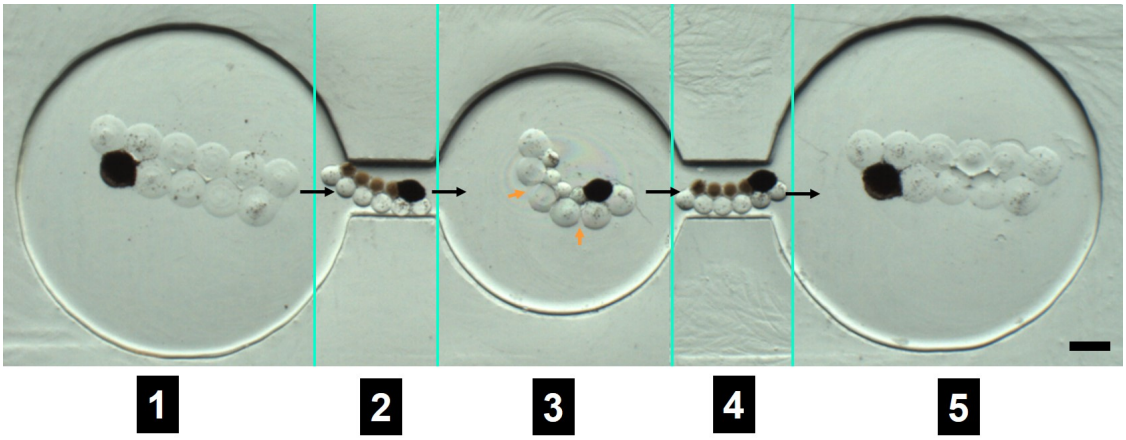

Figure 3.22: Brightfield images of the device moving through each stage **(1)-(5)** (see **Figure 3.21**) as a result of dual temperature and magnetic control. Green lines indicate where images are stitched together. Orange arrows indicate fissures between droplets causing increased curvature. Scale bar, 500 µm.

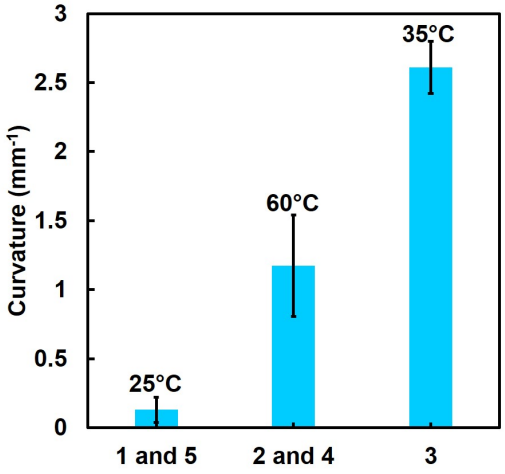

Figure 3.23: Curvature of dual-temperature responsive structures at each position and temperature from **(1)-(5)**. A structure was imaged at the temperature at each position at least three times. The mean curvature was calculated from the data extracted from these images. Error bars indicate one standard deviation about the mean curvature.

likely produced by the strain placed on the device during curling of the PNIPAm region, and caused increased curvature both at 35°C and 60°C.

3.5 Conclusion

This chapter has described the incorporation of functional additives into droplet-templated PNIPAm hydrogels with the aim of enabling shape change or locomotion in response to a variety of stimuli. These different additives were incorporated into the PNIPAm structures by further optimising the previously developed droplet-templating method.

Firstly, AuNPs were used for control of shape change using light. Photothermally controllable AuNPs were synthesised and stabilised such that they were active and reproducibly usable. A different photoinitiator, Irgacure 2959, was optimised to enable matched polymerization rates in the two different regions. With AuNP-PNIPAm and PNIPAm, a structure capable of photothermally controlled curling and temperature-controlled contraction was made. In addition, a 3D structure made from three types of droplet, also including PEGDAAm-NIPAm was made. With further optimisation of the gelation in the three regions, a structure capable of non-uniform responses in response to temperature and light could be made.

Secondly, magnetic beads were used, which allowed locomotion via magnetic control. With a designed mechanism for dual temperature control, a magnetically controlled gripper-like structure was fabricated. This device was able to contract such that it could move through different passages that it originally could not at 60°C, whilst it was able to curl at 35°C. It is envisaged that this structure could form a basis for a gripper that could be used to transport cargo. Once curled at 35°C, it would be able to enclose around an object. It could then be manipulated with a magnet, and release the object either by heating further, or by cooling.

4

Generation of PNIPAm hydrogels from picolitre droplets with a 3D droplet printer

In **Chapter 2**, up to 39 nL droplets were manually arranged into droplet networks and used to generate patterned PNIPam hydrogel structures. This chapter describes the use of a 3D droplet printer[86,87] to automate the fabrication of PNIPAm hydrogel structures templated by hundreds of NIPAm pre-gel droplets, whose manual assembly was outlined in **Chapter 2**. With the droplet printer, networks composed of pL droplets (50-100 µm) can be produced, resulting in higher resolution patterning. Furthermore, with automated droplet generation, the precise placement of hundreds to thousands of droplets in 3D is possible. In order to produce continuous PNIPAm hydrogel structures with the droplet printer, optimisation of both the PNIPAm photopolymerization and droplet printing methodologies was required. Firstly, the photopolymerization methodology was modified to enable its compatibility with smaller (sub-nL) droplets. Secondly, the printing strategy was adapted to allow reproducible printing of uniform, stable networks. These approaches would allow for the formation of PNIPAm hydrogels templated by 3D printed droplet networks. In future, successful implementation of this technology will therefore

allow the formation of multi-material responsive hydrogels from networks composed of thousands of droplets, patterned to a resolution of tens of microns.

Acknowledgement of collaboration

Droplet printing in this chapter was carried out by the author, as well as with assistance from Dr Michael Booth and Dr Ravinash Krishna Kumar, both postdoctoral researchers in the Bayley group. Printer modifications were designed by Dr Linna Zhou and Dr Stuart Box, postdoctoral researchers in the Bayley group.

4.1 Introduction

Using a 3D droplet printer to automate the generation of aqueous droplet networks in oil has enabled the construction of a variety of novel soft materials[82]. These include aqueous droplet networks possessing emergent properties resembling those of tissues, such as electrical signalling[86], folding[86], and light-activated protein expression[87]. However, these functionalities have yet to be realised in droplet networks stable in an aqueous environment[82] (see **Section 1.2.3**). Alternatively, if gelators are contained within the droplets, a solidified hydrogel matrix can be formed, whose patterning is based on the positions of droplets within the original network (see **Section 1.2.3**). By printing droplets containing live cells, this technology has application in the formation of cell-containing hydrogel-based microtissues, due to the high resolution patterning available to droplet printers[103]. Similarly, it was hypothesised that with the droplet printer, highly patterned responsive hydrogels could be fabricated. Here, the adaptation of the droplet printer for the formation of PNIPAm hydrogels is outlined.

4.1.1 Assembly of 3D droplet networks

Manual assembly techniques involving the use of micropipettes or syringes, such as those implemented in **Chapter 2** and **Chapter 3**, allow the straightforward assembly of small numbers (tens) of droplets, and remain useful for when only a few

copies of a particular designed network are desired[84]. Primarily, these techniques have been used to form 2D networks, but small 3D networks, comprising up to three layers of droplets, have also been assembled[88]. 3D droplet networks have also been assembled by incorporating paramagnetic beads into the droplets, and using a magnetic probe brought in proximity to the droplet for manipulation[88]; as well as with optical tweezers[89]. However, there is limited application of these techniques to the formation of large 3D structures, containing hundreds to thousands of droplets, and in cases in which many copies of a structure are required.

By automating droplet formation with microfluidics, large numbers of monodisperse droplets can be produced. However, although 2D and 3D droplet networks have been assembled in this way[91], patterning capabilities are limited, and networks are typically difficult to access or extract from within microfluidic devices as they are packed into capillary tubes[82]. To overcome these limitations, a droplet-based 3D printer was developed, able to produce precisely patterned droplet networks containing up to tens of thousands of pL droplets[86].

4.1.2 3D droplet printing setup

The droplet printer[86] comprised up to two stationary droplet generators, able to eject two types of aqueous droplet into a reservoir of lipid-in-oil **(Figure 4.1A)**. 3D droplet networks were assembled layer-by-layer, as the reservoir was moved in 3D by a micromanipulator, which was controlled by a computer. The reservoir, which could be made of PMMA or glass, was filled with lipid-in-oil, typically DPhPC (0.2 - 0.5 mg mL^{-1}, 0.2 – 0.6 mM) in 1:1 v/v hexadecane and silicone oil.

The droplet generator consisted of a glass nozzle protruding from a custom made PMMA chamber filled with printing solution, which also contained a piezoelectric transducer (piezo)[86] **(Figure 4.1B)**. The PMMA chamber was filled with up to 500 µL of printing solution, typically a buffered solution, which could also contain salts and dyes. It was possible to decrease the sample volume to a minimum of 3 µL for valuable samples, for example, containing the protein pore αHL. To do this, the PMMA chamber was instead filled with water, and a hexadecane plug was

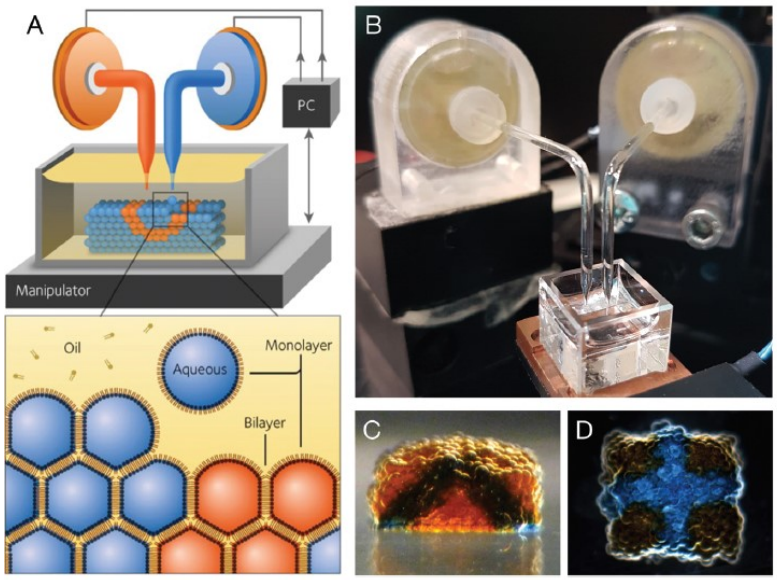

Figure 4.1: **(A)** Schematic of a droplet printer setup with two nozzles, printing an aqueous droplet network with two types of droplet[86]. **(B)** Photograph of the droplet generators and lipid-in-oil-containing reservoir[82]. **(C)** A patterned aqueous droplet network imaged from the side[86]. **(D)** A patterned aqueous droplet network imaged from the top[86].

drawn into the tip of the nozzle, before the smaller sample volume was then drawn into the nozzle. This hexadecane plug prevented mixing of the printing solution with the water filling the chamber. Overall control of the system was derived from custom-built computer software, able to trigger droplet ejection and synchronise it with micromanipulator motion, through use of a microcontroller. Droplet ejection was initiated via on-demand activation of the piezo by a driver unit, which would produce a pulse of up to 30 V. This pulse generated an acoustic wave causing the expulsion of a droplet from the end of the nozzle. After expulsion, droplets acquired a lipid monolayer in the lipid-in-oil, as they sank to the bottom surface of the reservoir, which could be made of PMMA or glass. Layer-by-layer assembly took place as a 2D map for each layer was read from a corresponding png image file. In the image files, droplets were represented by individual pixels colourised to reflect which of the printing nozzles were used for their ejection. The resulting droplet networks were patterned in 3D from two different droplet solutions **(Figure 4.1C-D)**.

There were a number of important considerations whilst printing[82,86]. Importantly, the droplet size (diameter: 10 - 200 µm; volume: 0.5 pL – 4 nL) was affected

by the magnitude of the voltage and length of the voltage pulse produced by the piezo. Droplet size and ejection was also dependent on the diameter of the nozzle, each of which was manually formed by hand-pulling a glass capillary, and on the fluid level within the PMMA chamber.

Spontaneous leakage of the printing solution from the nozzle could also occur, due to hydrostatic pressure (see **Section 4.4**). However, in general, this made printing unfeasible if the chamber of the droplet generator was positioned too much higher than the level of oil in the printing reservoir. In this case, leakage occurred in two phases[86]. In the first phase, which took several minutes, the fluid at the tip of the nozzle would protrude, with the aqueous-oil interface forming an approximately hemispherical shape. In the second phase, which occurred over a few seconds, the contents of the aqueous chamber emptied rapidly. If a droplet was ejected during the first phase, the interface between the printing solution and oil would become flat once more. This could be countered by the application of a particular voltage waveform, which did not cause droplet ejection. The typically used waveform was composed of three square pulses, with a length of 40 µs and amplitude of ~12V, each separated by a 20 ms interval. Subsequently, software improving the usability of the droplet printer has been developed by Dr Stuart Box[87,103], as well as several unpublished hardware modifications (see **Section 4.4.2**).

For the range of droplet sizes used, lipid monolayers were able to form within 1 second, allowing a typical droplet ejection rate of approximately 1 per second. As each lipid-coated droplet fell into place next to preceding droplets, a lipid bilayer formed between the two droplets over a finite time (typically 1 - 3 s[86]), and networks were built up accordingly. Theoretically, the structure of an ideal 3D printed droplet network would be a perfect hexagonal close packed lattice. In actuality, several obstacles preclude this. Viscous shear resulting from rapid printing speeds, and the force produced during ejection of a new droplet, could dislodge previously dispensed droplets that have not yet formed bilayers. However, this could be reduced by increasing the distance between the tip of the nozzle and the top layer of the printed network, adding delays during printing, or adjusting the densities of the droplets and

the printing oil used. In addition, as droplets were deposited on top of previously formed layers of droplets, edge droplets could roll down the sides of the network, due to the finite time required for a lipid bilayer to form and hold the droplet in place. Hence, the rate of formation of the bilayer was as important to the structure and stability of the network, as was the strength of the bilayer, with both factors dependent on the composition of lipid-in-oil used (see **Section 1.2.1**).

4.1.3 Functional materials from 3D printed droplet networks

The aqueous droplet networks in oil constructed with the initial printing conditions and setup (see **Section 4.1.2**) could be functionalised with membrane proteins, allowing communication via electrical signalling over a precisely defined path[86]. Programmed folding could also be designed into the networks, by patterning osmolarity gradients into the structures **(Figure 4.2)**[86]. However, later demonstrations of functional materials from 3D printed droplet networks have required modifications to the printing methodology. For example, a light-activated in vitro transcription translation (IVTT) system was encapsulated within 3D printed droplet networks[87]. Incorporating this system into the droplets resulted in a high concentration of proteins that destabilised the bilayers, resulting in droplet fusion. Consequently, lipids with PEGylated headgroups were used to counteract this.

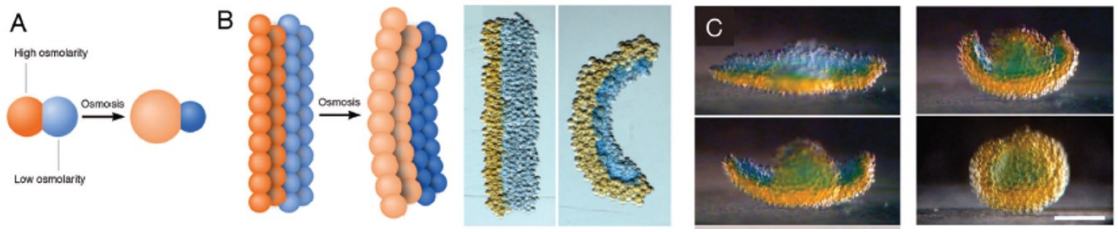

Figure 4.2: (A) In a droplet pair containing a droplet with a high salt concentration (orange), and a droplet with a low salt concentration (blue), water flows from the low osmolarity droplet to the high osmolarity droplet until osmotic balance is achieved. **(B)** 2D folding is caused by the osmotic flow of water in a droplet network. **(C)** 3D osmotic folding from a flower shape into a hollow ball. Scale bar, 200 µm. Reproduced from Villar et al.[86]

In initial studies on adapting the droplet printer for use as a bioprinter, cells suspended in a culture medium were also found to destabilise the networks[103]. Although stabilisation strategies and phase transfer methodologies were explored for cell-containing aqueous droplet networks, an approach in which hydrogels were incorporated into the printed networks as a scaffold was instead developed[103].

Importantly, the possible candidates for hydrogels incorporated into droplet-based systems are restricted to gelators whose crosslinking is triggered remotely, for example via temperature or UV[132]. An obstacle to chemically triggered gelation (e.g. via the addition of TMEDA and APS; or pH-mediated gelation of alginate) is the difficulty in introducing the initiator into the droplet network. Consequently, temperature-mediated, physically crosslinked gelators such as agarose have been chosen to fabricate cell-containing microtissues patterned using droplet networks[103].

In changing the printing solution from aqueous solutions to solutions containing gelators, certain modifications have been made to the printing process. For example, when using an ultra-low gelling temperature agarose, modification of the printing oil was necessary. Because the gelation temperature of agarose was below the freezing point of hexadecane (18°C), hexadecane was replaced with undecane, a structurally similar but lower density hydrocarbon (hexadecane, 770 mg mL^{-1}; undecane, 740 mg mL^{-1}). As a result, the proportion of silicone oil had to be increased to counteract the change in density of the oil mixture and ensuing increase in droplet sinking rate[132] (see **Section 4.1.2**).

Further unpublished modifications to the droplet printer in the Bayley lab have been made by Dr Linna Zhou to enable the printing of Matrigel. Matrigel is used due to its high suitability for use with specialised cell lines[133], and is liquid at low temperature (~4°C) and gels at physiological temperature[134]. As a result, one such modification was a temperature controller integrated with the droplet printer, which allowed printing at low temperatures. Another issue encountered whilst using Matrigel was its propensity for spontaneous leakage (see **Section 4.1.2**). Notably, the spontaneous leakage for Matrigel was much more severe in its rate and frequency compared to salt solutions previously used for printing. However,

leakage could be prevented with the use of narrow printing nozzles, whose inner tip surface was functionalised with (3-aminopropyl)trimethylsiloxane (3-APTMS). If the tip was not functionalised, oil infiltration, whereby oil was gradually able to creep up the inner surface of the nozzle, could occur. Finally, the high viscosity of the solution proved to reduce the efficacy of droplet ejection. A piezo driver with an increased voltage output of ±133V was built to address this by Dr Linna Zhou and the electronic workshop of the Chemistry Department, University of Oxford. The second generation driver enabled an increase in the possible force of the acoustic wave generated by the piezo.

4.2 Development of 3D printed droplet networks to form responsive hydrogels

Given the successful adaptation of the 3D droplet printer developed in the Bayley group to reproducibly form cell-containing microtissues, within a hydrogel matrix[103], it was hypothesised that the printing system might also be used to form responsive hydrogels templated by 3D printed droplet networks.

Chapter 2 described a novel fabrication method for responsive hydrogels, by templating from droplet networks formed from nL pre-gel droplets. These droplet networks could be assembled in one, two and three-dimensional geometries, as well as from multiple types of pre-gel. The resulting multi-material PNIPAm-based hydrogel structures could undergo reversible shape changes in response to a range of stimuli. It was initially hypothesised that the droplet printer could be used, similarly to nL droplets, to assemble 3D droplet networks containing NIPAm pre-gel, which could then be photopolymerized to form PNIPAm hydrogel structures (see **Chapter 2** and **3**). To achieve this, it was necessary to ensure the NIPAm pre-gel would be compatible for use with the droplet printer, such that it would allow reproducible formation of droplet networks containing pL droplets. In **Chapter 2**, a difference was observed between efficacy of gelation of single droplets and larger hexagonal structure. As a result, it would need to be determined whether the

NIPAm pre-gel networks produced by 3D droplet printing would be amenable to the photopolymerization process previously optimised for nL droplets (see **Chapter 2**).

This chapter demonstrates the optimisation of the 3D printer to allow the formation of NIPAm pre-gel networks from pL droplets, which could subsequently be photopolymerized into thermoresponsive continuous hydrogel structures. In preliminary experiments, parameters were chosen that had been used during experiments with manually assembled NIPAm pre-gel droplet networks. However, further optimisation of both the photopolymerization and printing processes were required due to a number of obstacles. Firstly, photopolymerization issues resulting from the reduced droplet size were addressed by introducing oxygen scavenging strategies into the fabrication process (see **Section 1.1.2**). Secondly, the NIPAm pre-gel was prone to rapid spontaneous leakage (see **Section 4.1.2**), so additional hardware was integrated to the printer to manage the hydrostatic pressure. Thirdly, different lipid and oil compositions, as well as additives to the printing solution, were tested to improve the stability of the networks. As a consequence of these modifications, PNIPAm hydrogels capable of reversible contraction could be formed from 3D printed droplet networks.

4.2.1 Printer setup and preliminary printing

In preliminary experiments, a printer setup with one droplet generator, was used as previously described (see **Section 4.1.2**), with two primary differences. Firstly, the second generation piezo driver built by Dr Linna Zhou, which was able to produce higher voltages if required, was used as standard. Secondly, the updated software (see **Section 4.1.2**) was also implemented. The **standard printing lipid-in-oil** chosen was the same 1:1 v/v mixture of hexadecane and silicone oil, containing 1.1 mM DPhPC, as the **standard lipid-in-oil** used for manual assembly of nL droplet networks (**Chapter 2** and **Chapter 3**). All pre-gels used in this chapter are listed in **Table 6.5**. For the printing solution, initially, NIPAm pre-gels were tested that had been successfully used to produce PNIPAm hydrogels when used

with nL droplet networks (0.76 M NIPAm with 7.5 mM MBA and 7.5 mM α-KGA; 1.53 M NIPAm with 13.6 mM MBA and 13.6 mM α-KGA). Upon beginning printing, two main obstacles were observed.

Firstly, due to spontaneous leakage of the NIPAm pre-gel solution from the nozzle, it was impossible to reproducibly print 3D networks comprising uniformly sized droplets. Rapid leakage of the NIPAm pre-gel could occur almost instantaneously upon immersing the nozzle in the oil reservoir, although this was variable between prints. Here, the formation of the hemispherical protrusion took seconds rather than minutes (see **Section 4.1.2**). One approach to counter this was ejecting droplets immediately upon submersing the nozzle. By beginning the automated print immediately after submersing the nozzle, it was possible to print networks with square bases **(Figure 4.3)**. The voltage waveform described in **Section 4.1.2** could also be utilised to prevent leakage during printing, depending on the rate of leakage in a given print, and the set delay before ejection of each droplet. For example, this waveform could be applied after each droplet was ejected, or after a row was finished, or after a layer was finished, as the nozzle returned to begin the next layer. However, these techniques were not always successful, and in some preliminary experiments, manually triggered droplets were ejected in rapid succession to form three dimensional, although irregular, droplet networks **(Figure 4.4A)**.

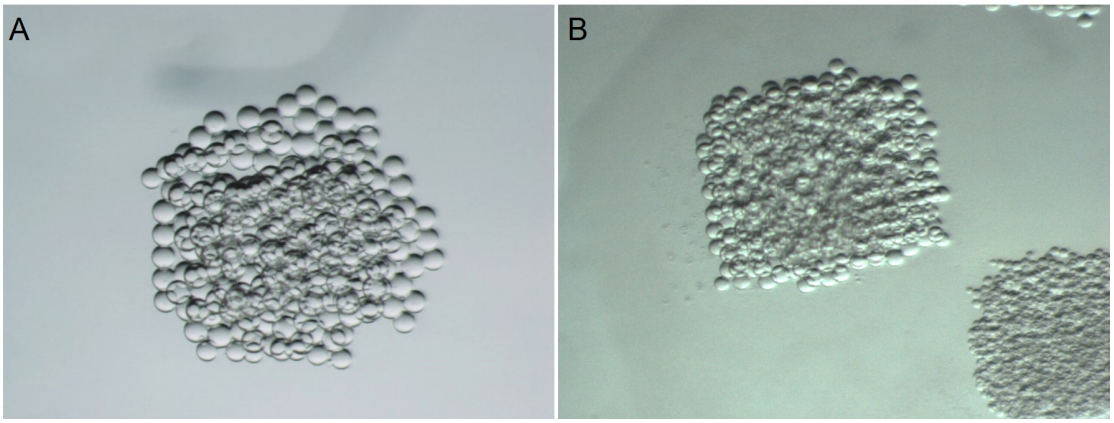

Figure 4.3: (A-B) Preliminary 3D printed droplet networks formed from NIPAm pre-gels. Typically, droplets formed were ~100 µm in diameter. See **Section 6.7**.

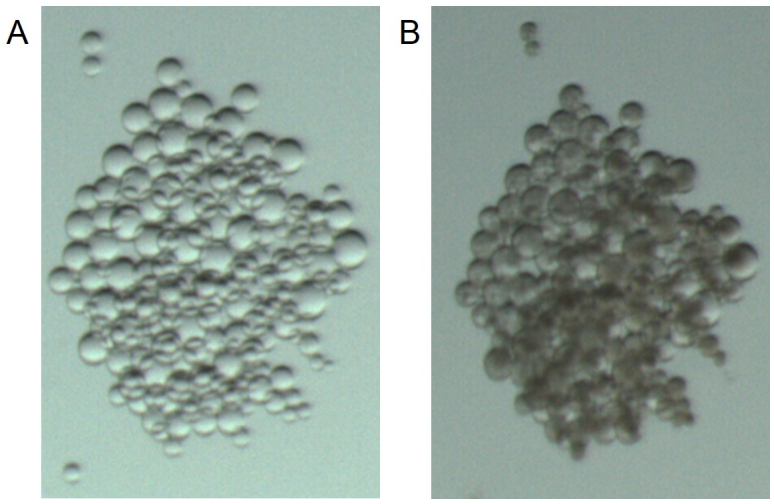

Figure 4.4: (A) A preliminary 3D printed NIPAm pre-gel droplet network after being subjected to UV irradiation. **(B)** The same network after heating to 42°C in an oven for 20 minutes, showing regions of polymer formation, rather than overall crosslinking. Typically, droplets formed were ~100 µm in diameter. See **Section 6.7**.

The second problem was encountered upon subjecting these printed networks to the photopolymerization process used for nL droplet networks. After UV irradiation, the structures appeared no different from a pre-gel droplet network **(Figure 4.4A)**, indicating that gelation had been unsuccessful. The bilayers were visibly intact, as the droplets were distinct from one another, indicating that a continuous structure was not formed. To demonstratively test whether polymerization had occurred, the structure was heated to 42°C. Although dark regions were visible in the microscope image, indicating that some polymer or gel formation had taken place in these regions **(Figure 4.4B)**, there was no overall size change of the network. Thus, despite using the same purging and photopolymerization steps that had resulting in successfully polymerized PNIPAm structures for nL droplets, a through-bilayer-crosslinked, solid PNIPAm hydrogel matrix was not formed when the printed networks were used instead.

4.3 Achieving gelation of printed NIPAm pre-gel droplets

Of the challenges impeding successful droplet printing of NIPAm, it was first decided to address the inadequate polymerization. Although spontaneous leakage precluded the reproducible formation of uniform 3D networks, it was possible to form irregular droplet networks with 3D regions. This would allow the testing of strategies to optimise polymerization on networks with a size regime and some structural features resembling target networks. Unlike nL droplets (see **Chapter 2** and **Chapter 3**), preliminary experiments on printed droplets showed that purging the environment surrounding droplet networks in oil was insufficient to allow the formation of hydrogel structures.

4.3.1 Printer-compatible oxygen reduction strategies

It was hypothesised that free radical polymerization in the smaller droplets produced by the printer would have a heightened susceptibility to oxygen inhibition, due to the droplets' increased surface area to volume ratio. For example, manually formed droplets, e.g. of approximately 50 nL volume, have a surface area to volume ratio of 13.1 m^{-1}; whereas printed droplets, e.g. 4 nL (approximately 100 µm diameter), have a surface area to volume ratio of 31 m^{-1}. Previous examples of responsive hydrogel structures with features hundreds of microns in size have required oxygen reduction approaches to successfully polymerize[42]. However, the strategy chosen to reduce oxygen inhibition needed to be compatible for use with the droplet printer. Pre-purging pre-gel solutions with an inert gas such as nitrogen or argon is a widely used method[22], but sustaining this minimised concentration of oxygen for steps downstream of solution preparation would be challenging for droplet printing. For example, the droplet printing setup requires constant exposure of both printing oil and printing solutions to air over a period of tens of minutes to hours. Although enclosed systems that can be purged of oxygen are available, such as gloveboxes and bags, preliminary experiments utilising the printer inside such a system (an Atmosbag^{TM}, Sigma-Aldrich) showed that this was impracticable **(Figure 4.5)**.

Figure 4.5: Operation of the droplet printer inside in an Atmosbag^{TM} (Sigma-Aldrich) was found to be impracticable. See **Section 6.7**.

4.3.2 Using glucose oxidase to scavenge oxygen

One widely used approach to reduce the concentration of oxygen inhibiting polymerization involves the use of oxygen scavenging molecules[22]. One such example is the enzyme glucose oxidase (GOx), which has been used to improve monomer conversion for thin films[135]. Glucose oxidase consumes glucose and oxygen, producing gluconolactone and hydrogen peroxide. When glucose and GOx were added to a UV-curable aqueous formulation containing poly(ethylene glycol) diacrylate (PEGDA), the monomer conversion during the formation of a thin film in ambient conditions was increased from approximately 25% to approximately 50% **(Figure 4.6A)**[135]. GOx has enhanced the polymerization of composite polyacrylamide- and PNIPAm-based composite hydrogel structures formed by extrusion printing **(Figure 4.6B)**[42]. In this example, structures were printed from a deoxygenated ink under ambient conditions, and rapidly cured by UV light for 200 s. Without GOx, printed features with dimensions of 200 µm could not be cured.

In a pilot experiment to test efficacy of enzymatic oxygen reduction, GOx and glucose were added to NIPAm pre-gels at concentrations that had resulted in successful polymerization in the literature[42]. These concentrations were 0.23% GOx and 3.8% glucose respectively. Hence, the concentrations tested were $\geq$ 230 U mL^{-1} GOx (equivalent to 2.3 mg mL^{-1}), and 211 mM glucose (equivalent to 38

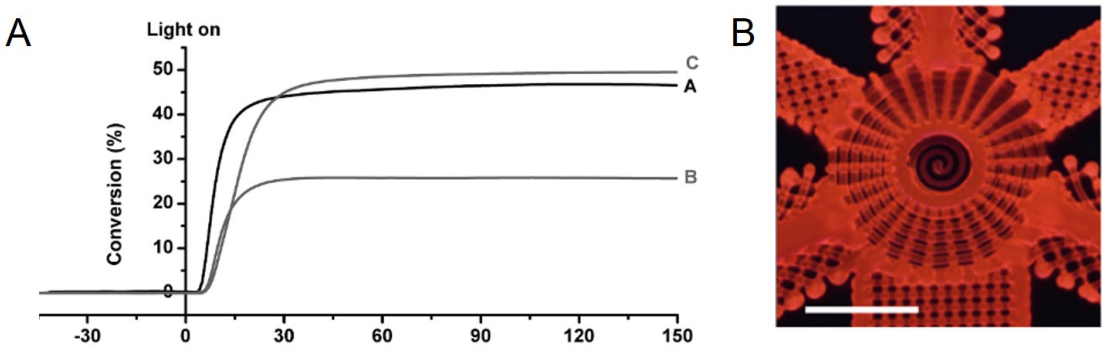

Figure 4.6: (A) Monomer conversion of a thin PEGDA film [A] with and [B] without GOx, compared to [C] under a nitrogen atmosphere. Reproduced from Oytun et al.[135] **(B)** Extrusion printed polyacrylamide-based composite hydrogel flower, reproduced from Gladman et al.[42] Scale bar, 5 mm.

mg mL^{-1}) respectively. The same NIPAm pre-gels which had been used for initial testing with the printer were utilised for this experiment, with a total volume of 250 µL (0.76 M NIPAm with 7.5 mM MBA and 7.5 mM α-KGA; 1.53 M NIPAm with 13.6 mM MBA and 13.6 mM α-KGA). Interestingly, when GOx and glucose were added to the vial containing the 0.76 M NIPAm pre-gel, a transparent PNIPAm hydrogel was formed in the vial within minutes **(Figure 4.7A)**, without UV light and irrespective of the ambient, oxygen-saturated conditions. Furthermore, for the vial containing the 1.53 M NIPAm pre-gel, within seconds of the addition of GOx and glucose, the solution began to turn an opaque white, indicating that polymerization had begun to take place[57]. A dense, opaque and solidified PNIPAm hydrogel was formed within minutes **(Figure 4.7B)**.

At these concentrations of GOx and glucose, polymerization was observed, which meant that the concentration of dissolved oxygen was sufficiently reduced. However, this polymerization was taking place independently of the UV-initiated breakdown of α-KGA. As a result, it would not be possible to use the droplet printer under these conditions, as the 1.53 M-containing NIPAm pre-gel would solidify before loading, whereas the rapidly increasing viscosity for the 0.76 M-containing NIPAm pre-gel would clog the nozzle. Hence, to be able to test NIPAm pre-gels containing GOx and glucose with the droplet printer, the concentrations of GOx and glucose would need to be lowered to slow the rate of premature polymerization, whilst still

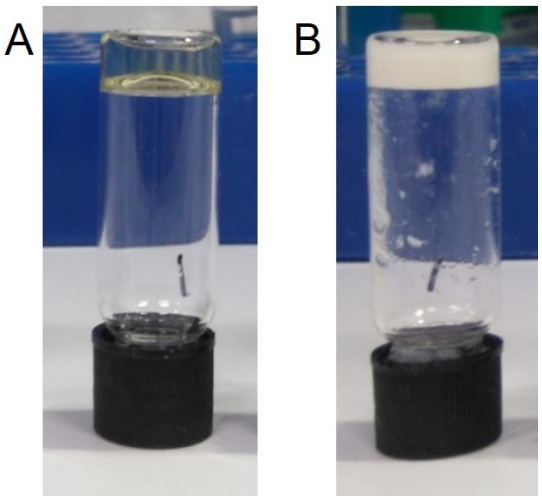

Figure 4.7: Premature gelation of bulk NIPAm pre-gels (250 µL) upon adding GOx ($\geq$ 230 U mL^{-1}) and glucose (211 mM) containing **(A)** 0.76 M NIPAm or **(B)** 1.53 M NIPAm. See **Section 6.7.3**.

Pre-gel	[GOx]	[Glucose]	Extent of gelation
1	$\geq$ 230 U mL^{-1}	211 mM	Gelation ($<$ 45 min)
2	$\geq$ 115 U mL^{-1}	106 mM	Gelation (1 hr 45 min)
3	$\geq$ 23 U mL^{-1}	21.1 mM	Gelation (1 hr 45 min)
4	$\geq$ 16 U mL^{-1}	10.5 mM	Partial gelation (1 hr 45 min)

Table 4.1: Effect of GOx and glucose concentrations on bulk gelation of 250 µL of 0.76 M NIPAm-containing pre-gel (containing 7.5 mM MBA and 7.5 mM α-KGA).

enabling photopolymerization after printing. For example, if the NIPAm pre-gel was still fluid 45 minutes after GOx addition, it might be compatible for use with the droplet printer. A range of concentrations of GOx and glucose were added to the 0.76 M-containing NIPAm pre-gel (see **Table 4.1**).

Given that NIPAm pre-gel (3) remained fluid for the first 45 minutes after GOx addition, it was subsequently tested with droplets in oil, to investigate its gelation efficacy for small droplets. Since printing was not yet optimised for leakage reduction, another method was needed to screen conditions. However, droplet formation with Hamilton syringes or pipetting would not be suitable, as droplets would not be of a relevant size to printed droplets. Instead, droplets in oil were formed by pipetting 5 µL of GOx-containing NIPAm pre-gel into 50 µL of lipid-in-oil, and briefly vortexing ($<$ 1 s). These emulsion droplets were then transferred by micropipette into wells of

a PMMA well array, where they formed an irregular droplet network. Although the size distribution of these droplets was visibly broad, it was possible to form smaller droplets than by pipette. In addition to this, droplet pairs with constituent droplets in the nL regime were formed via micropipette (~300 nL), which were expected to gel. After purging and photopolymerization, it was visibly apparent that the bilayer had ruptured for the nL droplet pair **(Figure 4.8A)**, indicating formation of a hydrogel matrix. Upon heating to 37°C, the droplet pair-templated PNIPAm hydrogel contracted **(Figure 4.8B)**. In contrast, there was no visible bilayer rupture for the UV-irradiated emulsion droplet network **(Figure 4.8C)**. Upon heating, very little change in appearance of the emulsion droplet network was observed, apart from some slight darkening of larger droplets **(Figure 4.8D)**. It was hypothesised that for 0.72 M NIPAm (pre-gel (3) in **Table 4.1**), a crosslinked hydrogel could not form in small droplets due to oxygen inhibition, despite the addition of GOx.

A higher concentration of NIPAm, 1.3 M, was instead tested, which contained 13 mM α-KGA and 13 mM MBA. Due to the more rapid polymerization rate of this higher concentration pre-gel, the GOx and glucose concentrations were lowered to $\geq$ 16 U mL^{-1} and 10.5 mM respectively. After purging and UV irradiation, the addition of GOx and glucose to the NIPAm pre-gel resulted in a hydrogel structure that appeared to be partially continuous **(Figure 4.9A)**. After heating above the LCST, the structure underwent an overall shape change **(Figure 4.9B)**, indicating that polymeric connections between droplets had formed. When the pre-gel did not contain GOx, although the formation of hydrogel regions upon UV irradiation was evident from the appearance of the structure **(Figure 4.9C)**, an overall shape change did not take place, as droplets contracted individually **(Figure 4.9D)**. This indicated that polymeric connections between droplets were not formed.

This pre-gel was then used with the droplet printer to print networks (hereafter denoted as **NIPAm printing pre-gel**). Despite issues with leakage, it was possible to print networks with square bases and more uniformly sized droplets (~90 µm diameter) using all of the previously described strategies (see **Section 4.2.1**), although this was not reproducible. Due to increasing viscosity resulting from

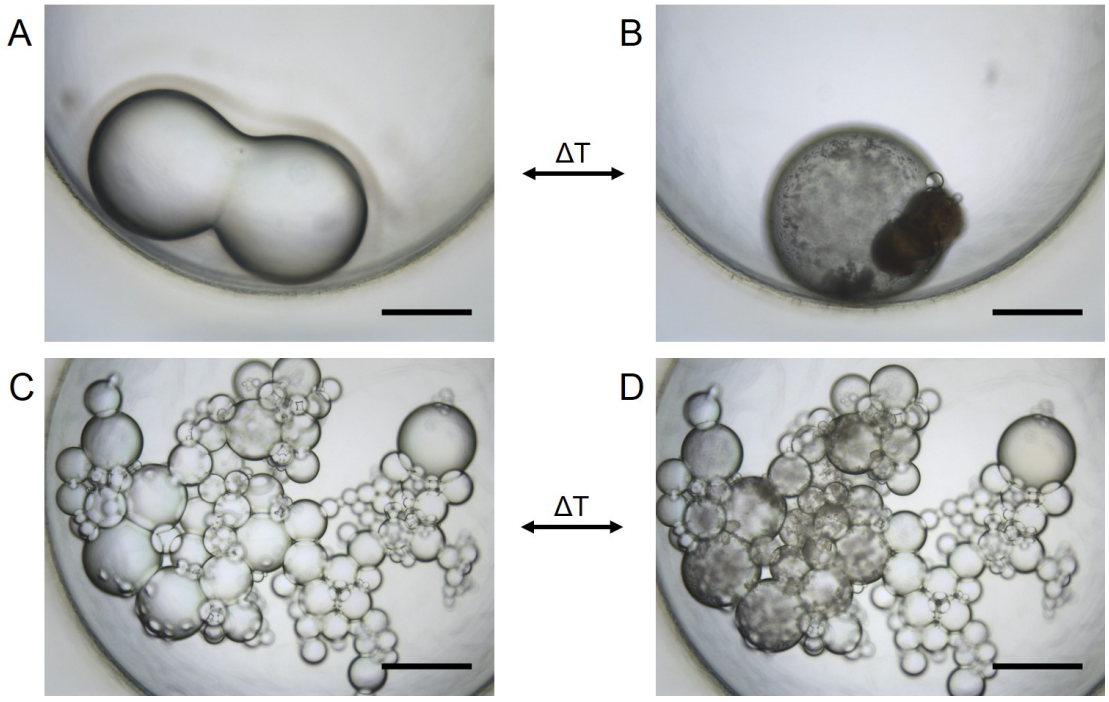

Figure 4.8: A droplet pair formed from the a GOx-containing NIPAm pre-gel (GOx at $\geq$ 23 U mL^{-1}; glucose 21.1 mM; 0.76 M NIPAm with 7.5 mM MBA and 7.5 mM α-KGA) **(A)** formed a continuous structure which **(B)** underwent an overall shape change upon heating above the LCST to 37°C. **(C)** An emulsion droplet network formed from the same pre-gel did not show visible signs of polymerization, and **(D)** upon heating above the LCST to 37°C, some regions darkened to indicate poor polymer formation. Scale bars, 250 µm. See **Section 6.7.4**.

premature polymerization, only a few prints were possible before the nozzle clogged. After purging and photopolymerization, unlike the emulsion-formed networks, visible hydrogel formation was not apparent **(Figure 4.10A)**. Upon heating above the LCST, there was no overall shape change or contraction of individual droplets. Instead, there was visible precipitation in central droplets as they darkened from their initial transparent appearance **(Figure 4.10B)**. This indicated that polymer formation had occurred in the droplets in the central region, rather than formation of a crosslinked hydrogel in any part of the structure. Remarkably, outer droplets remained transparent upon heating. It was hypothesised that an overall excess of oxygen had inhibited the polymerization throughout the pre-gel droplet network, exacerbated at the edge droplets due to diffusion of further dissolved oxygen from the oil. This effect likely counteracted the depletion of dissolved oxygen within the

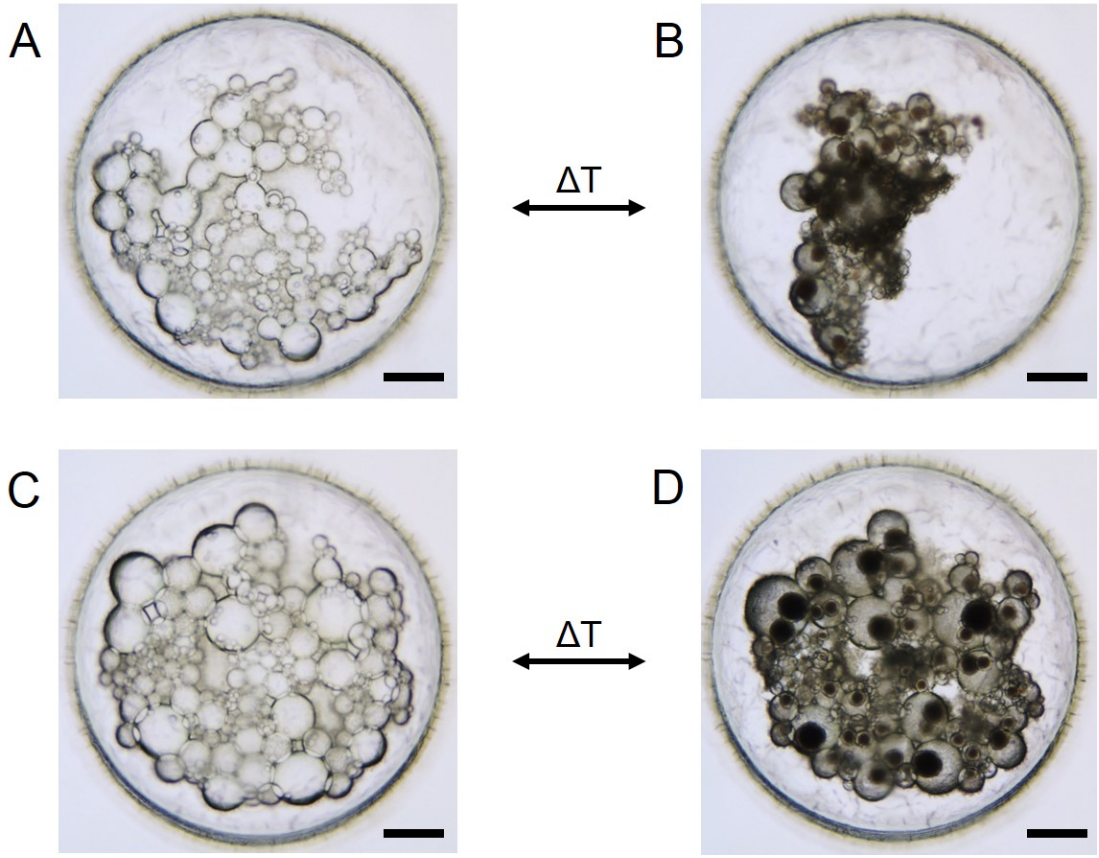

Figure 4.9: PNIPAm hydrogels formed from emulsion droplet networks, comprising droplets of heterogeneous sizes. When GOx was added to the NIPAm pre-gel, **(A)** a partially continuous hydrogel structure was formed which **(B)** underwent an overall shape change upon heating above the LCST to 37°C. **(C)** Without GOx, although hydrogel droplets were individually formed, **(D)** upon heating above the LCST to 37°C, droplets contracted individually and there was not an overall shape change. Scale bars, 250 µm.

pre-gel droplet network firstly by GOx, and additionally, by radicals generated at the beginning of photopolymerization (as discussed in **Section 1.1.2**).

4.3.3 Reducing the concentration of dissolved oxygen in the oil

To address oxygen inhibition **(Section 4.3.3)**, a degassing strategy was used to reduce the concentration of dissolved oxygen in the lipid-in-oil. Freeze-pump-thaw degassing was chosen, as it is considered one of the more effective strategies to remove dissolved oxygen for oxygen sensitive chemistry[136]. Once freeze-pump-thaw degassing of the lipid-in-oil was performed, printing was performed rapidly. This was firstly to minimise the time in which the oil was exposed to oxygen. The second

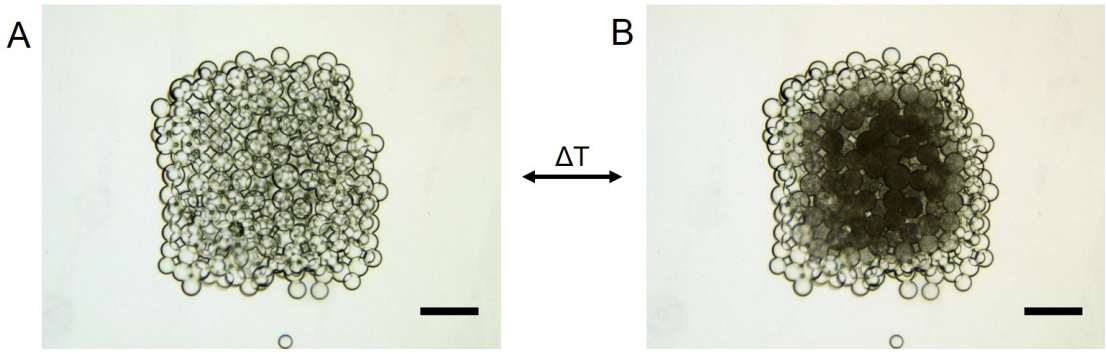

Figure 4.10: A droplet network printed with the **NIPAm printing pre-gel (A)** after irradiation with UV light and **(B)** after heating above the LCST (37°C). The darkened region had been oxygen-depleted due to consumption by GOx. Scale bars, 250 µm.

reason was the premature gelation of the GOx-containing NIPAm pre-gel, due to clogging of the nozzle. One difficulty arising from these factors was the short time window available to determine optimal printing parameters (such as voltage pulse amplitude and length) for a given print, which differed on every print. Moreover, in conjunction with the previously discussed problem of spontaneous leakage of the pre-gel into the oil (see **Section 4.1.2**), it remained challenging to form regularly shaped networks. If spontaneous leakage began to occur during an automated print, and applying the leak-countering voltage waveforms was unsuccessful, manually removing the nozzle from the oil reservoir forced the rapidly growing leaking droplet to bud from the nozzle, and printing could continue. However, droplets formed by leakage were typically substantially larger than those produced by a voltage pulse. Despite this, networks were printed which had three dimensional regions, and most constituent droplets in the networks had a diameter of ~130 µm. Subsequently, after purging and photopolymerization, a PNIPAm hydrogel structure had visibly formed from the NIPAm droplet network **(Figure 4.11A)**. Upon heating above the LCST, the entire structure underwent an overall shape change, and contracted **(Figure 4.11B)**. Not all droplets in proximity to this structure had become part of the continuous hydrogel structure, which was likely due to poor bilayer formation, due to the heterogeneity in droplet sizes and the irregular spacing between them. Upon cooling, the structure re-swelled to a shape

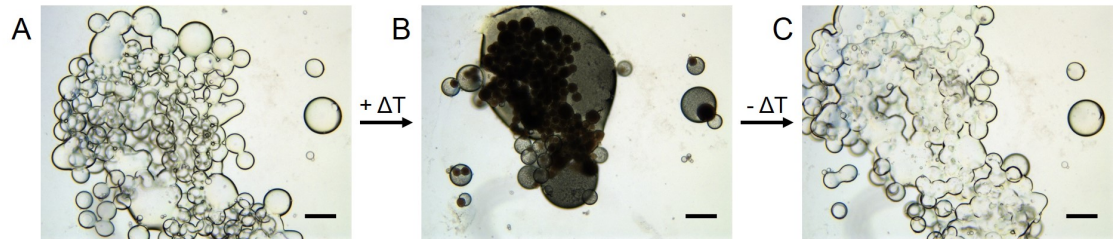

Figure 4.11: (A) A PNIPAm hydrogel structure printed in degassed lipid-in-oil with the **NIPAm printing pre-gel**. **(B)** When heated above the LCST, the structure underwent an overall contraction, expelling water in a large surrounding droplet. **(C)** The structure reswelled upon cooling to room temperature, taking up the expelled water. Scale bars, 250 µm. See **Section 6.7.5**.

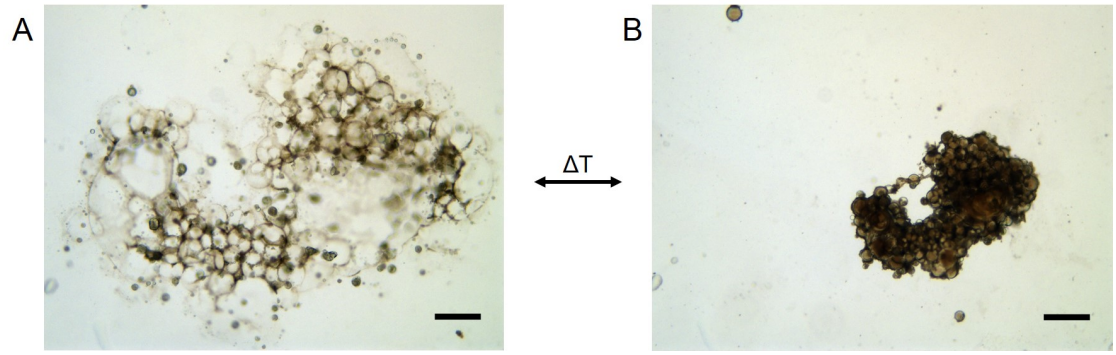

Figure 4.12: (A) A PNIPAm hydrogel structure printed in degassed lipid-in-oil with the **NIPAm printing pre-gel**, transferred into water. **(B)** The structure contracted uniformly when heated above the LCST. Scale bars, 250 µm. See **Section 6.7.8**.

with a slightly altered morphology, due to coalescences where the bilayers had not ruptured immediately after photopolymerization **(Figure 4.11C)**.

When the oil was then replaced with water, the hydrogel structures remained stable and swelled **(Figure 4.12A)**. Upon heating above the LCST, the structures underwent a uniform contraction **(Figure 4.12B)**, which was reversible upon cooling back to room temperature. The structure shown in **(Figure 4.12)** is a different structure, printed under the same conditions as that shown in **(Figure 4.11)**.

4.4 Reduction of NIPAm pre-gel leakage during printing

Now that the polymerization process had been optimised such that printed structures consisting of pL droplets could be gelled, the problem of rapid spontaneous leakage of

the NIPAm pre-gel needed to be addressed. Two approaches to do this were explored: functionalisation of the inner surface of the nozzles, and managing the hydrostatic pressure in the droplet generating system with an additional piece of hardware.

4.4.1 Nozzle functionalisation with 3-APTMS

Typically, a flat interface between the printing solution and the oil indicates desirable conditions for printing, with neither leakage, nor oil infiltration occurring. Upon immersion of a wider nozzle into the oil, rapid spontaneous leakage was typically observed **(Figure 4.13A)**. In contrast, narrow nozzles exhibited oil infiltration, which prevented droplet ejection, once the oil had infiltrated the nozzle to a certain height **(Figure 4.13B)**. Hence, as Matrigel had also exhibited these characteristics (see **Section 4.1.3**), the first approach investigated to reduce leakage of the NIPAm pre-gel was functionalisation of the tip of the inner surface of the nozzles with 3-APTMS, which had been successfully implemented to allow droplet printing with Matrigel. This functionalisation should result in hydrophilicity as the amino groups protruded from the surface. The protocol followed had been optimised by Dr Linna Zhou in unpublished work. Functionalisation of the inner tip of the printing nozzle was performed by dipping the narrow end of the printing nozzle into a 5% solution of APTMS in acetone, and allowing the nozzle to partially fill via capillary action. The tip was carefully wiped to minimise deposition onto its external surface. After ten minutes, acetone and ethanol were then used to clean the nozzle and remove residual APTMS. After cleaning, the nozzle could then be used as normal, and a flat interface was observed at the tip of the nozzle **(Figure 4.13C)**.

With the APTMS-functionalised nozzle, it was possible to form multiple networks in a printing session, with minimal disturbance from leaked droplets **(Figure 4.14A-C)**. Furthermore, the constituent droplets of these networks were of a homogenous size range compared to previous examples. Importantly, it was observed that the networks needed to stand for at least 5 minutes after printing, in order to form sufficient bilayers between droplets. Without this incubation time the network could break apart **(Figure 4.14C)**.

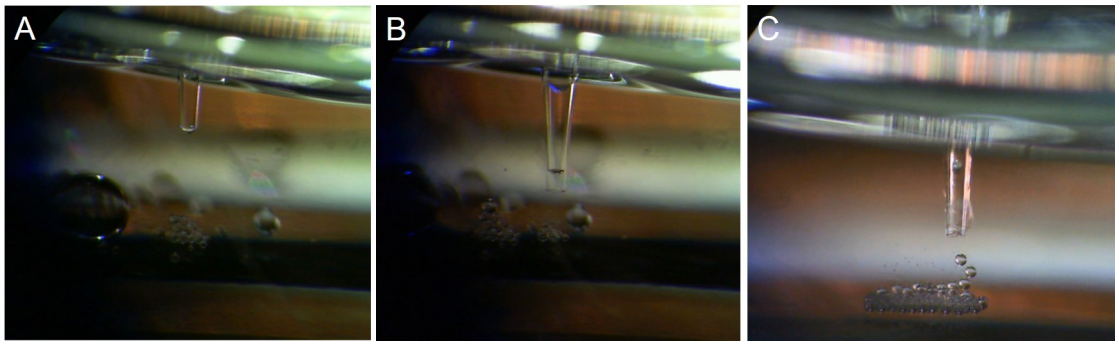

Figure 4.13: (A) Hemispherical protrusion from a leaking nozzle, with a large leaked droplet visible on the left. **(B)** Oil infiltration into the nozzle preventing droplet ejection. **(C)** Flat pre-gel/oil interface, suitable for printing.

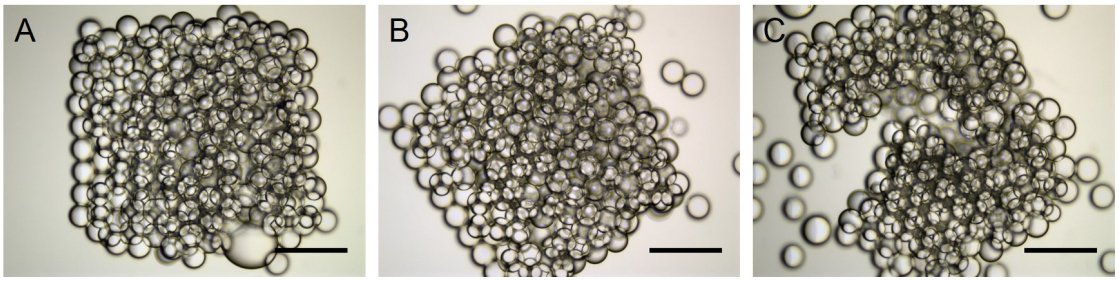

Figure 4.14: 3D printed droplet networks formed using the **NIPAm printing pre-gel** and with an APTMS-functionalised nozzle. **(A-B)** Networks with stably formed bilayers. **(C)** Broken network after insufficient bilayer incubation. Scale bars, 250 µm. See **Section 6.7.6**.

An additional observation from these **(Figure 4.14)** and previously printed **(Figure 4.3, 4.4, 4.9)** NIPAm pre-gel networks was the small bilayer size. For this reason, it was decided to test another lipid composition. In unpublished work by Dr Ravinash Krishna Kumar and Alessandro Alcinesio (a DPhil student, also of the Bayley group) it had been identified that the use of 1-palmitoyl-2-oleoyl-sn-glycero-3-phosphocholine (POPC) in addition to DPhPC in the lipid-in-oil results in increased contact angles formed between droplet pairs. This stronger adhesion between neighbouring droplets leads to more compact networks. As a result of this, in order to promote the formation of stable droplet networks with larger bilayers, the lipid-in-oil used for the following experiments contained a 1:1 mixture of DPhPC and POPC (final lipid concentration of 1.1 mM) in a 1:1 v/v mixture of hexadecane and silicone oil. However, complications arose from using this, which will be discussed in **Section 4.5**.

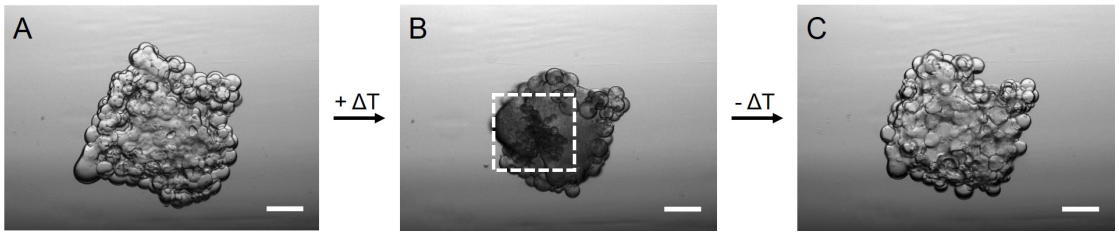

Figure 4.15: PNIPAm hydrogel structure formed from 3D printed **NIPAm printing pre-gel** networks in degassed oil with APTMS-functionalised nozzle. **(A)** Structure after gelation, **(B)** after heating above the LCST and **(C)** re-swollen after cooling to room temperature. White dashed box indicates contracted structure. Scale bars, 250 µm.

A 3D printed network was fabricated using the **NIPAm printing pre-gel** in the degassed lipid-in-oil with the APTMS-functionalised nozzle. After purging and photopolymerization, an approximately cuboidal PNIPAm hydrogel structure was formed **(Figure 4.15A)**. This structure partially contracted upon heating **(Figure 4.15B)**, before reswelling to approximately its original shape **(Figure 4.15C)**. As observed in **Figure 4.10B**, not all of the droplet network had become part of the interconnected hydrogel structure.

Despite the successful printing of multiple NIPAm pre-gel droplet networks, it was found that after the nozzle was used more than one or two times, gelled PNIPAm residue would be left on the inside of the tip. This residue was challenging to remove without a roughening agent such as sodium hydroxide, and the surface coating would need to be replaced. As a result, there was increased variability from the constant modifications to the nozzle. Furthermore, the efficacy of the surface modification was not reproducible, as leakage could still occur.

4.4.2 Modified droplet generator

An alternative approach to the functionalised nozzle, to address the issue of leakage, was an unpublished modified droplet generator designed by Dr Stuart Box to control the hydrostatic pressure on the fluid at the tip of the nozzle. This droplet generator comprised an extra water-filled reservoir affixed to a micromanipulator, attached via water-filled tubing to the PMMA chamber of a droplet generator, containing the piezo disk **(Figure 4.16A)**. By manually altering the z-height of the extra

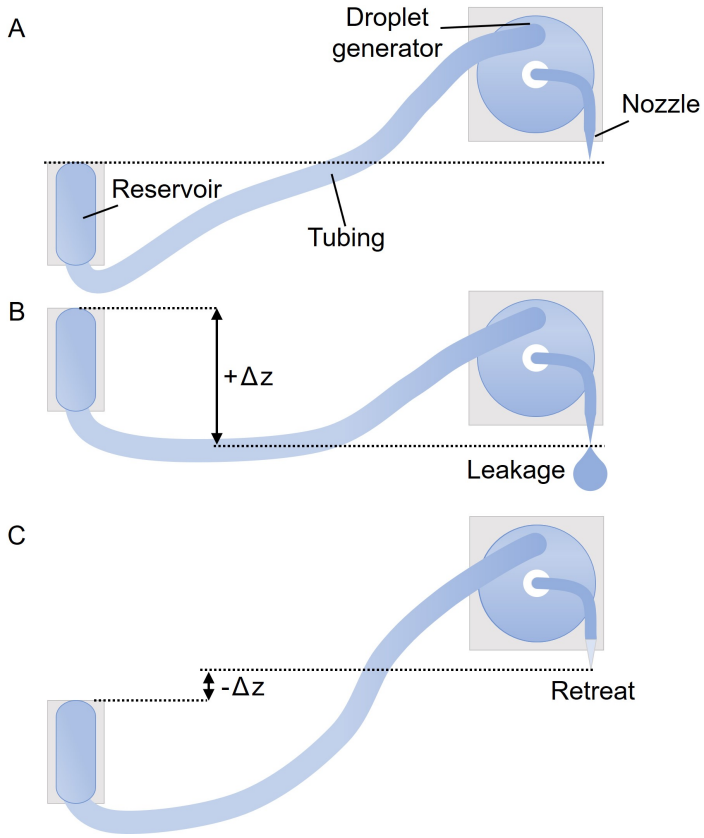

Figure 4.16: Schematic of modified droplet generator, where changing the z height of an additional reservoir lessens or increases leakage of NIPAm pre-gel solution from the nozzle. **(A)** When the top of the reservoir is aligned with the tip of the nozzle, there is no positive or negative pressure on the fluid in the nozzle resulting from the water in the reservoir. **(B)** When the top of the reservoir is at an increased z-height compared to the tip of the nozzle (+Δz), there is an additional positive pressure on the fluid in the nozzle and leakage is increased. **(C)** When the top of the reservoir is at a decreased z-height compared to the tip of the nozzle (-Δz), there is a negative pressure on the fluid in the nozzle and the fluid retreats up the nozzle. See **Section 6.7.7**.

reservoir above or below the tip of the nozzle, the hydrostatic pressure on the printing solution in the nozzle could be adjusted. With an increased z height of the reservoir, leakage would increase due to increased hydrostatic pressure **(Figure 4.16B)**. Alternatively, with a decreased z height, the leakage would decrease due to lessened hydrostatic pressure, which could also cause fluid to retreat up the nozzle when decreased by too much **(Figure 4.16C)**. Ideally, however, the interface would become flat (see **Section 4.4.1**).

Utilising the modified droplet generator yielded the most reproducible printing, and the same nozzle could be repeatedly used. A 3D printed droplet network,

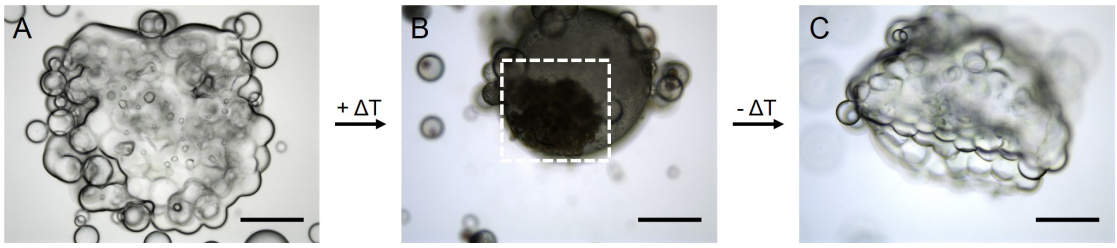

Figure 4.17: PNIPAm hydrogel structure formed from 3D printed **NIPAm printing pre-gel** droplet networks in degassed oil with the modified droplet generator. **(A)** Structure after gelation, **(B)** after heating above the LCST and **(C)** re-swollen after cooling to room temperature. Scale bars, 250 µm. See **Section 6.7.7**.

printed with the **NIPAm printing pre-gel** was photopolymerized and yielded a continuous hydrogel structure, in which the majority of the droplet network had become part of the interconnected structure **(Figure 4.17A)**. It underwent a reversible overall contraction upon heating to 42°C **(Figure 4.17B-C)**. During reswelling, the structure's orientation changed, such that a side view was visible. Due to the variability in the thickness of the structure (visible in **Figure 4.17C**), likely due to roll-off of droplets from the top layer of the network prior to gelation, a volumetric shrinkage ratio could not be calculated. Instead, a shrinkage ratio was calculated from the area of the base of the structure and found to be ~0.1.

This structure was transferred into an aqueous environment **(Figure 4.18A)**, where the same reversible contraction was performed **(Figure 4.18B-C)**. Excess polymerized material in the cuvette, as well as residual oil, were visible in these images.

4.5 Stability of printed networks

Although it was possible to photopolymerize continuous hydrogels by printing GOx-NIPAm in this lipid-in-oil **(Figure 4.15 and 4.17)**, some networks formed did not yield continuous hydrogels after photopolymerization. For instance, two networks fabricated in the same print yielded structures with dissimilar appearances after photopolymerization, with one forming a continuous hydrogel **(Figure 4.19A)**, and the other with a continuous sub-section, but primarily composed of single droplets **(Figure 4.19B)**. The poor polymerization exhibited by the network in **Figure**

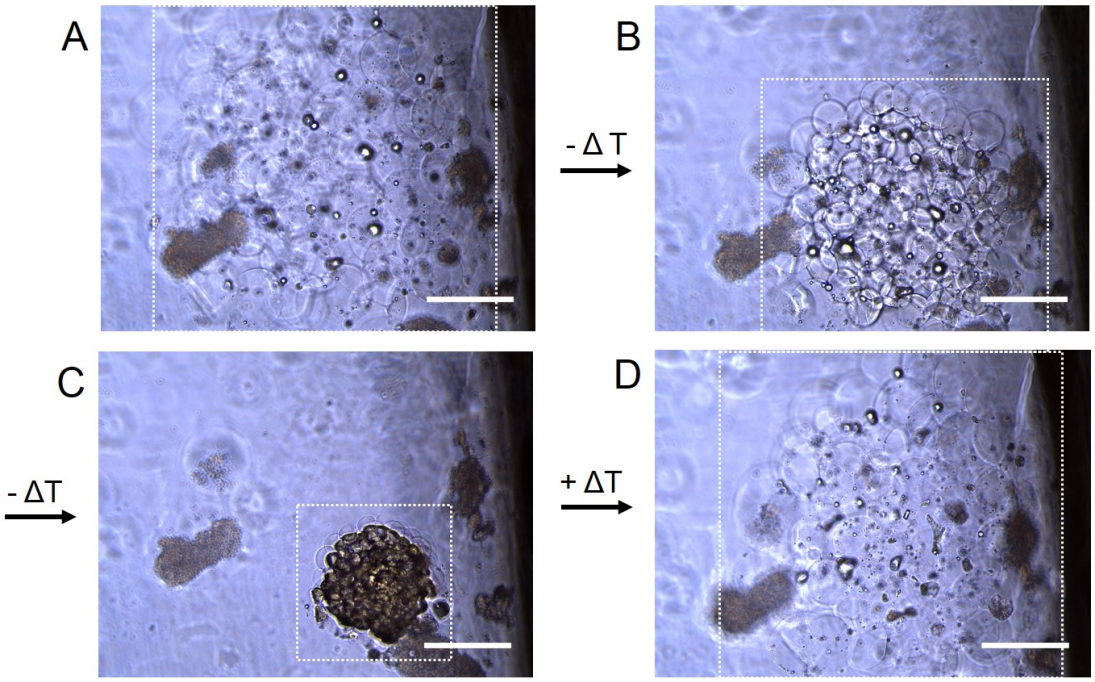

Figure 4.18: Phase transferred PNIPAm hydrogel structure formed from 3D printed **NIPAm printing pre-gel** networks, using degassed oil with the modified droplet generator. **(A)** Structure after transfer, **(B)** during contraction above the LCST and **(C)** fully contracted and **(D)** re-swollen after cooling to room temperature. Scale bars, 250 µm.

4.19B may have been due to heterogeneously dispensed pre-gel, resulting from its gradually changing viscosity and resulting clogging of the nozzle during printing due to premature polymerization. Interestingly, although this lipid combination had been adopted to try and improve packing in the networks, the droplets comprising the latter structure were connected to one another by very small bilayers. As well as the lipid-in-oil used, the contents of the droplets is known to be crucial for bilayer formation and strength[82]. Although in unpublished work from the Bayley group, the addition of POPC had been reported to increase bilayer size, it was unknown how this lipid would function with the NIPAm pre-gel as the droplet contents.

To investigate this further, droplet pairs were formed between nL NIPAm droplets in different lipid-in-oil mixtures. The **standard NIPAm pre-gel** was used instead of the **NIPAm printing pre-gel**, as the latter clogged in the Hamilton syringe. When **standard NIPAm pre-gel** droplets were formed in the 1:1 mixture of DPhPC and POPC (total concentration 1 mM) in 1:1 v/v of hexadecane and

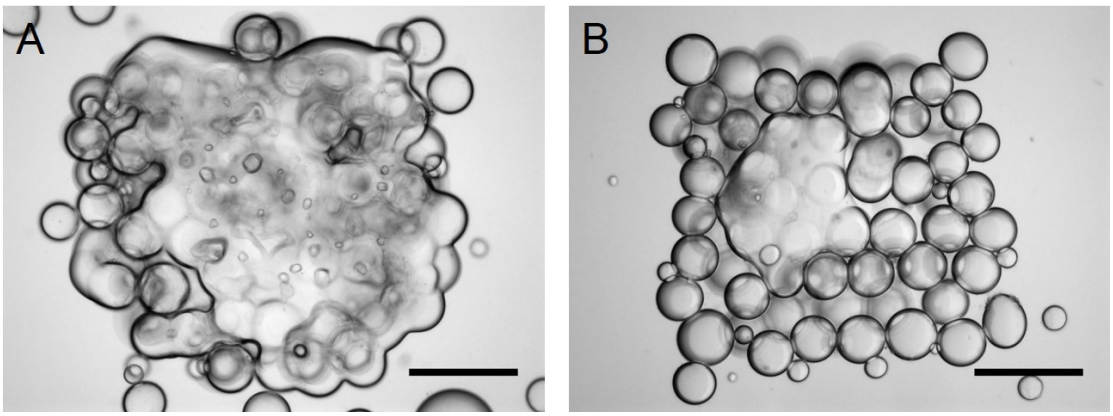

Figure 4.19: Two different printed structures after UV irradiation, fabricated from **NIPAm printing pre-gel** droplets. Both structures were printed in 1:1 POPC:DPhPC lipid mixture (1 mM total lipid concentration) in 1:1 v/v hexadecane to silicone oil. Scale bars, 250 µm. See **Section 6.7.9**.

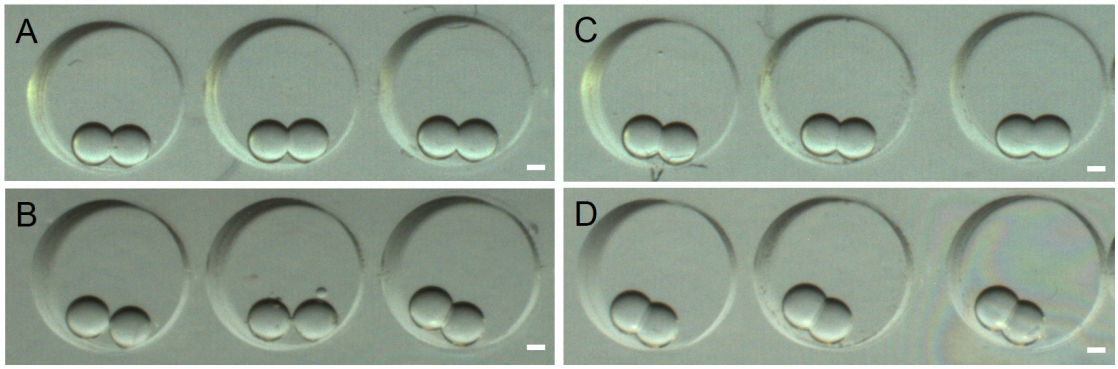

Figure 4.20: For **standard NIPAm pre-gel** droplet pairs, **(A)** bilayers formed easily when the lipid used was 1 mM DPhPC. In contrast, bilayer formation was inconsistent in **(B)** 1 mM of a 1:1 DPhPC:POPC mix. **(C-D)** However, if 50 mM Na_3PO_4 was added to the **standard NIPAm pre-gel**, bilayers appeared larger, and **(D)** formed more consistently. Three droplet pairs are shown to demonstrate differences in bilayer formation for **(B)**. Scale bars, 250 µm. See **Section 6.7.10**.

silicone oil, bilayer formation was much more inconsistent than if the same pre-gel was used to form droplet pairs in DPhPC (1 mM) with the same oils **(Figure 4.20A-B)**. It was hypothesised that if a buffer was added to the this pre-gel, it would facilitate bilayer formation. After adding 50 mM Na_3PO_4 to the standard NIPAm pre-gel, for the DPhPC only-containing lipid-in-oil, bilayers appeared larger **(Figure 4.20C)**. For the lipid-in-oil containing a 1:1 mixture of DPhPC and POPC, bilayers formed more consistently, as well as appearing larger relative to the bilayers formed in DPhPC-only oil **(Figure 4.20D)**.

To quantify this, a MATLAB script was implemented (see **Section 6.7.13**), which used a circle finding algorithm to locate the droplets. This script was modified from a script originally written by Oliver Meacock, a DPhil student in the Kevin Foster Group, University of Oxford. If a pair of droplets, with radii R_1 and R_2, were separated by distance L, the contact angle, θ, could be calculated according to **Equation 4.1**[137]:

$$\theta = \cos^{-1} \frac{L^2 - R_1^2 - R_2^2}{2R_1R_2} \tag{4.1}$$

The average contact angle for the **standard NIPAm pre-gel** was found to be 34.6 ± 0.5° for 1 mM DPhPC in a 1:1 v/v mixture of hexadecane and silicone oil **(Figure 4.20A)**. For 1 mM of a 1:1 mixture of DPhPC:POPC in 1:1 v/v hexadecane and silicone oil **(Figure 4.20B)**, only one bilayer formed from three pairs, with a calculated contact angle of 39.4°. However, if a buffer was added to the same NIPAm pre-gel (as previous, with 50 mM Na_3PO_4 added), the contact angles for the same lipid-in-oil mixtures were 43.0 ± 2.5° (DPhPC only) and 52.4 ± 1.8° (1:1 DPhPC:POPC).

This effect was also propagated to printed networks. A printed network of the standard NIPAm pre-gel in the 1:1 mixture of DPhPC and POPC yielded a structure with small bilayers **(Figure 4.21A)**. When 50 mM Na_3PO_4 was added to the pre-gel, the bilayers maximised to form a large, compact network **(Figure 4.21B)**.

4.6 Optimising the use of glucose oxidase

Given that only a few networks could be fabricated with each print due to clogging of the nozzle, it was important to solve the issue of premature polymerization. Interestingly, GOx has not only been utilised in polymer chemistry for oxygen scavenging, but also as a strategy to produce free radicals for polymerization[138,139]. In these examples, where GOx-mediated polymerization has been used in a signal amplification assay, free radical generation has been initiated with Fenton's reaction[138,139]. In the sequence of enzymatic reactions[138], β-D-glucose is first converted

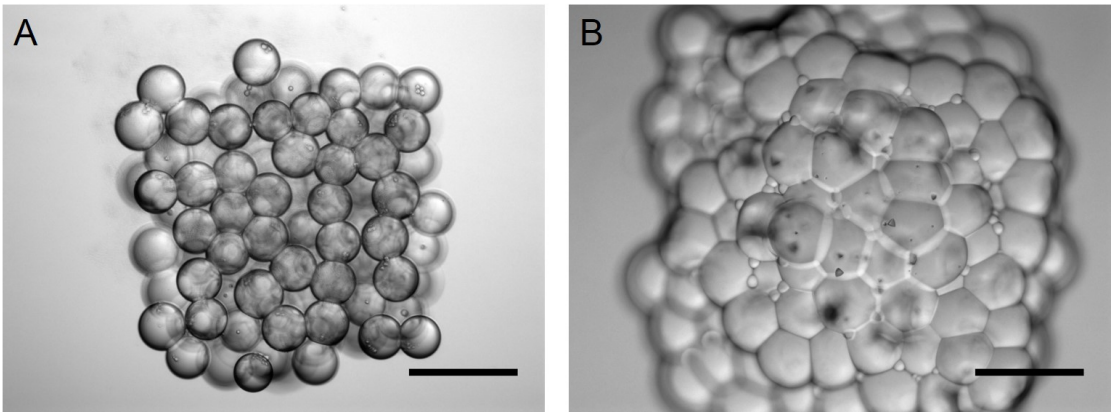

Figure 4.21: Bilayer formation in 3D printed droplet networks in a 1:1 mixture of DPhPC:POPC (final concentration 1 mM). **(A)** When the standard NIPAm pre-gel was used, smaller bilayers were formed than **(B)** when a NIPAm pre-gel containing 50 mM Na_3PO_4. Scale bars, 250 µm.

to δ-D-gluconolactone as GOx is reduced **(Equation 4.2)**. Molecular oxygen oxidises GOx and regenerates it, which produces hydrogen peroxide **(Equation 4.3)**. Hydrogen peroxide is converted to hydroxyl radicals in Fenton's reaction **(Equation 4.4)**[140], either via the addition of a ferrous salt[138] or due to trace amounts of metal ions[139]. The hydroxyl radicals generated can then initiate polymerization by activating monomers (M) to form propagating radicals (M·) **(Equation 4.5)**.

$$\beta\text{-D-glucose} + \text{GOx-FAD} \rightarrow \text{GOx-FADH}_2 + \delta\text{-D-gluconolactone} \tag{4.2}$$

$$\text{GOx-FADH}_2 + \text{O}_2 \rightarrow \text{GOx-FAD} + \text{H}_2\text{O}_2 \tag{4.3}$$

$$\text{H}_2\text{O}_2 + \text{Fe}^{2+} \rightarrow \text{OH}^- + \text{Fe}^{3+} + \cdot\text{OH} \tag{4.4}$$

$$\cdot\,\text{OH} + \text{M} \rightarrow \text{HOM}\cdot \tag{4.5}$$

When the trace metal ions, hypothesised to be the source of free radical generation, were removed with Chelex, a metal chelating resin, the polymerization resulting in signal amplification no longer occurred. When up to 50 ppb of iron or copper was subsequently re-added to the reaction mixture, polymerization was observed once more[139].

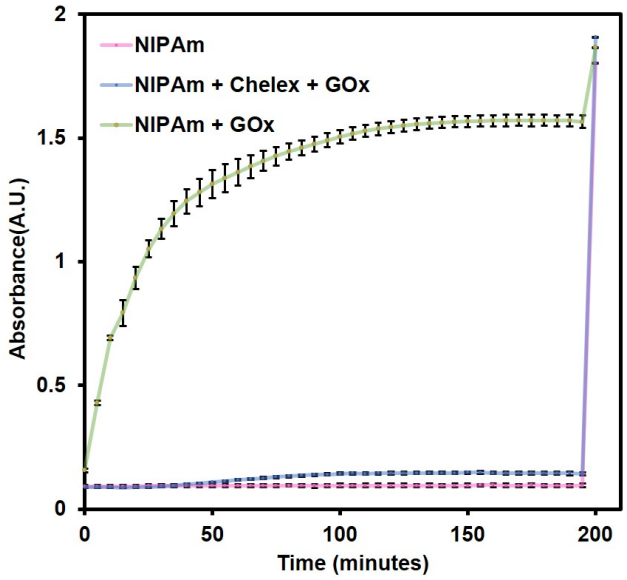

Figure 4.22: Absorbance of NIPAm pre-gels monitored over time. When GOx and glucose are added to the NIPAm pre-gel (green line), the absorbance increases over time. No change is observed for NIPAm (pink line) or NIPAm treated with Chelex, with GOx added (blue line). See **Section 6.7.11** and **Section 6.7.12**.

Based on these reported observations, it was hypothesised that trace metal ions present in the NIPAm pre-gels might be responsible for the premature polymerization upon addition of GOx and glucose, and that treatment of the NIPAm pre-gel with a metal chelating system would help prevent this. A Chelex column was used to remove metal ions from the **standard NIPAm pre-gel**, and its absorbance was monitored after adding GOx and glucose over 200 minutes. Simultaneously, the absorbance of the **NIPAm printing pre-gel**, containing GOx and glucose, and the **standard NIPAm pre-gel**, which did not contain GOx or glucose, were monitored. Premature polymerization in the **NIPAm printing pre-gel** resulted in a change in appearance from transparent to an opaque white **(Figure 4.22, green line)**. For the **standard NIPAm pre-gel**, which did not contain GOx or glucose, no increase in absorbance was observed **(Figure 4.22, pink line)**. However, when GOx was added to the Chelex-treated **standard NIPAm pre-gel**, there was little increase in absorbance **(Figure 4.22, blue line)**, relative to NIPAm pre-gel to which GOx had not been added. Upon irradiating the plate containing the samples for five minutes with UV light, the absorbance of all samples increased, to greater than 1.5.

4.7 Conclusion

In this chapter, the use of a 3D droplet printer to automate the fabrication of PNIPAm hydrogel structures templated by hundreds of droplets was described. To achieve this, adaptations were made to both the polymerization and droplet printing methodologies. To prevent rapid spontaneous leakage of the NIPAm pre-gel from the nozzle, additional hardware was used, which allowed the reproducible printing of uniform droplet networks. Strategies for oxygen scavenging, including the use of GOx, as well as the reduction of dissolved oxygen in the lipid-in-oil, were utilised in order to achieve successful gelation of pL droplets. However, the addition of GOx was found to cause premature polymerization via the presence of trace metals, which impeded reproducible printing. Subsequently, this was mitigated by treatment of the pre-gel with a chelating resin. Problems with network stability were also investigated, by examining bilayer formation with different lipid-in-oils and different pre-gel solutions.

To achieve improved, reproducible printing of 3D droplet networks, namely, networks that are uniform, cuboidal, and stable **(see Figure 4.1)**, optimised oxygen reduction and leakage prevention will need to be integrated. The formation of multiple networks in the same printing session must be achieved. Once the printing methodology is optimised, such that it is possible to print networks with monodisperse constituent droplets, the stability of the networks must be optimised. With monodisperse droplets, and an optimal combination of the lipid-in-oil and NIPAm pre-gel, a stable network base can be formed, allowing the formation of a well packed network.

It is envisaged that in future, this technology will be used to fabricate multi-material, multi-responsive hydrogels, from networks composed of thousands of droplets, and patterned to a resolution of tens of microns. To do this, gelation will first have to be optimised for additional NIPAm-based pre-gel solutions (see **Chapter 2** and **Chapter 3**). For example, stability of printed networks containing PEGDAAm or AuNPs will need to be examined. As in **Section 4.5** and in unpublished work from the Bayley group, the contact angle of droplet pairs can

be used to predict stability for printed networks. Finally, two or more nozzles, and therefore modified droplet generators, will be required to print networks from which multi-material hydrogels can be formed. Although modification of the nozzle surface was found to be inoptimal in the work demonstrated in this chapter, it may be useful to test the efficacy of other silanes, or revisit 3-APTMS, if the use of multiple modified droplet generators becomes impracticable.

5
Future directions

The development of new fabrication approaches to generate patterned, multi-material responsive hydrogels will aid their application in microscale soft robotic and biomedical devices. This thesis has described the development of a new fabrication approach from 2D and 3D droplet networks, aqueous droplets connected via lipid bilayers. With this droplet-templating approach, multi-material PNIPAm hydrogel structures capable of temperature- **(Chapter 2)** and light-controlled **(Chapter 3)** shape changes, and magnetically controlled locomotion **(Chapter 3)**, were fabricated. Furthermore, adaptations made to the droplet printing methodology have allowed the automated formation of 3D PNIPAm hydrogel structures, templated from droplet networks comprised of hundreds of pL droplets **(Chapter 4)**.

The gelation and printing processes were optimised in **Chapter 4** to generate 3D printed hydrogels from NIPAm pre-gel droplets. Beyond the progress already described, further optimisation will be required to successfully form multi-material responsive hydrogels, patterned to a resolution of tens of microns. Initially, the strategies outlined in **Chapter 4**, including oxygen minimisation, leak reduction, and stability optimisation, will need to be integrated. Following this, they will need to be used in conjunction with multiple nozzles to enable 3D, high resolution and multi-material hydrogel PNIPAm structures to be fabricated.

As droplet templating allows different pre-gels to be encapsulated within adjacent droplets, the gradient of temperature control, such as that described in **Section 3.4.2** could be further extended, by patterning domains with several different concentrations of PEGDAAm with the PNIPAm hydrogels. This would allow multiple distinct movements as the temperature is increased or decreased. Furthermore, there are many alternatives to the functional additives whose incorporation was outlined in **Chapter 3**. Plasmonic nanoparticles sensitive to other wavelengths of light could be incorporated, such as gold nanorods[55], reduced graphene oxide[73] or iron oxide nanoparticles[9], which are sensitive to near-IR light. The combination of gold nanoparticles **(Chapter 3)** and for example, gold nanorods, will generate PNIPAm hydrogels able to perform distinct movements under two different wavelengths of light. In addition to nanoparticles for photothermal control, other nanoparticles might be utilised to improve locomotion. For instance, platinum nanoparticles have been used in conjunction with PNIPAm for autonomous propulsion of polymeric stomatocyte-like capsules with LCST-regulated braking[113]. Droplet-templated PNIPAm hydrogels, containing platinum nanoparticles, would be able to propel themselves forward in addition to changing shape. Another avenue that may be of interest would be to replace the PNIPAm hydrogel matrix with a pH-[29], solvent-[29] or electrically-sensitive[71] hydrogel, to vary to external stimuli used to activate the hydrogel. Other water-soluble monomers compatible with photoinitiated free radical polymerization, should be readily substituted with NIPAm. For example, a pH-sensitive gel can be formed from hydroxyethyl methacrylate[72], whereas 2-acrylamido-2-methyl-1-propanesulfonic acid can be used to form an electrically sensitive gel[71].

In replacing traditional robotic mechanisms with small and soft tools, sub-millimetre 3D printed hydrogel structures are ideally sized for in vivo applications. For many in vivo applications, biodegradability may offer an advantage, and accordingly, labile bonds may be introduced in the polymer backbone or crosslinks[21]. Similarly, pH-sensitive hydrogels[72], or hydrogels sensitive to biological molecules such as DNA[61], may be more readily activated when access with visible light or an environmental temperature change is challenging.

An advantage of the use of droplet networks to template responsive hydrogels is that it will be possible to tailor the dimensions of their features to allow coupling to synthetic tissue-like materials[82,86,87], formed from droplet networks themselves. Such coupling might allow droplet networks to undergo rapid and reversible shape changes. Similarly, encasing droplet networks within a PNIPAm hydrogel, as has been demonstrated for an inert hydrogel[101], could allow temperature-controlled fusion of inner droplets. This would activate mixing and in-situ syntheses, followed by release of their contents.

Responsive hydrogels in general suffer from certain limitations for use in soft robotic devices. However, their use might be broadened by certain advances. For example, one obstacle is the weakness of hydrogels compared to other soft materials such as elastomers[122]. Possible approaches to improve mechanical performance include the formation of double network or nanocomposite hydrogels to improve strength and stretchability[42,57]. For example, alginate/polyacrylamide[59] and alginate/PNIPAm networks[141] with significantly improved mechanical properties have been previously demonstrated. As a result, a physical/chemical double network might be formed by incorporating a liquid alginate in the NIPAm pre-gel. Gelation of the alginate network could then be initiated via the oil phase after photopolymerization of PNIPAm[101]. Another approach to improve usability for soft robotic applications might be the bonding of these patterned hydrogels to elastomers[142].

The use of droplet-templating as a means to pattern responsive hydrogels has a number of key advantages over other fabrication approaches. For example, the functionality of devices such as soft actuators is limited by the lack of structural heterogeneity offered by current approaches[2]. As a result of the unique patterning capabilities made possible by compartmentalization within droplet networks, 3D patterning of multi-material structures will be possible to a resolution of tens of microns. This is in contrast to conventional methodologies, in which only layered sheets have previously been demonstrated. Furthermore, the state of the art in these approaches require multi-step fabrication processes with complex re-alignment

steps[9,61]. In contrast, droplet templating requires only assembly of the droplet network and its subsequent photopolymerization. This simple method, which has been realized for 2D and 3D patterning of multi-material responsive hydrogels, will open up possibilities for the design of miniaturised soft robotics, biomedical devices and other shape-changing soft materials.

6 Materials and methods

This chapter describes the experimental details of the work described in this thesis including materials and methods used for the experiments elaborated in **Chapter 2**, **3** and **4**.

6.1 Materials

Table 6.1: Reagents used throughout this work.

Reagent	Supplier
N-isopropylacrylamide (NIPAm)	Sigma-Aldrich, UK
methylene bis(acrylamide) (MBA)	Sigma-Aldrich, UK
α-ketoglutaric acid (α-KGA)	Sigma-Aldrich, UK
poly(ethylene glycol) diacrylamide	Sigma-Aldrich, UK
ethidium bromide bis(acrylamide)	Sigma-Aldrich, UK
1,2-diphytanoyl-sn-glycero-3-phosphocholine (DPhPC) (4ME 16:0 PC)	Avanti Polar Lipids
hexadecane	Sigma-Aldrich, UK
silicone oil AR20	Sigma-Aldrich, UK
chloroform	Sigma-Aldrich, UK

Continued on next page

Table 6.1 – *Continued from previous page*

Reagent	**Supplier**
Texas Red®-1,2-dihexadecanoyl-sn-glycero-3-phosphoethanolamine, triethylammonium salt (TR-DHPE)	Thermo Fisher Scientific
gold(III) chloride hydrate	Sigma-Aldrich, UK
sodium citrate tribasic dihydrate	Sigma-Aldrich, UK
poly(ethylene glycol) methyl ether thiol	Sigma-Aldrich, UK
Irgacure 2959	Sigma-Aldrich, UK
dimethyl sulfoxide (DMSO)	Sigma-Aldrich, UK
MagneHis^{TM} Ni-Particles	Promega, USA
glucose oxidase from *Aspergillus niger*, type VII	Sigma-Aldrich, UK
(3-aminopropyl)trimethylsiloxane	Sigma-Aldrich, UK
1-palmitoyl-2-oleoyl-sn-glycero-3-phosphocholine (POPC)	Avanti Polar Lipids, USA
Chelex® 100 resin	Sigma-Aldrich, UK
Dulbecco's Phosphate Buffered Saline (PBS)	Sigma-Aldrich, UK
Ultrapure MilliQ water	Merck Millipore, UK

6.2 Instruments

Table 6.2: Instruments used throughout this work.

Instrument	Supplier
7000.5 KH 0.5 µL syringe	Hamilton, USA
DMi8 inverted microscope	Leica, Germany
SP5 confocal microscope	Leica, Germany
Tokai Hit^{TM} TPX (Type HF) Thermo Plate	Leica, Germany
SZX10 upright microscope	Olympus, Japan
monoFab SRM-20 computer numerical control (CNC) machine	Roland, Japan
Cary 50 Bio UV-Visible spectrophotometer	Agilent
Fieldmaster lightmeter	Coherent, USA
PC-10 dual-stage glass micropipette puller	Narishige, Japan
3D droplet printer	Custom built (see **Section 4.1.2**)
Infinite M1000 PRO microplate reader	Tecan, Switzerland

6.3 Methods

6.4 General methods

6.4.1 NIPAm recrystallisation

NIPAm (~5 g) was added to hexane (~75 mL) in a conical flask and heated to boiling point whilst stirring. Once the NIPAm had dissolved, the solution was filtered whilst hot through filter paper (QL 100, Fisherbrand) into a conical flask to remove insoluble impurities. It was then left undisturbed for at least 30 minutes to allow crystallisation to proceed. If crystallisation had not taken place, a crystal of NIPAm was added to induce nucleation of crystal growth in the solution, before leaving undisturbed for another 30 minutes. Filter paper was trimmed to fit a perforated ceramic Büchner funnel, which was placed in a vacuum flask with a rubber bung to provide a tight vacuum seal. The contents of the flask were transferred into the Büchner funnel under vacuum to remove soluble impurities, and rinsed with ice cold hexane (~250 mL). To ensure that the crystals completely dried, they were transferred into a glass vial and placed in a desiccator for at least 30 minutes.

6.4.2 General procedure for preparation of NIPAm pre-gel

NIPAm, MBA and α-KGA were were individually dissolved in MilliQ water before combining to form the pre-gel solutions. Typically, NIPAm (271.7 mg, 2.4 mmol) was added to MilliQ water (1 mL) to yield a NIPAm stock solution (1.84 M, due to increase in volume); MBA (19.3 mg, 0.125 mmol) was added to MilliQ water (1 mL) to yield a MBA stock solution (125 mM), and α-KGA (95 mg, 0.65 mmol) was added to MilliQ water (1 mL) to yield a α-KGA stock solution (650 mM). The **standard NIPAm pre-gel** contained 90 µL of the NIPAm stock solution, 15 µL of the MBA stock solution, 2.5 µL of the α-KGA stock solution and 17.5 µL MilliQ water, resulting in a final concentration of 1.34 M NIPAm, 13.1 mM MBA and 13.1 mM α-KGA. The concentrations in other pre-gels used are listed in Table **6.3**, **6.4** and **6.5**.

6.4.3 Preparation of standard lipid-in-oil

DPhPC (25 mg, 29.5 µmol) was dissolved in chloroform. 5 mg aliquots of the dissolved DPhPC were transferred to glass vials, and the chloroform was evaporated by rotation under a gentle stream of nitrogen to form lipid films. The films were subsequently placed in a desiccator for at least three hours to ensure all residual chloroform was evaporated. To make a DPhPC lipid-in-oil stock, a 5 mg lipid film was dissolved in filtered hexadecane (500 µL). The DPhPC stock (typically 100 µL) was diluted with more filtered hexadecane (typically 400 µL), in addition to filtered silicone oil AR 20 (typically 500 µL). This resulted in the **standard lipid-in-oil**, which contained a final DPhPC concentration of 1.2 mM, and a final hexadecane and silicone oil composition of 1:1 v/v.

6.4.4 General nL droplet network formation

Droplets were formed in custom-made poly(methyl methacrylate) (PMMA) well arrays, produced using a computer numerical control (CNC) milling machine (monoFab SRM-20 Roland, Japan). Depending on the manual arrangement of the droplets in different shaped well arrays, arbitrary patterns could be formed. Typically, well arrays were filled with 175 µL of the lipid-in-oil. In each well, droplets of pre-gel solution were formed with a 0.5 µL syringe (7000.5 KH, Hamilton, USA). Droplet networks were then assembled by manually bringing droplets (50 nL, unless specified) into contact with one another and allowing bilayers to form at the interfaces, which happened within seconds. The capillary action of a gel-loading tip could be used to remove droplets, rearrange structures, and for 3D droplet placement. Further detail for assembly of droplet networks from nL droplets is provided in **Section 6.5** and **Section 6.6**.

6.4.5 Phase transfer of nL-droplet templated PNIPAm hydrogel structures

For single hydrogel droplets, each droplet was transferred via capillary action of a gel-loading pipette tip into the wells of a Lab-Tek® II Chamber Slide^{TM} 8-well

glass slide. 200 µL of water was then added to each well.

For larger structures formed in the 2x2 square and circular well arrays, oil was removed with a micropipette and carefully replaced with water.

For all other nL droplet-templated PNIPAm hydrogel structures, after photopolymerization, the surrounding lipid-containing oil was removed from the well array with a micropipette and 175 µL of fresh oil, containing no lipid, was added. This oil exchange was repeated a total of five times to further dilute the lipid. Two 1 µL droplets of water were then added to each well. These aqueous droplets were dropped on top of each hydrogel structure and allowed to coalesce, forming a hydrogel structure within an aqueous droplet. The surrounding oil was then removed and water was added, to first fill the PMMA wells, and then the whole chamber. The water was slowly added, in order to minimise disturbance of the gel structures.

6.4.6 Light and fluorescence microscopy

For brightfield microscopy performed on an upright microscope, an Olympus SZX10 was used. For brightfield and fluorescence imaging performed on an inverted light microscope, a Leica DMi8 was used with a 5x or 10x objective, unless otherwise stated. For confocal imaging, a Leica SP5 confocal microscope was used with a 10x objective.

6.4.7 Heating and cooling of structures

A Tokai Hit^{TM} Leica TPX (Type HF) Thermo Plate was used to heat the well arrays containing the hydrogel structures. Typically, the set temperature of the heat plate was initially adjusted to the desired temperature (typically 42°C, unless stated otherwise). Then, the temperature reported by the plate sensor was monitored until equilibrated at the desired temperature. For experiments heating the hydrogel structures in oil, contraction typically occurred within a minute of heating. However, due to the time taken for the water surrounding the hydrogel structures to reach the temperature reported by the plate sensor, at least 30 minutes were usually allowed before imaging the heated hydrogel structures. Upon cooling to room temperature,

the set temperature was adjusted to 25°C, approximately room temperature. Once the temperature reported by the plate sensor had equilibrated, 30 minutes were allowed for samples to cool down, before further imaging. See individual chapter methods for further detail.

6.5 Chapter 2 Methods

6.5.1 EBBA-NIPAm pre-gels

For the fluorescent EBBA-NIPAm pre-gel used in the hexagonal structures **(Figure 2.22)**, EBBA (2.5 mg, 5.0 µmol) was dissolved in water (1 mL) to yield an EBBA stock solution (2.5 mg mL^{-1}, 5.0 mM). A pre-gel was formed from NIPAm (0.72 M), MBA (7.1 mM), α-KGA (7.1 mM) and EBBA (0.1 mM). For the fluorescent EBBA-NIPAm pre-gels used to form single droplets in **Figure 2.14-2.16**, pre-gels were made with a constant concentration of EBBA (0.1 mM), whilst varying each of the other components: NIPAm (0.8-1.5 M), MBA (10-25 mM) and α-KGA (10-100 mM) (see **Section 2.2.3**).

6.5.2 ATTO-containing NIPAm pre-gel

For the experiment monitoring the diffusion of ATTO-488 after photopolymerization in **Figure 2.12**, a **standard NIPAm pre-gel** was made. An ATTO-488 stock was prepared by Alessandro Alcinesio, a DPhil student in the Bayley group. To make this stock, ATTO-488 was dissolved in DMSO at a concentration of 1 mM (1 µL) was diluted with water (9 µL), yielding a 100 µm ATTO-488 solution. 1.25 µL of the 100 µm ATTO-488 solution was added to the NIPAm pre-gel, resulting in an ATTO-NIPAm pre-gel containing a final concentration of 1 µM ATTO-488.

6.5.3 PEGDAAm-NIPAm pre-gels

PEGDAAm was added to the NIPAm pre-gel as a hydrophilic crosslinker, to modulate the LCST and swelling ratio of the resulting PEGDAAm-PNIPAm hydrogel. Typically, PEGDAAm (25 mg, 6.8 µmol) was dissolved in water (162

µL) to yield a PEGDAAm stock solution (42 mM). The **standard NIPAm pre-gel** was adjusted with the desired amount of the PEGDAAm stock and used for hydrogels in **Figure 2.23-2.28**. For the experiment varying the concentration of PEGDAAm in single droplets **(Figure 2.23)** concentrations of PEGDAAm used were 0 mM, 1 mM, 3 mM, 5 mM and 7 mM. NIPAm, MBA, α-KGA and EBBA concentrations were kept constant at 1.34 M, 13.1 mM, 13.1 mM and 0.1 mM respectively. For the differential contraction in a droplet pair-templated structure **(Figure 2.24-2.25)** and thermoresponsive curling hydrogels **(Figure 2.25-2.28)**, the PEGDAAm-PNIPAm hydrogel contained 8 mM PEGDAAm.

6.5.4 Pre-gels used in each experiment

Table 6.3: Pre-gels used in **Chapter 2**. **Standard NIPAm pre-gel**: 1.34 M NIPAm, 13.1 mM MBA, 13.1 mM α-KGA.

Figure	Description	Pre-gel
Figure 2.5	Single PNIPAm droplets	**Standard NIPAm pre-gel**
Figure 2.6	Single PNIPAm droplets	1.53 M NIPAM, 14 mM MBA, 14 mM α-KGA
Figure 2.7	Single EBBA-PNIPAm droplets	1.34 M NIPAm, 13.1 mM MBA, 13.1 mM α-KGA, 0.1 mM EBBA
Figure 2.8	PNIPAm droplets	**Standard NIPAm pre-gel**
Figure 2.10	PNIPAm droplet pair	**Standard NIPAm pre-gel**
Figure 2.11	PNIPAm droplet pair	**Standard NIPAm pre-gel**
Figure 2.12	PNIPAm droplet pair with ATTO-488 diffusion	**Standard NIPAm pre-gel**, ATTO-containing NIPAm
Figure 2.13	PNIPAm droplet pair	**Standard NIPAm pre-gel**

Continued on next page

Table 6.3 – *Continued from previous page*

Figure	Description	Pre-gel
Figure 2.14	Single EBBA-PNIPAm droplets (NIPAm variation)	0.8 - 1.5 M NIPAm, 20 mM MBA, 13.1 mM α-KGA
Figure 2.15	Single EBBA-PNIPAm droplets (MBA variation)	10 - 25 mM MBA, 1.34 M NIPAm, 13.1 mM α-KGA
Figure 2.16	Single EBBA-PNIPAm droplets (α-KGA variation)	10 - 100 mM α-KGA, 1.34 M NIPAm, 13 mM MBA
Figure 2.17	Chain, triangular and pyramidal PNIPAm structures	**Standard NIPAm pre-gel**
Figure 2.18	4-droplet PNIPAm chains	1.53 M NIPAm, 14 mM MBA, 14 mM α-KGA
Figure 2.20	Patterned hexagonal EBBA-PNIPAm and PNIPAm structures	PNIPAm: **Standard NIPAm pre-gel**; EBBA-PNIPAm: 1.34 M NIPAm, 13.1 mM MBA, 13.1 mM α-KGA, 0.1 mM EBBA
Figure 2.21	Hexagonal EBBA-PNIPAm and PNIPAm structure	As **Figure 2.20**
Figure 2.22	Hexagonal EBBA-PNIPAm structure	0.72 M NIPAm, 7.2 mM MBA, 7.2 mM α-KGA, 0.16 mM EBBA
Figure 2.23	Single EBBA-PEGDAAm-PNIPAm droplets	0 - 8 mM PEGDAAm, 1.34 M NIPAm, 13.1 mM MBA, 13.1 mM α-KGA
Figure 2.24-2.25	PNIPAm and PEGDAAm-PNIPAm droplet pair	PEGDAAm-NIPAm: 8 mM PEGDAAm, 1.34 M NIPAm, 13.1 mM MBA, 13.1 mM α-KGA NIPAm: **standard NIPAm pre-gel**

Continued on next page

Table 6.3 – *Continued from previous page*

Figure	Description	Pre-gel
Figure 2.26-2.27	PNIPAm and PEGDAAm-PNIPAm curling structures	PEGDAAm-NIPAm: 8 mM PEGDAAm, 1.34 M NIPAm, 13.1 mM MBA, 13.1 mM α-KGA NIPAm: **standard NIPAm pre-gel**

6.5.5 Extended droplet network formation

For structures made from between one and four droplets **(Figure 2.10-2.19)**, the PMMA well arrays used contained 4x4 circular wells, each of which was 1.5 mm in diameter. For hexagonal structures **(Figure 2.20-2.22)**, NIPAm pre-gel droplets and EBBA-NIPAm pre-gel droplets were assembled in a PMMA well array with 3x3 2 mm diameter circular wells, containing 175 µL of the lipid-in-oil stock. Upon filling the well with droplets, the structure would rearrange to form a hexagonal shape as the bilayers maximised. The structure was photopolymerized as previously described. Patterned hexagonal structures were formed and photopolymerized by David Lunn.

For self-folding structures **(Figure 2.26-2.28)**, NIPAm pre-gel droplets and PEGDAAm-NIPAm pre-gel droplets were assembled in a custom-made PMMA well array with 2x2 square wells with side length 8mm. Each well contained 150 µL of the lipid-in-oil stock. Droplets were ejected at the top edge of a well and rolled via gravity to the bottom edge, to allow for monolayer incubation before forming bilayers.

6.5.6 Monitoring bilayer rupture with diffusion of ATTO-488 dye

For fluorescent lipid-in-oil stocks, DPhPC (25 mg) was dissolved in chloroform (1 mL) to make a 25 mg mL^{-1} (29.5 mM) stock, and TR-DHPE (1 mg) was dissolved in chloroform (1 mL) to make an 1 mg mL^{-1} (0.72 mM) stock. These stocks were made by Dr Ravinash Krishna Kumar and Alessandro Alcinesio. 39 µL of the

DPhPC stock and 1.6 µL of the TR-DHPE stock were transferred to a glass vial, and the chloroform was evaporated under nitrogen and then desiccated as previously described, resulting in a lipid film. Hexadecane (500 µL) and silicone oil AR20 (500 µL) were added, to yield a final concentration of 1.2 mM DPhPC with 0.01 mol % TR-DHPE, and a final hexadecane and silicone oil composition of 1:1 v/v.

Droplet pairs were made from one NIPAm droplet and one ATTO-NIPAm droplet in a well array filled with 175 µL of the fluorescent lipid-in-oil stock **(Figure 2.12)**. After bilayer formation, 175 µL of DPhPC lipid-in-oil was added to dilute the free fluorescent lipid in the oil and thus reduce background fluorescence. A micropipette was used to gently displace the oil surrounding the droplets in the wells. After removing 175 µL of the lipid-in-oil in the well array, the dilution procedure was repeated five times to for optimal fluorescence background reduction. Fluorescence imaging of pre-gel droplets and photopolymerized structures was performed on a Leica SP5 confocal microscope with a 10x objective lens (HC PL FLUOTAR, Leica) with an overall laser power of 20%. All microscope settings were kept the same for images taken before and after UV.

6.5.7 Time-dependent temperature response of single PNIPAm droplets

To monitor shrinkage of single PNIPAm droplets in water over time **(Figure 2.8)**, the set temperature of the heat stage was first adjusted to 42°C and the plate sensor allowed to equilibrate. Three individual droplets were imaged using a time lapse, beginning from the plate temperature equilibration. Once the droplets had contracted to a minimum size (at approximately 21 minutes) the temperature of the heat stage was re-adjusted to room temperature. The time lapse continued as the droplets re-swelled, finishing after a total time of 38 minutes. Radii of the droplets were extracted using ImageJ and the MATLAB script described in **Section 6.5.13**.

6.5.8 Temperature response of small droplet network-templated PNIPAm hydrogel structures

The heating and cooling cycle was performed as previously described (see **Section 2.2.4**), multiple times over different days. Radii of the droplets comprising each structure were extracted using the previously described MATLAB script, and the shrinkage ratio was calculated when the structures were fully contracted and fully reswollen **(Figure 2.19)**.

6.5.9 Temperature response of hexagonal EBBA-PNIPAm and PNIPAm structures

Hexagonal structures which had contained 1.34 M NIPAm were heated in oil, and were allowed 20 minutes for contraction **(Figure 2.21)**. FIJI was used to measure dimensions of the hexagonal structure, including the area of the base, and the diameter of individual droplets. The volume was estimated by multiplying the area of the base by the diameter of an individual droplet. Hexagonal structures which contained 0.72 M NIPAm were heated as previously described. Fluorescence microscopy settings were kept the same throughout the experiment **(Figure 2.22)**. Fluorescence intensity plot profiles were generated with FIJI (ImageJ). Lines used to generate the profiles were of the same length and were drawn across the same region of the structure. The same approach was then used to measure dimensions and estimate volumes.

6.5.10 Temperature response of PEGDAAm-PNIPAm single droplets

PEGDAAm-NIPAm pre-gel droplets with different concentrations of PEGDAAm were formed in individual wells, and photopolymerized and phase transferred into an 8-well glass slide as previously described. The volume of water in all of the wells was kept constant at 200 µL. A temperature probe (Tokai Hit^{TM} Leica TPX (Type HF) Thermo Plate) was placed in a control well which contained the same volume of water as the wells in which the samples were placed. To monitor their shrinkage at

different temperatures, the temperature was adjusted, and left for approximately 15 minutes to equilibrate. Once the readout from the temperature probe had reached a constant temperature, the droplets were allowed an extra 20 minutes to allow for any change in volume to take place. Fluorescence imaging was performed on the Leica DMi8 inverted microscope. For the radii data, at least three individual droplets were imaged for each PEGDAAm concentration at each time. Radii of the droplets were extracted using the previously described MATLAB script, and used to calculated shrinkage ratios **(Figure 2.23)**. The fluorescence images shown in **Figure 2.7** were also of droplets monitored this way, which contained no PEGDAAm.

6.5.11 Temperature response of structures containing PNIPAm and PEGDAAm-PNIPAm

NIPAm and PEGDAAm-NIPAm pre-gel droplet pairs **(Figure 2.24-2.25)** and bilayer strips **(Figure 2.26-2.27)** were assembled, photopolymerized and phase transferred as previously described. The heat stage was used as previously described whilst imaging fully contracted structures. For curvature data, images of three curling structures were taken over a 29 minute period. The plate sensor was allowed to equilibrate to 42°C before imaging as previously. When heated to 42°C, the resulting concentration of PEGDAAm in the droplets increased the LCST and decreased the swelling ratio such that it behaved as an inert gel with a minimal temperature response, resulting in curling as the PNIPAm droplets shrunk. The temperature was then reduced to room temperature after the structure had reached a maximum curvature (approximately 15 minutes). Curvature data were extracted from images of the structures at each temperature using the previously described MATLAB script **(Figure 2.28)**.

6.5.12 Image processing

Image processing, including image segmentation with thresholding, and radius of curvature analysis, was performed with custom scripts written utilising the MATLAB Image Processing toolbox (see **Appendix A.1**, **A.2** and **A.3** for code),

as well as FIJI (ImageJ). Extracted data enabled the analysis of hydrogel droplet radii, and hydrogel bilayer strip curvature.

6.5.13 Radii extraction methodology

To extract radii from images, first, FIJI was used to convert images from the .lif file into .jpgs. These were read into MATLAB, where they could be thresholded using an inbuilt function, creating a binary image in which any droplets present were distinct from the background (see **Figure 6.1**). FIJI could also be used to threshold the image. For either type of thresholding, the binary image was compared with the original image to ensure that the region analysed was approximately the same size as was visible in the original image. Then, an inbuilt function that could analyse properties of image regions was used to extract the approximate radius of each droplet in pixels. This could then be converted into microns, using the scale from the original image's metadata, and used as is. Alternatively, it could be used to calculate a shrinkage ratio, based on the fully swollen radius of the droplet.

6.5.14 Curvature extraction methodology

An upright microscope was used to image the curling structures, which did not store the associated metadata such as scale. As a result, FIJI was used to set the scale, based on the approximate size of the well (8 mm sides for square wells; 4 mm diameter for circular wells). The .jpgs were read into MATLAB, and an inbuilt function was used to select points along the PNIPAm region. The points were selected at the centre of each droplet, and the coordinates of each point were stored. Then, a circle was fitted to the set of coordinates which had been stored, using an open source function. This function[143] was based on a method originally devised by U. M. Landau[144] and later developed by Chan and Thomas[145]. The circle could be plotted on the image (see **Figure 6.2**), allowing verification of the fit. The corresponding radius of curvature was saved, and converted into millimetres. From this, the curvature was calculated from the reciprocal of the radius of curvature.

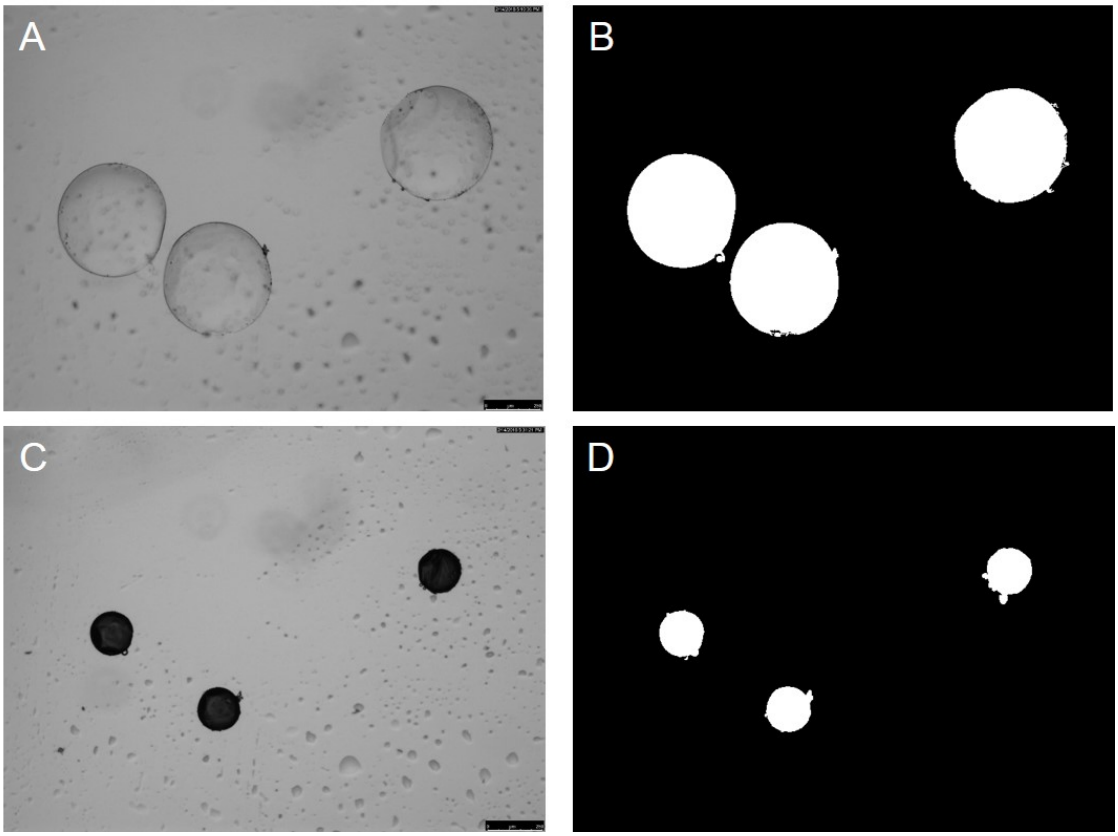

Figure 6.1: **(A)** Brightfield and **(B)** thresholded images of three PNIPAm hydrogel droplets at room temperature. **(C)** Brightfield and **(D)** thresholded images of the droplets once fully contracted, after heating to 42°C.

6.6 Chapter 3 Methods

6.6.1 Synthesis of AuNPs using Bunte salts as ligand precursors

A previously reported Bunte salt synthetic procedure[128] was used to synthesise the ligand precursor by George Klemperer.

6.6.2 Synthesis of AuNPs using citrate reduction procedure

Citrate-stabilised AuNPs were synthesised by Dr David Lunn. In aqua regia cleaned glassware, a solution of gold(III) chloride hydrate (20 mg, 0.06 mmol assuming anhydrous) in water (50 mL) was stirred and heated to 100°C. A solution of sodium citrate tribasic dihydrate (60 mg, 0.20 mmol) in deionised water (1.2 mL, 50 mg

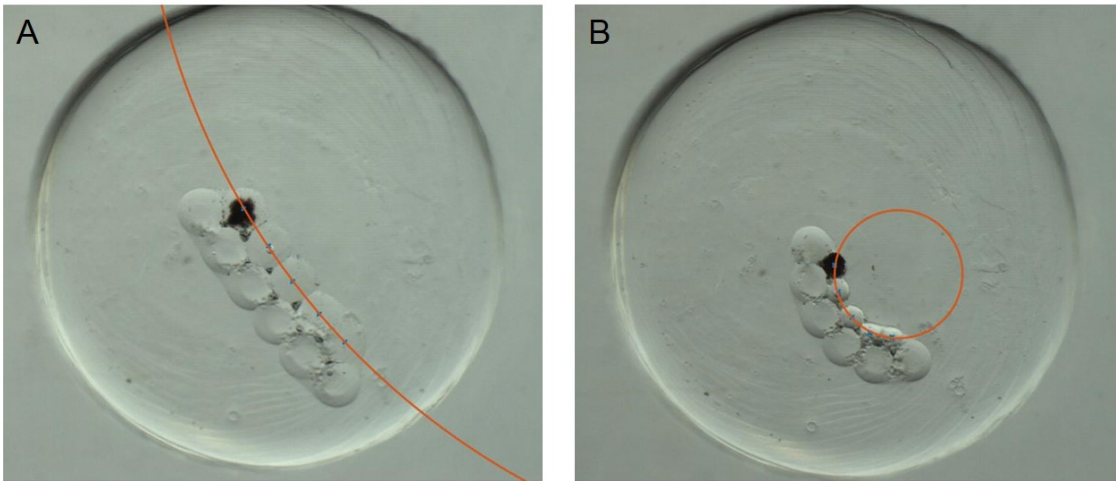

Figure 6.2: Brightfield images of the curling structures shown in **Figure 3.19** with overlaid circle (orange line) fitted using the script described in **Section 6.5.14**. The structure is shown at **(A)** 25°C and **(B)** 35°C.

mL^{-1}) was added in one portion. The reaction was stirred for 30 minutes at 100°C, over which time it changed colour from pale yellow to ruby red. The reaction mixture was allowed to cool to room temperature and transferred to a refrigerator for storage. Assuming a complete synthesis reaction due to the excess of reducing agent used, the final concentration of AuNPs in the dispersion was taken to be 0.4 mg mL^{-1}. The λ_{max} was determined to be approximately 523 nm by UV-Vis spectroscopy.

6.6.3 UV-Vis spectroscopy of AuNPs

The absorbance of AuNPs in solution was monitored using a UV-Visible spectrophotometer (Cary 50 Bio, Agilent, USA). For measurement of the synthesised AuNPs, 100 µL of citrate-stabilised AuNPs dispersed in water was diluted with 900 µL water in a polystyrene cuvette (Fisherbrand, UK). For stabilised AuNPs, 100 µL of citrate-stabilised AuNPs were stabilised, the residual PEG_{800}-SH was removed, water was added to the remaining quantity of AuNPs to result in a final volume of 1 mL. For the AuNP-NIPAm pre-gel sample, 100 µL of an AuNP-NIPAm pre-gel which contained PEG-stabilised AuNPs was diluted with 900 µL water. Differences in absorption maxima could be attributed to loss of AuNPs during washing steps of the stabilisation process.

6.6.4 Stabilisation of AuNPs

PEG_{800}-SH (20 mg, 25 µmol) was dissolved in water (200 µL) to yield a PEG_{800}-SH stock solution (100 mg mL^{-1}, 125 mM). 160 µL of the PEG_{800}-SH stock solution was incubated with 500 µL of the dispersion of AuNPs for 1 hour. Following incubation, the solution was centrifuged at 21000 rpm for 15 minutes to collect the PEGylated AuNPs. After removing the supernatant, the collected PEGylated AuNPs were washed twice with 500 µL of water to remove any unreacted PEG_{800}-SH, centrifuging for 30 minutes and removing the supernatant after each wash. This resulted in between 10-20 µL of the PEGylated AuNP suspension. Lower equivalents of PEG_{800}-SH resulted in incomplete stabilisation of the nanoparticles. The λ_{max} after PEGylation was determined to be approximately 524 nm by UV-Vis spectroscopy.

6.6.5 AuNP-NIPAm pre-gel

For AuNP-containing hydrogels, Irgacure 2959 (30 mg, 0.13 mmol) was dissolved in DMSO (30 µL). Irgacure 2959 was used as an additional photoinitiator, to counteract disruption of polymerization by the AuNPs. 1 µL of this was diluted in 19 µL water, resulting in a solution of 5% w/v Irgacure 2959. The previously described quantities of NIPAm and MBA stock solutions were added to the collected PEGylated AuNPs along with 5 µL of the 5% w/v Irgacure 2959 solution.

6.6.6 Pre-gels for dual-temperature responsive and magnetically responsive hydrogels

To form the dual-temperature and magnetically responsive hydrogels, two PEGDAAm-NIPAm pre-gels were used, containing different concentrations of the hydrophilic cross-linker PEGDAAm. Additionally, a magnetically responsive pre-gel was used to form the magnetic handle.

For the lower PEGDAAm concentration pre-gel (low LCST domain), the PEGDAAm stock solution (1.2 µL) was added to a NIPAm pre-gel, resulting in a final PEGDAAm concentration of 0.4 mM with 1.34 M NIPAm, 13.1 mM MBA and 13.1 mM α-KGA.

For the higher PEGDAAm concentration pre-gel (high LCST domain), the PEGDAAm stock solution (11.1 µL) was added to a NIPAm pre-gel, resulting in a final PEGDAAm concentration of 3.5 mM with 1.34 M NIPAm, 13.1 mM MBA and 13.1 mM α-KGA.

For the magnetically responsive NIPAm pre-gel, 1 µL of the MagneHis^{TM} Ni-Particle suspension was added to 10 µL of the lower concentration PEGDAAm-NIPAm pre-gel.

6.6.7 Pre-gels used in each experiment

Table 6.4: Pre-gels used in **Chapter 3**. **Standard NIPAm pre-gel**: 1.34 M NIPAm, 13.1 mM MBA, 13.1 mM α-KGA.

Figure	Description	Pre-gel
Figure 3.4	3-droplet AuNP-PNIPAm chain	**Standard NIPAm pre-gel** added to Bunte-AuNPs
Figure 3.7	PNIPAm and AuNP-PNIPAm droplet pairs	(A-B) NIPAm: **standard NIPAm pre-gel**; AuNP-NIPAm: **standard NIPAm pre-gel** added to PEG-stabilised AuNPs (C) PNIPAm: **standard NIPAm pre-gel**; AuNP-PNIPAm: 1.34 M NIPAm, 13.1 mM MBA, excess α-KGA added to PEG-stabilised AuNPs
Figure 3.8	PNIPAm and AuNP-PNIPAm droplet pairs	(A) 1.34 M NIPAm, 13.1 mM MBA, 0.1 wt % Irgacure added to PEG-stabilised AuNPs (B) **Standard AuNP-NIPAm pre-gel**: 1.34 M NIPAm, 13.1 mM MBA, 0.5 wt % Irgacure added to PEG-stabilised AuNPs

Continued on next page

Table 6.4 – *Continued from previous page*

Figure	Description	Pre-gel
Figure 3.9	PNIPAm and AuNP-PNIPAm droplet pair	**Standard NIPAm pre-gel** and **standard AuNP-NIPAm pre-gel**
Figure 3.10	PNIPAm and AuNP-PNIPAm droplet pair	As **Figure 3.9**
Figure 3.11	AuNP-PNIPAm 3-droplet chain	**Standard AuNP-NIPAm pre-gel**
Figure 3.12	PNIPAm and AuNP-PNIPAm curling structures	**Standard AuNP-NIPAm pre-gel** and **standard NIPAm pre-gel**
Figure 3.13	PNIPAm and AuNP-PNIPAm curling structures	As **Figure 3.12**
Figure 3.14	3D patterned droplet network	Clear: **standard NIPAm pre-gel**; blue: 1.34 M NIPAm, 13.1 mM MBA, 13.1 mM α-KGA, 260 µM xylene cyanol; orange: 1.34 M NIPAm, 13.1 mM MBA, 13.1 mM α-KGA, 8 mM PEGDAAm, 330 µM orange G.
Figure 3.15	3D patterned PNIPAm curling structure	High PEGDAAm-PNIPAm: **standard NIPAm pre-gel** with additional 8 mM PEGDAAm; Low PEGDAAm-PNIPAm: **Standard NIPAm pre-gel** with addition 1 mM PEGDAAm; AuNP-PNIPAm: **standard NIPAm pre-gel** with additional 0.4 mM PEGDAAm and 0.5 wt % Irgacure added to PEG-stabilised AuNPs

Continued on next page

Table 6.4 – *Continued from previous page*

Figure	Description	Pre-gel
Figure 3.16	PNIPAm and magnetic bead-containing PNIPAm droplet pair	**Standard NIPAm pre-gel**; **standard magnetic NIPAm pre-gel**
Figure 3.17	PNIPAm and magnetic bead-containing PNIPAm droplet pair	As **Figure 3.16**
Figure 3.18	Magnetic curling structure	**Standard NIPAm pre-gel**; 1.34 M NIPAm, 13.1 mM MBA, 13.1 mM α-KGA, 3.5 mM PEGDAAm; **standard magnetic NIPAm pre-gel**
Figure 3.19	Magnetic curling structure	As **Figure 3.18**
Figure 3.22	Magnetic curling structure	As **Figure 3.18**

6.6.8 Extended droplet network formation

For curling structures in **Figure 3.12-3.13**, **Figure 3.19** and **Figure 3.22**, NIPAm pre-gel droplets and AuNP-NIPAm or magnetically responsive NIPAm pre-gel droplets were assembled in a PMMA well array with 2x2 circular wells with diameter 4 mm. The well array contained 175 µL of the lipid-in-oil stock. Droplets were ejected at the top edge of a well and rolled via gravity to the bottom edge, to allow for monolayer incubation before forming bilayers. Single droplets of different pre-gels could be placed adjacent to one another with this method. As before, capillary action of a gel-loading tip could be used to rearrange structures and for 3D droplet placement.

For 3D structures in **Figure 3.14-3.15**, NIPAm pre-gel droplets and PEGDAAm-NIPAm pre-gel droplets or AuNP-NIPAm pre-gel droplets were assembled as for

the curling structures described previously, with additional pre-gel droplet placed on top using a gel-loading tip.

6.6.9 Light and temperature response of structures containing AuNP-PNIPAm

For structures in **Figure 3.12-3.13**, droplet networks were assembled from AuNP-NIPAm and NIPAm pre-gel droplets, as well as additional PEGDAAm-NIPAm pre-gel droplets for the structure pictured in **Figure 3.15**. Networks were then photopolymerized and phase transferred as previously described. Brightfield imaging and light activation were performed on the Leica DMi8 inverted microscope. For temperature activation, the heat stage was used as previously described. For the light activation, the Texas Red filter cube was used (excitation 540-580 nm), with the shutter intensity at its highest setting. The maximum measured intensity was found to be 50 mW with a Fieldmaster lightmeter (Coherent, USA). Contraction of irradiated regions of the structures occurred within seconds, and imaging was performed immediately after illumination.

6.6.10 Dual temperature response and magnetic movement of structures containing PEGDAAm-PNIPAm and magnetically responsive PNIPAm

Droplet networks were assembled from the **standard magnetic NIPAm pre-gel**, as well as NIPAm and PEGDAAm-NIPAm pre-gel droplets, then photopolymerized and phase transferred as previously described. For curvature data, the temperature of the heat stage was adjusted to each desired temperature and allowed 25 minutes for the temperature in the well array to reach that of the plate. Curvature data were extracted from images of three structures at each temperature using the previously described MATLAB script. Magnetic movement was performed by placing a stack of twenty adjoined 5 mm^3 neodymium magnets (N42, first4magnets), with an equivalent pull of 1 kg, proximally above the structure, and moving it manually.

6.7 Chapter 4 Methods

A 3D droplet printer was used with a setup as previously described[86,87] with some modifications: namely, the second generation piezo driver built by Dr Linna Zhou and the updated software which was developed by Dr Stuart Box (see **4.1.2**). The setup used throughout **Chapter 4** consisted of one droplet generator which could eject aqueous-based droplets into a reservoir of a lipid-in-oil. The reservoir was moved in 3D by a micromanipulator (PatchStar 7000, Scientifica, UK) which was controlled by a computer via a microcontroller (Arduino Uno). Droplet generators used were fabricated from a micromachined PMMA chamber containing a piezoelectric transducer, from which a glass printing nozzle protruded. Glass nozzles were manually pulled from 100 µm-diameter capillaries (Drummond) using a dual-stage glass micropipette puller (PC-10, Narishige). The pulled capillary was bent at a 90° angle over a flame and trimmed ~3.5 cm from the bend. Before use, printing nozzles were cleaned with detergent, water and ethanol, and dried under a stream of N_2. To ensure completely dry, N_2-dried nozzles were then air-dried for at least ten minutes.

Filling the droplet generator was performed as previously described[86,87]. The chamber in the droplet generator was filled with water via an inlet on the top of the device with a micropipette. Once the chamber was full, the nozzle would spontaneously fill due to capillary action. Then, the tip of the nozzle was placed in an Eppendorf containing hexadecane, and a hexadecane plug (~5 µL) was drawn into the tip by applying suction at the top inlet of the chamber. Similarly, the chosen printing solution (~5 µL) (see **Table 6.5**) was then drawn into the tip. Printing was then performed either manually or via the automated program, as described in detail in **Chapter 4**.

For use with the Atmosbag^{TM} **(Figure 4.5)**, the printer was placed inside the bag. To minimise the amount of oxygen present, air was removed from the bag by placing it under a vacuum, before refilling it with nitrogen. This was then repeated twice more. In addition, all reagents were purged with nitrogen before use.

6.7.1 NIPAm printing pre-gel

For the NIPAm printing pre-gel, the same concentrations of NIPAm, MBA and α-KGA were used as the **standard printing pre-gel**. $\geq$ 16 U mL^{-1} GOx and 10.5 mM glucose were additionally incorporated.

6.7.2 Pre-gels used in each experiment

Table 6.5: Pre-gels used in **Chapter 4**. **Standard NIPAm pre-gel**: 1.34 M NIPAm, 13.1 mM MBA, 13.1 mM α-KGA.

Figure	Description	Pre-gel
Figure 4.3	Preliminary printed networks	0.76 M NIPAm, 7.5 mM MBA and 7.5 mM a-KGA; 1.53 M NIPAm, 13.6 mM MBA and 13.6 mM α-KGA
Figure 4.4	Preliminary printed networks	1.53 M NIPAm, 13.6 mM MBA and 13.6 mM α-KGA
Figure 4.7	Bulk NIPAm pre-gels	0.76 M NIPAm, 7.5 mM MBA and 7.5 mM α-KGA with $\geq$ 230 U mL^{-1} GOx and 211 mM glucose; 1.53 M NIPAm, 13.6 mM MBA and 13.6 mM α-KGA with $\geq$ 230 U mL^{-1} GOx and 211 mM glucose
Figure 4.8	Droplet pair and emulsion droplet network	0.76 M NIPAm, 7.5 mM MBA and 7.5 mM α-KGA with $\geq$ 230 U mL^{-1} GOx and 211 mM glucose
Figure 4.9	Emulsion droplet network	**NIPAm printing pre-gel**
Figure 4.10	Printed, semi-polymerized droplet network	**NIPAm printing pre-gel**
Figure 4.11	Printed PNIPAm hydrogel structure	**NIPAm printing pre-gel**
Figure 4.12	Printed PNIPAm hydrogel structure	As **Figure 3.11**

Continued on next page

Table 6.5 – *Continued from previous page*

Figure	Description	Pre-gel
Figure 4.14	Printed NIPAm pre-gel droplet networks	**NIPAm printing pre-gel**
Figure 4.15	Printed PNIPAm hydrogel structure	**NIPAm printing pre-gel**
Figure 4.17	Printed PNIPAm hydrogel structure	**NIPAm printing pre-gel**
Figure 4.18	Printed PNIPAm hydrogel structure	As **Figure 3.17**
Figure 4.19	Printed PNIPAm hydrogel structure	As **Figure 3.17**
Figure 4.20	Droplet pairs	(A-B) **standard NIPAm pre-gel**; (C-D) **standard NIPAm pre-gel** with additional 50 mM Na_3PO_4
Figure 4.20	Printed NIPAm pre-gel droplet networks	(A) **standard NIPAm pre-gel**; (B) **standard NIPAm pre-gel** with additional 50 mM Na_3PO_4

6.7.3 GOx testing in bulk

For the preliminary experiments testing the use of glucose oxidase with the NIPAm pre-gels, the pre-gels (see **Table 6.5**) were made up in glass vials to 250 µL. Once glucose oxidase was added, the vials were sealed and left on the bench. The vials were gently shaken at 15 minute intervals to check whether gelation was proceeding. Once the reaction appeared to be complete, tube inversion was performed (see **Figure 4.7**).

6.7.4 Formation of emulsion droplet networks

To test the efficacy of oxygen removal with glucose oxidase in droplet networks in oil containing ca. sub-nL droplets **(Figure 4.8-4.9)**, 5 µL of the GOx-containing

NIPAm pre-gel was pipetted into 50 µL of lipid-in-oil and briefly vortexed. These emulsion droplets were transferred into a PMMA well array, and purged and photopolymerized as previously described. ~300 nL droplets were formed for comparison using a micropipette.

6.7.5 Freeze-pump-thaw degassing of lipid-in-oil

A round flask with two outlets was attached to a Schlenk line. The flask was filled with nitrogen via one outlet, with the other outlet sealed with a rubber septum (Suba Seal, Sigma Alrich, UK). The chosen lipid-in-oil was prepared in a 7 mL vial with a stirrer bar, sealed with a rubber septum and parafilm. A needle was inserted into the septum as an inlet. The vial was placed inside the round flask, and the flask was filled with nitrogen and evacuated under vacuum three times to remove oxygen in the surrounding environment. The flask was again filled with nitrogen and the lipid-in-oil frozen by immersion in a dewar of liquid nitrogen. The vacuum was then applied to the flask for five minutes. The vial was then allowed to thaw with a warm water bath until just melted. The freezing, vacuum and thawing steps were then repeated twice more, and finally the vial was sealed under nitrogen and used immediately.

6.7.6 Nozzle functionalization

The narrow end of the printing nozzle was dipped into a 5% solution of APTMS in acetone, and allowed to partially fill via capillary action. After careful wiping to minimise deposition on the external surface, the nozzle was left for ten minutes. Acetone and ethanol were then used to clean the nozzle and remove residual APTMS. APTMS-functionalised nozzles were then cleaned and used as previously described.

6.7.7 Use of modified droplet generator

The extra reservoir of the modified droplet generator was filled with water from a 1 mL-capacity micropipette. The height of the reservoir was adjusted relative to the droplet network such that severe leakage would not occur. Typically, once the nozzle

was loaded with the hexadecane plug and the printing solution, leakage did not take place unless either the nozzle was immersed in the lipid-in-oil reservoir; or the height of the reservoir had been incorrectly adjusted. Once immersed in the lipid-in-oil reservoir, the height of the reservoir was tuned until leakage no longer occurred.

6.7.8 Phase transfer of 3D printed PNIPAm structures

To phase transfer 3D printed PNIPAm structures into an aqueous environment, oil was carefully removed with a micropipette and replaced with water.

6.7.9 Preparation of 1:1 POPC:DPhPC lipid-in-oil

25 mg ampoules of DPhPC and POPC were dissolved in chloroform to make 25 mg mL^{-1} stocks (33 mM and 34 mM respectively) and kept at -20°C. These stocks were prepared by Dr Ravinash Krishna Kumar and Alessandro Alcinesio. To make 1:1 POPC:DPhPC lipid films, POPC (1 µmol; 30.2 µL of chloroform stock) and DPhPC (1 µmol; 29.4 µL of chloroform stock) were added to a glass vial and dried by rotation under a gentle stream of nitrogen. The film was dried in a desiccator for at least 30 minutes and used immediately. 1 mL hexadecane and 1 mL silicone oil were then added to the lipid film, resulting in a final lipid concentration of 1 mM.

6.7.10 Preparation of sodium phosphate buffer

Following a previously reported protocol[146], monobasic and dibasic sodium phosphate were individually dissolved in water to make stock solutions with a final concentration of 1 M. 8.77 mL of the monobasic sodium phosphate stock was added to 1.23 mL of the dibasic sodium phosphate stock resulting in a 1 M sodium phosphate buffer, with a pH of 6.

6.7.11 Use of Chelex to remove metal ions from NIPAm pre-gels

Chelex columns were used to remove metal contaminants from NIPAm pre-gel or PBS, which was used to dissolve glucose oxidase. For each Chelex column formed, a small piece of cotton wool was placed inside a glass Pasteur pipette to act as a

stopper at the narrow end. The resin was added to the column and several column volumes of either water or PBS were poured through the column and then discarded. NIPAm pre-gel or PBS was then passed through the column and collected.

6.7.12 Absorbance measurements of NIPAm pre-gels with GOx and glucose

A microplate reader (Infinite M1000 PRO, Tecan, Switzerland) was used to monitor the absorbance of NIPAm pre-gels to which glucose oxidase and glucose had been added. Three replicates of each sample were monitored in a polystyrene transparent flat-bottomed 96-well plate (Costar®, Corning®, USA) over 195 minutes.

6.7.13 Contact angle extraction methodology

Images analysed were normally of ~15 DIBs in separate wells, taken with the Olympus SZX10 upright microscope. A MATLAB script was implemented, which used a circle finding algorithm to locate the droplets, and was modified from a script originally written by Oliver Meacock (a DPhil student in the Kevin Foster Group, University of Oxford). The original script was designed to find the contact angle between two droplets, from an image of a single droplet pair, using **Equation 6.7.13**[137]:

$$\theta = \cos^{-1} \frac{L^2 - R_1^2 - R_2^2}{2R_1R_2} \tag{6.1}$$

The modified script was designed to increase the throughput, allowing analysis of multiple DIB contact angles instead of a single DIB contact angle. The script first read an image into MATLAB, and converted it to black and white. User input could increase the contrast of the image to aid an inbuilt circle-finding algorithm, *imfindcircles*. Then, an inbuilt tool *imdistline* was used to determine an approximate range of radii of the droplets. This range was utilised by *imfindcircles* to locate circles (corresponding to invididual droplets) in the image. The circles extracted were then plotted on the image to allow verification **(Figure 6.3)**. The

imfindcircles algorithm extracted the coordinates of the centres of each pair of circles, and their radii, and used them to calculate the contact angle. The coordinates were used to calculate the distance between the centres. If a pair of droplets, with radii R_1 and R_2, were separated by distance L, the contact angle, θ, could be calculated according to Equation 1.

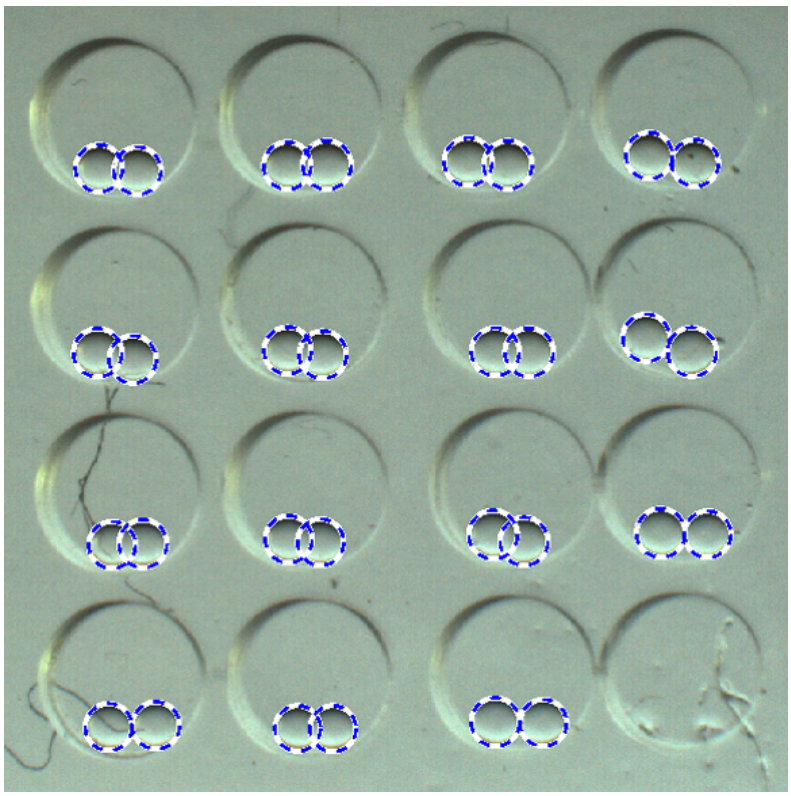

Figure 6.3: Brightfield image of fifteen DIBs formed in a well array, with overlaid blue and white lines delineating circles extracted using the MATLAB *imfindcircles* algorithm.

Appendices

A
Appendix

Matlab Code

A.1 MATLAB script for radii extraction

The following script was used to extract the radii of single PNIPAm hydrogel droplets from images taken with the Leica DMi8 inverted microscope. See **Section 6.5.13** for a description of the script.

```
%% Script to find radii of single PNIPAm hydrogel droplets in batches of images
% Modified code from MATLAB website - "Detection of a Cell" algorithm and "regionprops" function examples

% Section 1: Read all images in a given directory into MATLAB, and store
% data in a cell array.

imagefiles = dir('*.jpg');
nfiles = length(imagefiles);    % Number of files found

for ii=1:nfiles
    currentfilename = imagefiles(ii).name;
    currentimage = imread(currentfilename);
    bw_image = rgb2gray(currentimage);
    images{ii} = currentimage;
    images_names{ii} = currentfilename;
end
```

```
17
18
19 %% Section 2: Threshold so only desired number of largest
       circles are visible
20
21 % Create a cell array to store the extracted image data
22 images_Extracted = cell(5,length(imagefiles));
23
24 % Process each image - create binary images showing only
       hydrogel droplet
25 % outlines. For this part, the MATLAB website example "
       Detection of a Cell"
26 % was used
27
28 for i=1:nfiles
29     % Convert image to grayscale
30     I = rgb2gray(images{i});
31
32     % Use 'Canny' method for edge detection
33     [~, threshold] = edge(I, 'canny');
34     fudgeFactor = 1.2;
35     BW_Edge = edge(I,'canny', threshold * fudgeFactor);
36             %figure, imshow(BW_Edge), title('binary
                   gradient mask');
37
38     % Dilate lines so all circles are joined up
39     se90 = strel('line', 4, 90);
40     se0 = strel('line', 4, 0);
41     BWsdil = imdilate(BW_Edge, [se90 se0]);
42             %figure, imshow(BWsdil), title('dilated
                   gradient mask');
43
44     % Fill connected objects
45     BWdfill = imfill(BWsdil, 'holes');
46             %figure, imshow(BWdfill);
47             %title('binary image with filled holes');
48
49     % Retain only 3 largest objects
50     BW_extracted = bwareafilt(BWdfill,3);
51
52     % Export to cell array
53     images_Extracted{1,i} = BW_extracted;
54
55 end
56
```

```
57 %% Section 3: Write images to file
58
59 % Change extension on file name to png
60
61 new_name = cell(1,length(imagefiles));
62
63 for iv=1:nfiles
64     imwrite(images_Extracted{1,iv},sprintf('FD427_Analysed_
       %d.png',iv));
65 end
66
67 %% Section 4: Read all pngs of the thresholded images in
68
69 imagefiles_output = dir('*.png');
70 nfiles_output = length(imagefiles_output);     % Number of
    files found
71
72 for v=1:nfiles_output
73    currentfilename = imagefiles_output(v).name;
74    currentimage = imread(currentfilename);
75    images_output{v} = currentimage;
76    images_output_names{v} = currentfilename;
77 end
78
79 montage(images_output_names)
80
81 %% Section 5: Analyse the properties of the image using the
     function "regionprops"
82
83 radii_Extracted=zeros(3,length(nfiles));
84 x_Extracted=zeros(3,length(nfiles));
85 y_Extracted=zeros(3,length(nfiles));
86
87 for iii=1:nfiles
88     % The "regionprops" function is applied to each image,
       and extracts
89     % data which is subsequently used to calculate the
       radii of the hydrogel droplets
90     stats = regionprops('table',images_Extracted{1,iii},'
       Centroid','MajorAxisLength','MinorAxisLength','
       EquivDiameter');
91     centers = stats.Centroid;
92     diameters = mean([stats.MajorAxisLength stats.
       MinorAxisLength],2)
93     radii = diameters/2;
```

```
94
95      % Store the data extracted from the images.
96      images_Extracted{2,iii} = radii(1);
97      images_Extracted{3,iii} = radii(2);
98      images_Extracted{4,iii} = radii(3);
99
100     radii_Extracted(:,iii)=radii;
101     x_Extracted(:,iii) = centers(:,1);
102     y_Extracted(:,iii) = centers(:,2);
103 end
104
105
106 %%
107 % Output the radii extracted in each image
108 mean_radii = mean(radii_Extracted,1);
109 stdev_radii = std(radii_Extracted,1);
```

A.2 MATLAB script for curvature extraction

The following script was used to extract the radii of single PNIPAm hydrogel droplets from images taken with the Olympus SZX10 upright microscope. See **Section 6.5.14** for a description of the script.

```
1  %% Script to find radius of curvature for each image for
       curling PNIPAm hydrogel structures
2  % Section 1: Read all images in a given directory into
       MATLAB, and store
3  % data in a cell array.
4
5  imagefiles = dir('*.jpg');
6  nfiles = length(imagefiles);    % Number of files found
7
8  % Read over all of the image data in the array and convert
       to grayscale for
9  % ease of analysis.
10
11 for ii=1:nfiles
12     currentfilename = imagefiles(ii).name;
13     currentimage = imread(currentfilename);
14     bw_image = rgb2gray(currentimage);
15     images{ii} = currentimage;
16     images_names{ii} = currentfilename;
17 end
18
```

```
%% Section 2: Extract curvature
% Each image will be opened in MATLAB with "imshow", and a point selection function "getpts" is used to select coordinates along the structure.
% The coordinates are saved in a cell array, and used with an open source
% circle fitting function, "Fast circle fitting using Landau method". The
% circle is plotted on the image, along with the points, to allow
% verification of the fit.

% Create arrays to store coordinate and radii data

coordinate_data = cell(4,length(imagefiles));
radii = zeros(length(imagefiles),1);

for i=1:(length(images));
    FD426_Image = images{1,i};
    imshow(FD426_Image);

    % Select coordinates on the image
    [x, y] = getpts
    pause

    % Store coordinate data
    coordinate_data{1,i} = x;
    coordinate_data{2,i} = y;

    % Input coordinate data into the open source function "Landau_Smith"
    [xcnew,ycnew,Rnew] = Landau_Smith(x,y);

    % Save radii data in the previously created array.
    radii(i) = Rnew;
end

%% Section 3: A function called in Section 2 to plot the circles on the images, for verification.
% This comprises part of the code of the open source function "Fast circle
% fitting using Landau method".

[xcnew,ycnew,Rnew] = Landau_Smith(x,y);
 theta=0:pi/180:2*pi;
```

```
xcircle = Rnew*cos(theta')+xcnew;
ycircle = Rnew*sin(theta')+ycnew;
plot(x,y,'x',xcircle,ycircle,'LineWidth',2);
axis equal;
```

A.3 MATLAB script for contact angle extraction

The following script was used to extract the contact angles of multiple NIPAm pre-gel droplet pairs from images taken with the Olympus SZX10 upright microscope. See **Section 6.7.13** for a description of the script.

```
% Code partially adapted from Oli Meacock from the Foster group
% This code was designed for images taken on the upright microscope e.g.
% contrast alterations useful for that. Primarily, alterations were made so that many droplet pairs could be analysed at once.

%% 1. Open file and display image
% Navigate to the desired image using the pop-up window. Change the file type to "All files *.*" rather than "All MATLAB files",
% so the chosen image type can be opened e.g. jpg, tiff. This will display the chosen image.
verbose = true;

% User navigates to desired folder
% For convenience in browsing, set a starting folder from which to browse.
startingFolder = 'C:\Users\hbgroup\Documents\Flo\Experiment Planning and Analysis\DIB Contact Angles';
if ~exist(startingFolder, 'dir')
        % If that folder doesn't exist, just start in the current folder.
        startingFolder = pwd;
end

% Get name of file user wants to use
defaultFileName = fullfile(startingFolder, '*.*');
[baseFileName, folder] = uigetfile;
if defaultFileName == 0
    % User clicked cancel
    return;
```

```
24 end
25
26 fullFileName = fullfile(folder,baseFileName);
27 ImportImage = imread(fullFileName);
28
29 % Display image
30 imshow(ImportImage);
31
32 %% 2. Alter contrast to facilitate circle finding
33
34 % Converts to black and white, so that user interface
     allows user to change contrast of
35 % image (this is done with the black and white circular
     icon), and exports (File > Export to Workspace) as "I".
36
37 bw_ImportImage = rgb2gray(ImportImage);
38 imtool(bw_ImportImage);
39
40 %% Show new image and predict size of radius with draggable
      line
41
42 % Drag the line to determine the diameter of some droplets.
43 % Right click line and Export to Workspace as D1 and D2 (e.
     g. for a droplet
44 % that appears larger, and one that appears smaller, to
     ensure all of the
45 % droplets are covered by the range generated by these
     values).
46
47 DropletImage = I;
48 imshow(DropletImage);
49 d = imdistline;
50
51 %%
52 % Using the measured line lengths, a range of radii is
     generated [rmin,
53 % rmax]. This can be manually changed if it appears that
     the algorithm needs a
54 % larger range to work from
55
56 rmin = ((D1/2)-5);
57 rmax = ((D2/2)+20);
58 radiusRange = [rmin, rmax];
59
60 %% 3. Locate circles in image
```

```
61 % See documentation online for "imfindcircles" that explains each of the
62 % parameters within the brackets. Essentially, it takes the image
63 % (stored in MATLAB as DropletImage, it's the same I which was exported after
64 % contrast was changed), and applies a circle finding algorithm to it. If
65 % it's not working well, the sensitivity can be increased (might give false circles though), and change
66 % 'ObjectPolarity' (whether the object is dark or bright compared to the
67 % background.
68
69 radiusRange = int16(radiusRange)
70 [centres,radii] = imfindcircles(DropletImage, radiusRange,'ObjectPolarity', 'dark','Sensitivity',0.92); % may want to split into multiple imfindcircles if takes too long
71
72 %% This section will demonstrates how well imfindcircles worked
73
74 % Draw circles on top of original image
75 figure
76 imshow(ImportImage);
77 h = viscircles(centres,radii,'EdgeColor','b', 'LineStyle','--'); % centres = coordinates of each centre, radii = radius of each circle
78
79 % Count number of droplets
80 no_droplets = size(centres,1);
81
82
83 %% 4. Find contact angle
84 % This section (part of which was modified from Oliver Meacock of the Kevin Foster Group, University of Oxford) takes all the droplets and calculates a contact angle based
85 % on the formulae in 2012 Langmuir Dixit paper.
86
87 % If there are only two droplets:
88 if no_droplets == 2
89     L = pdist(centres); %pdist finds the distance between the two centres
90     R1 = radii(1);
```

```
91      R2 = radii(2);
92
93      contactAngle = acos(((L*L) - (R1*R1) - (R2*R2))/(2*R1*
            R1));
94
95  % If there are multiple droplet pairs in the image
96  elseif no_droplets > 2
97      warning('Number of droplets detected is greater than 2.
            Calculating which are pairs...');
98      dists = pdist2(centres,centres); % looks for  distances
            between all droplets - INSERT CENTRES
99
100      for i = 1:size(dists,1)
101          dists(i,i) = NaN;
102      end
103
104      [D,I] = pdist2(centres,centres,'euclidean','Smallest'
             ,2); % looks for 2 nearest droplets to each droplet
105      NearestDroplet = transpose(vertcat(D(2,:), I(2,:)));
106
107
108      x = zeros(size(dists,1),7);
109
110      for eachDroplet = 1:size(dists,1)
111          L = NearestDroplet(eachDroplet,1);
112          Droplet2 = NearestDroplet(eachDroplet,2);
113          R1 = radii(eachDroplet);
114          R2 = radii(Droplet2);
115
116          if L > 3*R1
117              contactAngle = NaN;
118              Droplet2 = NaN;
119          else
120
121              contactAngle = acos(((L*L) - (R1*R1) - (R2*R2))
                    /(2*R1*R2));
122              contactAngle = contactAngle/2;
123
124          % If the contact angle is complex, the contact
               angle is changed to
125          % 0.
126
127              tf = isreal(contactAngle);
128              contactAngle = contactAngle*tf;
129              angleInDegrees = radtodeg(contactAngle);
```

```
130             end
131
132             x(eachDroplet,:) = [L, R1, R2, eachDroplet,
                    Droplet2, contactAngle, angleInDegrees];
133         end
134
135         angleInDegrees = (x(:,7));
136         Droplet1Index = (x(:,4));
137         Droplet2Index = (x(:,5));
138
139     elseif total_centres < 2
140     warning('Number of droplets detected is less than 2.
            Skipping...');
141
142     contactAngle = NaN;
143 end
144
145 %% 5. Label circle centres
146 % Labels each droplet with the contact angle in degrees,
      two indices related to what order it and the closest
      droplet to it were found by the imfindcircles
147 % algorithm, and the coordinates of their centres.
148
149 str = cell(no_droplets, 1);
150 text_str_position = cell(no_droplets, 1);
151
152 dropletInfo = zeros(size(dists,1),5);
153
154 for eachDroplet=1:no_droplets
155     displayed_info_1 = [angleInDegrees(eachDroplet),
            Droplet1Index(eachDroplet), Droplet2Index(
            eachDroplet), centres(eachDroplet,1), centres(
            eachDroplet,2)]
156     displayed_info_2 = [angleInDegrees(eachDroplet),
            centres(eachDroplet,1), centres(eachDroplet,2)];
157     displayed_info_3 = [angleInDegrees(eachDroplet),
            Droplet1Index(eachDroplet), Droplet2Index(
            eachDroplet)];
158     dropletInfo(eachDroplet,:) = [angleInDegrees(
            eachDroplet), Droplet1Index(eachDroplet),
            Droplet2Index(eachDroplet), centres(eachDroplet,1),
            centres(eachDroplet,2)];
159     str{eachDroplet} = [num2str(displayed_info_1, '%.1f\n')
            ];
160 end
```

```
161
162 RGB = insertText(ImportImage,centres,str,'FontSize', 20, '
    BoxOpacity', 0, 'TextColor','black');
163
164 figure
165 imshow(RGB);
166 h = viscircles(centres,radii,'EdgeColor','b','LineStyle','
    --');
```

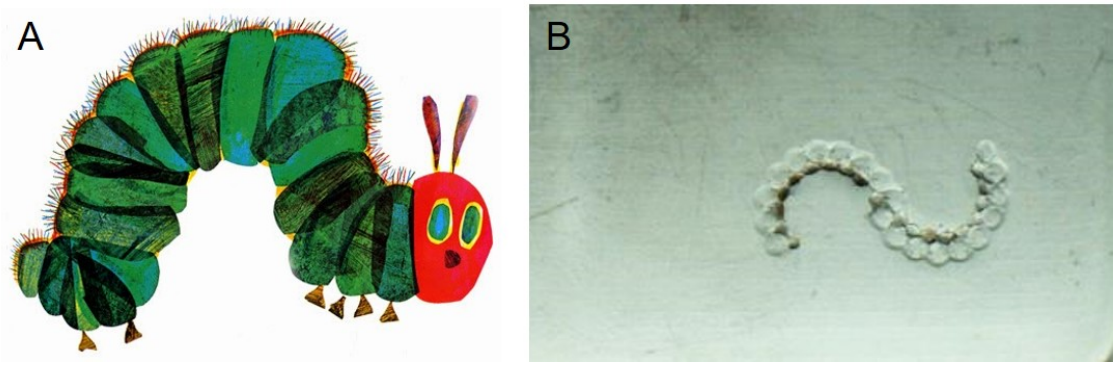

Figure A.1: **(A)** A very hungry caterpillar[147]. **(B)** A droplet-templated caterpillar.

On Saturday, he ate through one piece of chocolate cake, one ice-cream cone, one pickle, one slice of Swiss cheese, one slice of salami, one lollipop, one piece of cherry pie, one sausage, one cupcake, and one slice of watermelon. That night, he had a stomach ache.

— Eric Carle, *The Very Hungry Caterpillar*[147]

Bibliography

[1] Kristi S. Anseth, Christopher N. Bowman, and Lisa Brannon-Peppas. Mechanical properties of hydrogels and their experimental determination. *Biomaterials*, 17(17):1647–1657, 1996.

[2] Yu Shrike Zhang and Ali Khademhosseini. Advances in engineering hydrogels. *Science*, 356(6337):eaaf3627, 2017.

[3] Dror Seliktar. Designing cell-compatible hydrogels for biomedical applications. *Science*, 336(6085):1124–1128, 2012.

[4] Jianyu Li and David J. Mooney. Designing hydrogels for controlled drug delivery. *Nature Reviews Materials*, 1(12):16071, 2016.

[5] Mark W. Tibbitt and Kristi S. Anseth. Hydrogels as extracellular matrix mimics for 3D cell culture. *Biotechnology and Bioengineering*, 103(4):655–663, 2009.

[6] Leonid Ionov. Biomimetic Hydrogel-Based Actuating Systems. *Advanced Functional Materials*, 23(36):4555–4570, 2013.

[7] Lauren D. Zarzar, Philseok Kim, Mathias Kolle, C. Jeffrey Brinker, Joanna Aizenberg, and Bryan Kaehr. Direct writing and actuation of three-dimensionally patterned hydrogel pads on micropillar supports. *Angewandte Chemie - International Edition*, 50(40):9356–9360, 2011.

[8] Zhibing Hu, Xiaomin Zhang, and Yong Li. Synthesis and application of modulated polymer gels. *Science*, 269(5223):525–527, 1995.

[9] Hen Wei Huang, Mahmut Selman Sakar, Andrew J. Petruska, Salvador Pané, and Bradley J. Nelson. Soft micromachines with programmable motility and morphology. *Nature Communications*, 7(12263):1–10, 2016.

[10] Liang Dong, Abhishek K. Agarwal, David J. Beebe, and Hongrui Jiang. Adaptive liquid microlenses activated by stimuli-responsive hydrogels. *Nature*, 442(7102):551–554, 2006.

[11] Courtney D. Sorrell, Matthew C.D. Carter, and Michael J. Serpe. Color tunable poly(*N*-isopropylacrylamide)-co-acrylic acid microgel-Au hybrid assemblies. *Advanced Functional Materials*, 21(3), 2011.

[12] Jinlian Hu, Harper Meng, Guoqiang Li, and Samuel I. Ibekwe. A review of stimuli-responsive polymers for smart textile applications. *Smart Materials and Structures*, 21(5):053001, 2012.

[13] Xinyue Liu, Hyunwoo Yuk, Shaoting Lin, German Alberto Parada, Tzu Chieh Tang, Eléonore Tham, Cesar de la Fuente-Nunez, Timothy K. Lu, and Xuanhe Zhao. 3D Printing of Living Responsive Materials and Devices. *Advanced Materials*, 30(4):1704821, 2018.

[14] Mitsuhiro Shibayama and Toyoichi Tanaka. Volume phase transition and related phenomena of polymer gels. In *Responsive Gels: Volume Transitions*, pages 1–62. Springer, Berlin, Heidelberg, 1993.

[15] Richard A. L. Jones. *Soft Condensed Matter*. Oxford University Press, 2002.

[16] Toyoichi Tanaka. Collapse of gels and the critical endpoint. *Physical Review Letters*, 40(12):820–823, 1978.

[17] Toyoichi Tanaka and David J. Fillmore. Kinetics of swelling of gels. *The Journal of Chemical Physics*, 70(3):1214, 1979.

[18] Malcolm P. Stevens. *Polymer Chemistry*. Oxford University Press, New York, 1990.

[19] Masao Doi. *Introduction to Polymer Physics*. 1996.

[20] Jon A. Rowley, Gerard Madlambayan, and David J. Mooney. Alginate hydrogels as synthetic extracellular matrix materials. *Biomaterials*, 20(1): 45–53, 1999.

[21] Wim E. Hennink and Cornelus F. van Nostrum. Novel crosslinking methods to design hydrogels. *Advanced Drug Delivery Reviews*, 54(1):13–36, 2002.

[22] Samuel Ligon, Branislav Husár, Harald Wutzel, Richard Holman, and Robert Liska. Strategies to reduce oxugen inhibition in photoinduced polymerization. *Chem. Rev.*, 114(1):557–589, 2014.

[23] Heinrich F. Gruber. Photoinitiators for free radical polymerization. *Progress in Polymer Science*, 17:953–1044, 1992.

[24] April M. Kloxin, Andrea M. Kasko, Chelsea N. Salinas, and Kristi S. Anseth. Photodegradable hydrogels for dynamic tuning of physical and chemical properties. *Science*, 324(5923):59–63, 2009.

[25] Matthias P. Lutolf, Janelle L. Lauer-Fields, Hugo G. Schmoekel, Andrew T. Metters, Franz E. Weber, Greg B. Fields, and Jeffrey A. Hubbell. Synthetic matrix metalloproteinase-sensitive hydrogels for the conduction of tissue regeneration: Engineering cell-invasion characteristics. *Proceedings of the National Academy of Sciences*, 100(9):5413–5418, 2003.

[26] Takayuki Amiya and Toyoichi Tanaka. Phase Transitions in Cross-Linked Gels of Natural Polymers. *Macromolecules*, 20(5):1162–1164, 1987.

[27] Michal Ilavský, Jaroslav Hrouz, and Karel Ulbrich. Phase transition in swollen gels. *Polymer Bulletin*, 7(2-3):107–113, 1982.

[28] Yoshitsugu Hirokawa and Toyoichi Tanaka. Volume phase transition in a nonionic gel. *The Journal of Chemical Physics*, 81(12):6379, 1984.

[29] Toyoichi Tanaka, David Fillmore, Shao-Tang Sun, Izumi Nishio, Gerald Swislow, and Arati Shah. Phase Transition in Ionic Gels. *Physical Review Letters*, 45(20):1636–1639, 1980.

[30] Toyoichi Tanaka, Izumi Nishio, Shao Tang Sun, and Shizue Ueno-Nishio. Collapse of gels in an electric field. *Science*, 218(4571):467–469, 1982.

[31] Atsushi Suzuki and Toyoichi Tanaka. Phase transition in polymer gels induced by visible light. *Nature*, 346(6282):345–347, 1990.

[32] Hiroki Katono, Atsushi Maruyama, Kohei Sanui, Naoya Ogata, Teruo Okano, and Yasuhisa Sakurai. Thermo-responsive swelling and drug release switching of interpenetrating polymer networks composed of poly(acrylamide-co-butyl methacrylate) and poly(acrylic acid). *Journal of Controlled Release*, 16(1-2): 215–227, 1991.

[33] Jan Seuring and Seema Agarwal. Polymers with upper critical solution temperature in aqueous solution: Unexpected properties from known building blocks. *ACS Macro Letters*, 2(7):597–600, 2013.

[34] Mengge Xia, Yanhua Cheng, Zhouqi Meng, Xiaoze Jiang, Zhigang Chen, Patrick Theato, and Meifang Zhu. A Novel Nanocomposite Hydrogel with Precisely Tunable UCST and LCST. *Macromolecular Rapid Communications*, 36(5):477–482, 2015.

[35] Howard G. Schild. Poly(*N*-isopropylacrylamide): experiment, theory and application. *Progress in Polymer Science*, 17(2):163–249, 1992.

[36] Allan S. Hoffman. Stimuli-responsive polymers: Biomedical applications and challenges for clinical translation. *Advanced Drug Delivery Reviews*, 65(1): 10–16, 2013.

[37] Michael Heskins and James E. Guillet. Solution Properties of Poly(*N*-isopropylacrylamide). *Journal of Macromolecular Science: Part A - Chemistry*, 2(8):1441–1455, 1968.

[38] Toyoichi Tanaka, Eriko Sato, Yoshitsugu Hirokawa, Shunsuke Hirotsu, and Joyce Peetermans. Critical Kinetics of Volume Phase Transition of Gels. *Physical Review Letters*, 55(22):2455–2458, 1985.

[39] Shunsuke Hirotsu, Yoshitsugu Hirokawa, and Toyoichi Tanaka. Volume-phase transitions of ionized *N*-isopropylacrylamide gels. *The Journal of Chemical Physics*, 87(2):1392–1395, 1987.

[40] Yael Klein, Efi Efrati, and Eran Sharon. Shaping of elastic sheets by prescription of non-Euclidean metrics. *Science*, 315(5815):1116–20, 2007.

[41] Jungwook Kim, James A. Hanna, Myunghwan Byun, Christian D. Santangelo, and Ryan C. Hayward. Designing responsive buckled surfaces by halftone gel lithography. *Science*, 335(6073):1201–1205, 2012.

[42] A. Sydney Gladman, Elisabetta A. Matsumoto, Ralph G. Nuzzo, L. Mahadevan, and Jennifer A. Lewis. Biomimetic 4D printing. *Nature Materials*, 15(4): 413–418, 2016.

[43] Chi Wu and Xiaohui Wang. Globule-to-Coil Transition of a Single Homopolymer Chain in Solution. *Physical Review Letters*, 80(18):4092–4094, 1998.

[44] Mark A. Ward, Theoni K. Georgiou, and Theoni K. Georgiou. Thermoresponsive Polymers for Biomedical Applications. *Polymers*, 3(3):1215–1242, 2011.

[45] Ryo Yoshida, Katsumi Uchida, Yuzo Kaneko, Kiyotaka Sakai, Akihiko Kikuchi, Yasuhisa Sakurai, and Teruo Okano. Comb-type grafted hydrogels with rapid deswelling response to temperature changes. *Nature*, 374(6519):240–242, 1995.

[46] Xue Shen Wu, Allan S. Hoffman, and Paul Yager. Synthesis and characterization of thermally reversible macroporous poly(*N*-isopropylacrylamide) hydrogels. *Journal of Polymer Science Part A: Polymer Chemistry*, 30(10): 2121–2129, 1992.

[47] Eunsu Lee, Dowan Kim, Haneul Kim, and Jinhwan Yoon. Photothermally driven fast responding photo-actuators fabricated with comb-type hydrogels and magnetite nanoparticles. *Scientific Reports*, 5:15124, 2015.

[48] Liang Yin Chu, Jin Woong Kim, Rhutesh K. Shah, and David A. Weitz. Monodisperse thermoresponsive microgels with tunable volume-phase transition kinetics. *Advanced Functional Materials*, 17(17):3499–3504, 2007.

[49] Herman Feil, You Han Bae, Jan Feijen, and Sung Wan Kim. Effect of Comonomer Hydrophilicity and Ionization on the Lower Critical Solution Temperature of *N*-Isopropylacrylamide Copolymers. *Macromolecules*, 26(10): 2496–2500, 1993.

[50] Vered Pardo-Yissar, Ran Gabai, Andrew N. Shipway, Tatyana Bourenko, and Itamar Willner. Gold nanoparticle/hydrogel composites with solvent-switchable electronic properties. *Advanced Materials*, 13(17):1320–1323, 2001.

[51] Ivan Gorelikov, Lora M. Field, and Eugenia Kumacheva. Hybrid microgels photoresponsive in the near-infrared spectral range. *Journal of the American Chemical Society*, 126(49):15938–15939, 2004.

[52] Mallika Das, Nicolas Sanson, Daniele Fava, and Eugenia Kumacheva. Microgels Loaded with Gold Nanorods: Photothermally Triggered Volume Transitions under Physiological Conditions†. *Langmuir*, 23(1):196–201, 2007.

[53] Chun Wang, Nolan T. Flynn, and Robert Langer. Controlled structure and properties of thermoresponsive nanoparticle-hydrogel composites. *Advanced Materials*, 16(13):1074–1079, 2004.

[54] Adam W. Hauser, Arthur A. Evans, Jun Hee Na, and Ryan C. Hayward. Photothermally reprogrammable buckling of nanocomposite gel sheets. *Angewandte Chemie - International Edition*, 54(18):5434–5437, 2015.

[55] Amy Sutton, Tanya Shirman, Jaakko V. I. Timonen, Grant T England, Philseok Kim, Mathias Kolle, Thomas Ferrante, Lauren D Zarzar, Elizabeth Strong, and Joanna Aizenberg. Photothermally triggered actuation of hybrid materials as a new platform for in vitro cell manipulation. *Nature Communications*, 8:14700, 2017.

[56] Dawan Kungwatchakun and Masahiro Irie. Photoresponsive polymers. Photocontrol of the phase separation temperature of aqueous solutions of poly-[*N*-isopropylacrylamide-co-*N*-(4-phenylazophenyl)acrylamide]. *Die Makromolekulare Chemie, Rapid Communications*, 9(4):243–246, 1988.

[57] Kazutoshi Haraguchi and Toru Takehisa. Nanocomposite hydrogels: A unique organic-inorganic network structure with extraordinary mechanical, optical, and swelling/De-swelling properties. *Advanced Materials*, 14(16):1120–1124, 2002.

[58] Jian Ping Gong, Yoshinori Katsuyama, Takayuki Kurokawa, and Yoshihito Osada. Double-network hydrogels with extremely high mechanical strength. *Advanced Materials*, 15(14):1155–1158, 2003.

[59] Jeong Yun Sun, Xuanhe Zhao, Widusha R. K. Illeperuma, Ovijit Chaudhuri, Kyu Hwan Oh, David J. Mooney, Joost J. Vlassak, and Zhigang Suo. Highly stretchable and tough hydrogels. *Nature*, 489(7414):133–136, 2012.

[60] Hyunwoo Yuk, Teng Zhang, German Alberto Parada, Xinyue Liu, and Xuanhe Zhao. Skin-inspired hydrogel-elastomer hybrids with robust interfaces and functional microstructures. *Nature Communications*, 7:12028, 2016.

[61] Angelo Cangialosi, Chang Kyu Yoon, Jiayu Liu, Qi Huang, Jingkai Guo, Thao D. Nguyen, David H. Gracias, and Rebecca Schulman. DNA sequence–directed shape change of photopatterned hydrogels via high-degree swelling. *Science*, 357(6356):1126–1130, 2017.

[62] Randall M. Erb, Jonathan S. Sander, Roman Grisch, and André R. Studart. Self-shaping composites with programmable bioinspired microstructures. *Nature Communications*, 4(1):1712, 2013.

[63] Seog-Jin Jeon, Adam W. Hauser, and Ryan C. Hayward. Shape-Morphing Materials from Stimuli-Responsive Hydrogel Hybrids. *Accounts of Chemical Research*, 50(2):161–169, 2017.

[64] Amirali Nojoomi, Hakan Arslan, Kwan Lee, and Kyungsuk Yum. Bioinspired 3D structures with programmable morphologies and motions. *Nature Communications*, 9(1):3705, 2018.

[65] Georgi Stoychev, Nikolay Puretskiy, and Leonid Ionov. Self-folding all-polymer thermoresponsive microcapsules. *Soft Matter*, 7(7):3277–3279, 2011.

[66] Tae Soup Shim, Shin Hyun Kim, Chul Joon Heo, Hwan Chul Jeon, and Seung Man Yang. Controlled origami folding of hydrogel bilayers with sustained reversibility for robust microcarriers. *Angewandte Chemie - International Edition*, 51(6):1420–1423, 2012.

[67] Joyce C. Breger, Changkyu Yoon, Rui Xiao, Hye Rin Kwag, Martha O. Wang, John P. Fisher, Thao D. Nguyen, and David H. Gracias. Self-folding thermo-magnetically responsive soft microgrippers. *ACS Applied Materials and Interfaces*, 7(5):3398–3405, 2015.

[68] Hongyan He, Jingjiao Guan, and James L. Lee. An oral delivery device based on self-folding hydrogels. *Journal of Controlled Release*, 110(2):339–346, 2006.

[69] Haneul Kim, Hyeonjin Lee, Keum Yong Seong, Eunsu Lee, Seung Yun Yang, and Jinhwan Yoon. Visible Light-Triggered On-Demand Drug Release from Hybrid Hydrogels and its Application in Transdermal Patches. *Advanced Healthcare Materials*, 4(14):2071–2077, 2015.

[70] Basma Hashmi, Lauren D. Zarzar, Tadanori Mammoto, Akiko Mammoto, Amanda Jiang, Joanna Aizenberg, and Donald E. Ingber. Developmentally-inspired shrink-wrap polymers for mechanical induction of tissue differentiation. *Advanced Materials*, 26(20):3253–3257, 2014.

[71] Yoshihito Osada, Hidenori Okuzaki, and Hirofumi Hori. A polymer gel with electrically driven motility. *Nature*, 355(6357):242–244, 1992.

[72] Gu Han Kwon, Joong Yull Park, Jeong Yoon Kim, Megan L. Frisk, David J. Beebe, and Sang Hoon Lee. Biomimetic soft multifunctional miniature aquabots. *Small*, 4(12):2148–2153, 2008.

[73] Eddie Wang, Malav S. Desai, and Seung-Wuk Lee. Light controlled graphene-elastin composite hydrogel actuators. *Nano Lett.*, 13(6):2826–2830, 2013.

[74] Yuwei Hu, Chun-Hua Lu, Weiwei Guo, Miguel Angel Aleman-Garcia, Jiangtao Ren, and Itamar Willner. A Shape Memory Acrylamide/DNA Hydrogel Exhibiting Switchable Dual pH-Responsiveness. *Advanced Functional Materials*, 25(44):6867–6874, 2015.

[75] Limei Huang, Ruiqi Jiang, Jingjun Wu, Jizhou Song, Hao Bai, Bogeng Li, Qian Zhao, and Tao Xie. Ultrafast Digital Printing toward 4D Shape Changing Materials. *Advanced Materials*, 29(7):1605390, 2017.

[76] Yihui Zhang, Fan Zhang, Zheng Yan, Qiang Ma, Xiuling Li, Yonggang Huang, and John A. Rogers. Printing, folding and assembly methods for forming 3D mesostructures in advanced materials. *Nature Reviews Materials*, 2(17019), 2017.

[77] David B. Kolesky, Kimberly A. Homan, Mark A. Skylar-Scott, and Jennifer A. Lewis. Three-dimensional bioprinting of thick vascularized tissues. *Proceedings of the National Academy of Sciences*, 113(12):3179–3184, 2016.

[78] Tapomoy Bhattacharjee, Steven M. Zehnder, Kyle G. Rowe, Suhani Jain, Ryan M. Nixon, W. Gregory Sawyer, and Thomas E. Angelini. Writing in the granular gel medium. *Science Advances*, 1(8):e1500655–e1500655, 2015.

[79] Sean V. Murphy and Anthony Atala. 3D bioprinting of tissues and organs. *Nature Biotechnology*, 32(8):773–785, 2014.

[80] Wanjun Liu, Yu Shrike Zhang, Marcel A. Heinrich, Fabio De Ferrari, Hae Lin Jang, Syeda Mahwish Bakht, Mario Moisés Alvarez, Jingzhou Yang, Yi-Chen Li, Grissel Trujillo-de Santiago, Amir K. Miri, Kai Zhu, Parastoo Khoshakhlagh, Gyan Prakash, Hao Cheng, Xiaofei Guan, Zhe Zhong, Jie Ju, Geyunjian Harry Zhu, Xiangyu Jin, Su Ryon Shin, Mehmet Remzi Dokmeci, and Ali Khademhosseini. Bioprinting: Rapid Continuous Multimaterial Extrusion Bioprinting. *Advanced Materials*, 29(3), 2017.

[81] Hagan Bayley, Brid Cronin, Andrew Heron, Matthew A. Holden, William L. Hwang, Ruhma Syeda, James Thompson, and Mark Wallace. Droplet interface bilayers. *Molecular BioSystems*, 4(12):1191–208, 2008.

[82] Michael J. Booth, Vanessa Restrepo Schild, Florence G. Downs, and Hagan Bayley. Functional aqueous droplet networks. *Molecular BioSystems*, 13(9): 1658–1691, 2017.

[83] Christiane A. Helm, Jacob N. Israelachvili, and Patty McGuiggan. Role of Hydrophobic Forces in Bilayer Adhesion and Fusion. *Biochemistry*, 31(6): 1794–1805, 1992.

[84] Matthew A. Holden, David Needham, and Hagan Bayley. Functional bionetworks from nanoliter water droplets. *Journal of the American Chemical Society*, 129(27):8650–8655, 2007.

[85] Giovanni Maglia, Andrew J. Heron, William L. Hwang, Matthew A. Holden, Ellina Mikhailova, Qiuhong Li, Stephen Cheley, and Hagan Bayley. Droplet networks with incorporated protein diodes show collective properties. *Nature Nanotechnology*, 4(7):437–440, 2009.

[86] Gabriel Villar, Alexander D. Graham, and Hagan Bayley. A Tissue Like Printed Material. *Science*, 340(6128):48–52, 2013.

[87] Michael J. Booth, Vanessa Restrepo Schild, Alexander D. Graham, Sam N. Olof, and Hagan Bayley. Light-activated communication in synthetic tissues. *Science Advances*, 2(4):e1600056–e1600056, 2016.

[88] Tobias Wauer, Holger Gerlach, Shiksha Mantri, Jamie Hill, Hagan Bayley, and K. Tanuj Sapra. Construction and manipulation of functional three-dimensional droplet networks. *ACS Nano*, 8(1):771–779, 2014.

[89] Mark S. Friddin, Guido Bolognesi, Yuval Elani, Nicholas J. Brooks, Robert V. Law, John M. Seddon, Mark A. A. Neil, and Oscar Ces. Optically assembled droplet interface bilayer (OptiDIB) networks from cell-sized microdroplets. *Soft Matter*, 12(37):7731–7734, 2016.

[90] Michael J. Booth, Vanessa Restrepo Schild, Stuart J. Box, and Hagan Bayley. Light-patterning of synthetic tissues with single droplet resolution. *Scientific Reports*, 7(1):9315, 2017.

[91] Yuval Elani, Andrew J. Demello, Xize Niu, and Oscar Ces. Novel technologies for the formation of 2-D and 3-D droplet interface bilayer networks. *Lab on a Chip*, 12(18):3514–3520, 2012.

[92] Yuval Elani, Antony Gee, Robert V. Law, and Oscar Ces. Engineering multi-compartment vesicle networks. *Chemical Science*, 4(8):3332, 2013.

[93] Nan-Nan Deng, Maaruthy Yelleswarapu, and Wilhelm T. S. Huck. Monodisperse Uni- and Multicompartment Liposomes. *Journal of the American Chemical Society*, 138(24):7584–7591, 2016.

[94] Yuval Elani, Robert V. Law, and Oscar Ces. Vesicle-based artificial cells as chemical microreactors with spatially segregated reaction pathways. *Nature Communications*, 5(1):5305, 2014.

[95] Yuval Elani, Robert V. Law, and Oscar Ces. Protein synthesis in artificial cells: using compartmentalisation for spatial organisation in vesicle bioreactors. *Physical Chemistry Chemical Physics*, 17(24):15534–15537, 2015.

[96] Gabriel Villar, Andrew J. Heron, and Hagan Bayley. Formation of droplet networks that function in aqueous environments. *Nature Nanotechnology*, 6 (12):803–808, 2011.

[97] Yuval Elani, Xavier C. I. Solvas, Joshua B. Edel, Robert V. Law, and Oscar Ces. Microfluidic generation of encapsulated droplet interface bilayer networks (multisomes) and their use as cell-like reactors. *Chemical Communications*, 52(35):5961–5964, 2016.

[98] Andrew J. Heron, James R. Thompson, Bríd Cronin, Hagan Bayley, and Mark I. Wallace. Simultaneous Measurement of Ionic Current and Fluorescence from Single Protein Pores. *Journal of the American Chemical Society*, 131(5): 1652–1653, 2009.

[99] Shuo Huang, Mercedes Romero-Ruiz, Oliver K. Castell, Hagan Bayley, and Mark I. Wallace. High-throughput optical sensing of nucleic acids in a nanopore array. *Nature Nanotechnology*, 10(11):986–991, 2015.

[100] Vanessa Restrepo Schild, Michael J. Booth, Stuart J. Box, Sam N. Olof, Kozhinjampara R. Mahendran, and Hagan Bayley. Light-Patterned Current Generation in a Droplet Bilayer Array. *Scientific Reports*, 7(1):46585, 2017.

[101] Divesh K. Baxani, Alex J. L. Morgan, William D. Jamieson, Christopher J. Allender, David A. Barrow, and Oliver K. Castell. Bilayer Networks within a Hydrogel Shell: A Robust Chassis for Artificial Cells and a Platform for Membrane Studies. *Angewandte Chemie - International Edition*, 55(46): 14240–14245, 2016.

[102] Mariam Bayoumi, Hagan Bayley, Giovanni Maglia, and K. Tanuj Sapra. Multi-compartment encapsulation of communicating droplets and droplet networks in hydrogel as a model for artificial cells. *Scientific Reports*, 7(45167), 2017.

[103] Alexander D. Graham, Sam N. Olof, Madeline J. Burke, James P. K. Armstrong, Ellina A. Mikhailova, James G. Nicholson, Stuart J. Box, Francis G. Szele, Adam W. Perriman, and Hagan Bayley. High-Resolution Patterned Cellular Constructs by Droplet-Based 3D Printing. *Scientific Reports*, 7(1):7004, 2017.

[104] K. Tanuj Sapra and Hagan Bayley. Lipid-coated hydrogel shapes as components of electrical circuits and mechanical devices. *Scientific Reports*, 2 (1):848, 2012.

[105] Stephen A. Sarles, L. Justin Stiltner, Christopher B. Williams, and Donald J. Leo. Bilayer Formation between Lipid-Encased Hydrogels Contained in Solid Substrates. *ACS Applied Materials & Interfaces*, 2(12):3654–3663, 2010.

[106] William L. Hwang, Min Chen, Brid Cronin, Matthew A. Holden, and Hagan Bayley. Asymmetric Droplet Interface Bilayers. *Journal of the American Chemical Society*, 130(18):5878–5879, 2008.

[107] Elio J. Challita, Joseph S. Najem, Rachel Monroe, Donald J. Leo, and Eric C. Freeman. Encapsulating networks of droplet interface bilayers in a thermoreversible organogel. *Scientific Reports*, 8(1):6494, 2018.

[108] Joel R. Fried. *Polymer Science Technology*. Prentice-Hall, 2003.

[109] Yong Li and Toyoichi Tanaka. Kinetics of swelling and shrinking of gels. *The Journal of Chemical Physics*, 92(2):1365–1371, 1990.

[110] John Olmsted and David R. Kearns. Mechanism of ethidium bromide fluorescence enhancement on binding to nucleic acids. *Biochemistry*, 16 (16):3647–3654, 1977.

[111] Clément C. Campillo, André P. Schröder, Carlos M. Marques, and Brigitte Pépin-Donat. Volume transition in composite poly(NIPAM) giant unilamellar vesicles. *Soft Matter*, 4(12):2486, 2008.

[112] Kurt K. Dietliker. *Chemistry and technology of UV and EB formulation for coatings, inks and paints*. SITA, 1991. ISBN 0947798102.

[113] Yingfeng Tu, Fei Peng, Xiaofeng Sui, Yongjun Men, Paul B. White, Jan C. M. van Hest, and Daniela A. Wilson. Self-propelled supramolecular nanomotors with temperature-responsive speed regulation. *Nature Chemistry*, 9(5):480–486, 2016.

[114] Satish Nayak and L. Andrew Lyon. Photoinduced Phase Transitions in Poly(*N*-isopropylacrylamide) Microgels. *Chem. Mater.*, 16(13):2623–2627, 2004.

[115] Xuanhe Zhao, Jaeyun Kim, Christine A. Cezar, Nathaniel Huebsch, Kangwon Lee, Kamal Bouhadir, and David J. Mooney. Active scaffolds for on-demand drug and cell delivery. *Proceedings of the National Academy of Sciences*, 108 (1):67–72, 2011.

[116] Vincenzo Amendola, Roberto Pilot, Marco Frasconi, Onofrio M Maragò, and Maria Antonia Iatì. Surface plasmon resonance in gold nanoparticles: a review. *Journal of Physics: Condensed Matter*, 29(20):203002, 2017.

[117] Younan Xia and Naomi J. Halas. Shape-Controlled Synthesis and Surface Plasmonic Properties of Metallic Nanostructures. *MRS Bulletin*, 30(05): 338–348, 2005.

[118] Ke Jiang, David A. Smith, and Anatoliy Pinchuk. Size-Dependent Photothermal Conversion Efficiencies of Plasmonically Heated Gold Nanoparticles. *The Journal of Physical Chemistry C*, 117(51):27073–27080, 2013.

[119] Anna Zielińska-Jurek. Progress, challenge, and perspective of bimetallic TiO2-based photocatalysts. *Journal of Nanomaterials*, pages 1–17, 2014.

[120] Ralph Weissleder. A clearer vision for in vivo imaging. *Nature Biotechnology*, 19(4):316–317, 2001.

[121] Jinxing Li, Berta Esteban-Fernández de Ávila, Wei Gao, Liangfang Zhang, and Joseph Wang. Micro/nanorobots for biomedicine: Delivery, surgery, sensing, and detoxification. *Science Robotics*, 2(4):eaam6431, 2017.

[122] Yoonho Kim, Hyunwoo Yuk, Ruike Zhao, Shawn A. Chester, and Xuanhe Zhao. Printing ferromagnetic domains for untethered fast-transforming soft materials. *Nature*, 558(7709):274–279, 2018.

[123] Sylvain Martel. Beyond imaging: macro- and microscale medical robots actuated by clinical MRI scanners. *Science Robotics*, 2(3):eaam8119, 2017.

[124] Sangwon Kim, Famin Qiu, Samhwan Kim, Ali Ghanbari, Cheil Moon, Li Zhang, Bradley J. Nelson, and Hongsoo Choi. Fabrication and characterization of magnetic microrobots for three-dimensional cell culture and targeted transportation. *Advanced Materials*, 25(41):5863–5868, 2013.

[125] Friedhelm Serwane, Alessandro Mongera, Payam Rowghanian, David A. Kealhofer, Adam A. Lucio, Zachary M. Hockenbery, and Otger Campàs. In vivo quantification of spatially varying mechanical properties in developing tissues. *Nature Methods*, 14(2):181–186, 2017.

[126] Jürgen Rahmer, Christian Stehning, and Bernhard Gleich. Spatially selective remote magnetic actuation of identical helical micromachines. *Science Robotics*, 2(3), 2017.

[127] Wenqi Hu, Guo Zhan Lum, Massimo Mastrangeli, and Metin Sitti. Small-scale soft-bodied robot with multimodal locomotion. *Nature*, 554(7690):81–85, 2018.

[128] Young-Seok Shon, Stephen M. Gross, Brent Dawson, Marc Porter, , and Royce W. Murray. Alkanethiolate-Protected Gold Clusters Generated from Sodium S-Dodecylthiosulfate (Bunte Salts). *Langmuir*, 16(16):6555–6561, 2000.

[129] Wei Wang, Qin-Qin Wei, Jun Wang, Bi-Cui Wang, Sai-hui Zhang, and Zhi Yuan. Role of thiol-containing polyethylene glycol (thiol-PEG) in the modification process of gold nanoparticles (AuNPs): Stabilizer or coagulant? *Journal of Colloid and Interface Science*, 404:223–229, 2013.

[130] Gert Frens. Controlled Nucleation for the Regulation of the Particle Size in Monodisperse Gold Suspensions. *Nature Physical Science*, 241(105):20–22, 1973.

[131] Timothy G. Leong, Christina L. Randall, Bryan R. Benson, Noy Bassik, George M. Stern, and David H. Gracias. Tetherless thermobiochemically actuated microgrippers. *Proceedings of the National Academy of Sciences*, 106(3):703–708, 2009.

[132] Alexander D. Graham. *The Design and Implementation of a 3D Bioprinter*. PhD thesis, Doctor of Philosophy Thesis, University of Oxford, 2015.

[133] Chris S. Hughes, Lynne M. Postovit, and Gilles A. Lajoie. Matrigel: a complex protein mixture required for optimal growth of cell culture. *Proteomics*, 10 (9):1886–1890, 2010.

[134] Shiri Uriel, Edwardine Labay, Megan Francis-Sedlak, Monica L. Moya, Ralph R. Weichselbaum, Natalia Ervin, Zdravka Cankova, and Eric M. Brey. Extraction and assembly of tissue-derived gels for cell culture and tissue engineering. *Tissue engineering. Part C, Methods*, 15(3):309–21, 2009.

[135] Faruk Oytun, Muhammet U. Kahveci, and Yusuf Yagci. Sugar overcomes oxygen inhibition in photoinitiated free radical polymerization. *Journal of Polymer Science, Part A: Polymer Chemistry*, 51(8):1685–1689, 2013.

[136] D. Gilroy and J. E. O. Mayne. The de-aeration of aqueous solutions. *Journal of Applied Chemistry*, 12(8):382–384, 1962.

[137] Sanhita S. Dixit, Alexandra Pincus, Bin Guo, and Gregory W Faris. Droplet shape analysis and permeability studies in droplet lipid bilayers. *Langmuir*, 28(19):7442–51, 2012.

[138] Brad J. Berron, Leah M. Johnson, Xiao Ba, Joshua D. McCall, Nicholas J. Alvey, Kristi S. Anseth, and Christopher N. Bowman. Glucose oxidase-mediated polymerization as a platform for dual-mode signal amplification and biodetection. *Biotechnology and Bioengineering*, 108(7):1521–1528, 2011.

[139] Adam J. Gormley, Robert Chapman, and Molly M. Stevens. Polymerization Amplified Detection for Nanoparticle-Based Biosensing. *Nano Letters*, 14(11): 6368–6373, 2014.

[140] Cheves Walling. Fenton's reagent revisited. *Accounts of Chemical Research*, 8 (4):125–131, 1975.

[141] Wen Jiang Zheng, Ning An, Jian Hai Yang, Jinxiong Zhou, and Yong Mei Chen. Tough Al-alginate/Poly(*N*-isopropylacrylamide) Hydrogel with Tunable LCST for Soft Robotics. *ACS Applied Materials & Interfaces*, 7(3):1758–1764, 2015.

[142] Hyunwoo Yuk, Teng Zhang, German Alberto Parada, Xinyue Liu, and Xuanhe Zhao. Skin-inspired hydrogel-elastomer hybrids with robust interfaces and functional microstructures. *Nature Communications*, 7(May):1–11, 2016.

[143] Sumith, Yesu Dasan. Fast Circle fitting using Landau method, 2015. URL `https://uk.mathworks.com/matlabcentral/fileexchange/44219-fast-circle-fitting-using-landau-method`.

[144] Uri M. Landau. Estimation of a circular arc center and its radius. *Computer Vision, Graphics, and Image Processing*, 38(3):317–326, 1987.

[145] Samuel M. Thomas and Yiu-Tong Chan. A simple approach for the estimation of circular arc center and its radius. *Computer Vision, Graphics, and Image Processing*, 45(3):362–370, 1989.

[146] Sodium phosphate. *Cold Spring Harbor Protocols*, 2006(1):pdb.rec8303, 2006.

[147] Eric Carle. *The Very Hungry Caterpillar*. 1969.